ELUCIDATING THE ROLE OF ADSORBED STATES OF HYDROGEN, WATER AND CARBON DIOXIDE OVER TiO_2 AND Pd/TiO_2

A THESIS SUBMITTED TO
THE GRADUATE SCHOOL OF NATURAL AND APPLIED SCIENCES
OF
MIDDLE EAST TECHNICAL UNIVERSITY

BY

BEGÜM YILMAZ

IN PARTIAL FULFILLMENT OF THE REQUIREMENTS
FOR
THE DEGREE OF MASTER OF SCIENCE
IN
CHEMICAL ENGINEERING

JANUARY 2020

Approval of the thesis:

ELUCIDATING THE ROLE OF ADSORBED STATES OF HYDROGEN, WATER AND CARBON DIOXIDE OVER TiO_2 AND Pd/TiO_2

submitted by **BEGÜM YILMAZ** in partial fulfillment of the requirements for the degree of **Master of Science in Chemical Engineering Department, Middle East Technical University** by,

Prof. Dr. Halil Kalıpçılar _____
Dean, Graduate School of **Natural and Applied Sciences**

Prof. Dr. Pınar Çalık _____
Head of Department, **Chemical Engineering**

Prof. Dr. Deniz Üner _____
Supervisor, **Chemical Engineering, METU**

Examining Committee Members:

Assist. Prof. Dr. Emre Büküşoğlu
Chemical Engineering, METU _____

Prof. Dr. Deniz Üner
Chemical Engineering, METU _____

Assist. Prof. Dr. Bahar İpek Torun
Chemical Engineering, METU _____

Assist. Prof. Dr. Harun Koku
Chemical Engineering, METU _____

Assoc. Prof. Dr. Özcan Köysüren
Energy Engineering, Ankara University _____

Date: 27.01.2020

I hereby declare that all information in this document has been obtained and presented in accordance with academic rules and ethical conduct. I also declare that, as required by these rules and conduct, I have fully cited and referenced all material and results that are not original to this work.

Name, Last Name: Begüm Yılmaz

Signature :

ABSTRACT

ELUCIDATING THE ROLE OF ADSORBED STATES OF HYDROGEN, WATER AND CARBON DIOXIDE OVER TiO_2 AND Pd/TiO_2

Yılmaz, Begüm
M.S., Department of Chemical Engineering
Supervisor: Prof. Dr. Deniz Üner

January 2020, 104 pages

Artificial photosynthesis studies aim to utilize solar energy for conversion of CO_2 into valuable organics using H_2O; however, developments in the area are far from realistic level applications due to the low production rates. In order to understand the mechanism, CO_2 and H_2O adsorption isotherms over TiO_2 P25 were investigated by using a volumetric chemisorption technique with and without an illumination source.

Adsorption isotherms revealed indirect evidences on local temperature rise on the surface indicating photo-induced thermal chemistry upon charge recombination. Desorption was observed during CO_2 adsorption over TiO_2 P25 under illumination. Calculation of adsorbed amounts according to estimation for local temperature rise (to 160°C) on the surface yielded a reasonable adsorption isotherm under illumination. Similarly, H_2O adsorption isotherm under illumination showed Langmuir type of adsorption isotherm indicating presence of only strongly bound molecules under illumination. In this study, weakly adsorbed molecules were claimed to be desorbed due to local temperature rise on the catalyst surface upon charge recombination resulting in similar chemistry with heating of the sample cell to 150°C. Additionally, the attempts on direct heat release measurement upon charge recombination via microcalorimeter were explained.

Moreover, H_2 and CO_2 adsorption isotherms over Pd/TiO_2 surface were investigated

using a chemisorption manifold connected to a Setaram C80 microcalorimeter to understand the effect of presence of precious metal on TiO_2 support. 0.5% Pd/TiO_2 showed relatively well dispersed palladium on support. Enhanced CO_2 adsorption observed on 0.5% Pd/TiO_2 was related to increase in oxygen vacancy concentration due to spilled hydrogen during the reduction of surface. Evidences for presence of palladium bulk on 2.0% Pd/TiO_2 were presented via H_2-TPR results, especially.

According to these evidences, it is understood that the effect of heat release upon charge recombination on chemistry is highly underrated in literature. The local temperature rise can affect the chemistry significantly;however, uncontrollable temperature conditions are not desired. Last but not least, metal hydrogen systems over metal oxide support can offer a strategy for enhanced reduction reactions by utilizing stored hydrogen on surface.

Keywords: Photocatalysis, CO_2 adsorption, H_2O adsorption, TiO_2 P25, Pd/TiO_2

ÖZ

TiO_2 VE Pd/TiO_2 ÜZERİNDE HİDROJEN, SU VE KARBONDİOKSİT ADSORPLANMA HALLERİNİN ROLÜNÜN AYDINLATILMASI

Yılmaz, Begüm
Yüksek Lisans, Kimya Mühendisliği Bölümü
Tez Yöneticisi: Prof. Dr. Deniz Üner

Ocak 2020 , 104 sayfa

Yapay fotosentez çalışmaları, CO_2'in H_2O kullanılarak değerli organik maddelere dönüştürülmesi için güneş enerjisinden faydalanmayı amaçlamakla birlikte, bu alandaki gelişmeler düşük üretim hızları nedeniyle gerçekçi seviyedeki uygulamalardan uzaktır. Mekanizmayı anlamak için, TiO_2 P25 üzerindeki CO_2 ve H_2O adsorpsiyon izotermleri bir ışık kaynağı ile veya bir ışık kaynağı olmadan hacimsel kemisorpsiyon tekniği kullanılarak araştırılmıştır.

Adsorpsiyon izotermleri, yük rekombinasyonu üzerine yüzeydeki yerel sıcaklık artışından dolayı foto-kaynaklı termal kimyayı gösteren dolaylı kanıtlar ortaya koymuştur. Aydınlatma altında TiO_2 P25 üzerine CO_2 adsorpsiyonu sırasında desorpsiyon gözlendi. Yüzeydeki yerel sıcaklık artışı (160°C'ye) tahminine göre adsorbe edilen miktarların hesaplanması, aydınlatma altında makul bir adsorpsiyon izotermi verdi. Benzer şekilde, aydınlatma altında H_2O adsorpsiyon izotermi, aydınlatma altında sadece kuvvetle bağlı moleküllerin varlığını gösteren Langmuir tipi adsorpsiyon izotermini göstermiştir. Bu çalışmada zayıf adsorbe edilmiş moleküllerin, yük rekombinasyonu üzerine katalizördeki yerel sıcaklık artışından ötürü desorbe edildiği iddia edilmektedir, bu da numune hücresinin 150°C'ye ısıtılması ile benzer şekilde kimyayı etkilemektedir. Buna ek olarak, mikrokalorimetre yoluyla yük rekombinasyonu üzerine salınan ısının doğrudan ölçülmesi için olan girişimler açıklanmıştır.

Ayrıca, değerli metal varlığının TiO_2 üzerindeki etkisini anlamak için Pd/TiO_2 yüzeyi üzerinde H_2 ve CO_2 adsorpsiyon izotermleri bir Setaram C80 mikrokalorimetresine bağlı kemisorpsiyon manifoldu kullanılarak araştırıldı.%0.5 Pd/TiO_2, destek üzerinde paladyumun nispeten daha iyi dağılımını gösterdi. Muhtemelen yayılan (spilled) hidrojene bağlı olarak oluşan oksijen boşluklarından dolayı %0.5 Pd/TiO_2 üzerinde artış göstermiş CO_2 adsorpsiyonunu gözlemlenmiştir. %2.0 Pd/TiO_2 üzerinde bulk paladyumun bulunmasına dair kanıtlar da sunulmuştur.

Bu delillere göre, yük rekombinasyonu üzerine açığa çıkan ısının kimya üzerindeki etkisine literatürde oldukça az değer biçildiği sonucuna varılmıştır. Yerel sıcaklık artışı kimyayı önemli ölçüde etkileyebilir, ancak kontrol edilemeyen sıcaklık koşulları istenmez. Son olarak önemli noktalardan bir tanesi de, metal oksit üzerinde metal hidrojen sistemleri yüzeyde hidrojen kullanarak iyileştirilmiş indirgeme reaksiyonları için bir strateji sunabilir.

Anahtar Kelimeler: Fotokataliz, CO_2 adsorpsiyonu, H_2O adsorpsiyonu, TiO_2 P25, Pd/TiO_2

To my family

ACKNOWLEDGMENTS

I would like start by expressing my sincerest gratitude to my supervisor, Prof. Dr. Deniz Üner, for her unmatched guidance both in my master study and in my life. Coming across with her at the beginning of my master education was a turn of fate for me and I consider myself really lucky.

Besides, I would like to thank Uner group members, past and present, for their help throughout my study. I am grateful to Dr. Asmae Bouziani with her help with TPR, TEM and ICP experiments. In addition, I want to offer my deepest thanks to Dr. Mustafa Yasin Aslan and Dr. Atalay Çalışan for their help in the laboratory when I needed most. I would also like to thank Dr. Emre Büküşoğlu for lending UV lamp in his laboratory when needed without a question. Furthermore, I thank workshop people in the department, especially İsa Çağlar, for their help with laboratory equipment during my study.

I want to express my great gratitude to Aygün Şahin for her endless support and her valuable friendship since the beginning of my METU story. I want to thank Ahsen Gür, Nazlıdeniz Aktan and Merve Kocataş; my high school girl gang, for their friendship more than 10 years. I thank my colleagues in the department; Öznur Doğan, Berkan Atman, Salih Ermiş, Duygu Sezen Polat, Merve Sarıyer, Candan Karaeyvaz, Seda Sivri, Özge Batır and Ahmet Fırat Taşkın for their support and help in my life, in my study and in my job.

Most of all, I want to thank my one and only family from the deepest of my heart. I am blessed with love of my mother, Berrin; my father, Mehmet; my brother, Alp; my sister, Ayşenur and my sister in law, Tuğba. I cannot express my gratitude for them with words. They made me who I am by building a life for me full of love, respect, honour, dignity and self-confidence. Their belief in education and culture led me to the point where I stand right now, happily and thankfully. Above all, I would like thank Defne; my beautiful and too smart niece who brought nothing but joy into my life.

Lastly, I would like to thank TÜBİTAK project (No:117M040) for financial support.

TABLE OF CONTENTS

APPENDICES

LIST OF TABLES

TABLES

LIST OF FIGURES

FIGURES

LIST OF ABBREVIATIONS

ABBREVIATIONS

AFM	Atomic force microscopy
BET	Brunauer-Emmett-Teller
CB	Conduction band
CSP	Crystallographic shear planes
HREELS	High resolution electron loss spectroscopy
HRTEM	High resolution transmission electron microscope
HOMO	Highest occupied molecular orbital
LUMO	Lowest unoccupied molecular orbital
PL	Photoluminescence
SMSI	Strong metal support interaction
STM	Scanning tunneling microscopy
TAS	Time-resolved adsorption spectroscopy
TEM	Transmission electron microscope
TPD	Temperature programmed desorption
TPR	Temperature programmed reduction
UV	Ultraviolet
VB	Valence band

CHAPTER 1

INTRODUCTION

1.1 Photosynthesis

Solar energy storage process in chemical bonds (i.e glucose) by green plants and photosynthetic bacteria is named as photosynthesis. An extensive position paper published recently by Weitze (2018) stated followings on photosynthesis. The event started around 3 billion years ago by the bacteria. Thereafter, higher organisms like algae and plants started to carry out this process upon evolution of chloroplasts. Photosynthesis is still the most extensive and accomplished process on earth. Stable molecules like CO_2 and H_2O are converted to organics ($(CH_2O)_n$) through spatially and temporarily separated two step reactions according to the net reaction given in Equation 1.1. In the first step - "light reactions", sunlight is absorbed and H_2O splits resulting in formation of O_2 and H^+. In the second step - "Dark reactions", protons drive the reactions for CO_2 reduction to organics without needing sunlight.

$$\begin{gathered} 6CO_2 + 12H_2O \xrightarrow{LightEnergy} C_6H_{12}O_6 + 6O_2 + 6H_2O \\ \Delta G = 2880kJ/mol\ C_6H_{12}O_6 \end{gathered} \tag{1.1}$$

Photosynthesis is a highly sophisticated and complex catalytic process with several protein components, metal centers, cofactors, pigments and so on. Despite its complexity, photosynthesis comes into view as an ideal process by offering a clean and sustainable path to reduce CO_2 to organics through utilization of sunlight. Reducing CO_2 to valuable chemicals with a sustainable energy source provides the answer for the most critical problems of today: limited reservoir of fossil fuels and high CO_2 emission yielding global warming.

1.2 Utilization of fossil fuels and CO_2 emission

World's energy supply depends on fossil energy mostly.(Figure 1.1) Yet, 1973 oil crisis turned attention to alternative energy sources including solar energy (Schneider, Bahnemann, Ye, Li Puma, & Dionysiou, 2016). Global companies like BP and Shell have made serious investments for energy production from renewable sources and they are now considered as energy companies rather than oil companies (Pickl, 2019). Today, the largest growth in energy supply is expected to be from renewable energy sources (BP, 2019a). Energy production from solar energy shows a dramatic increase within the renewable sources reaching to 584.6 Terawatt-hours by the end of 2018 (Figure 1.2) (BP, 2019b).

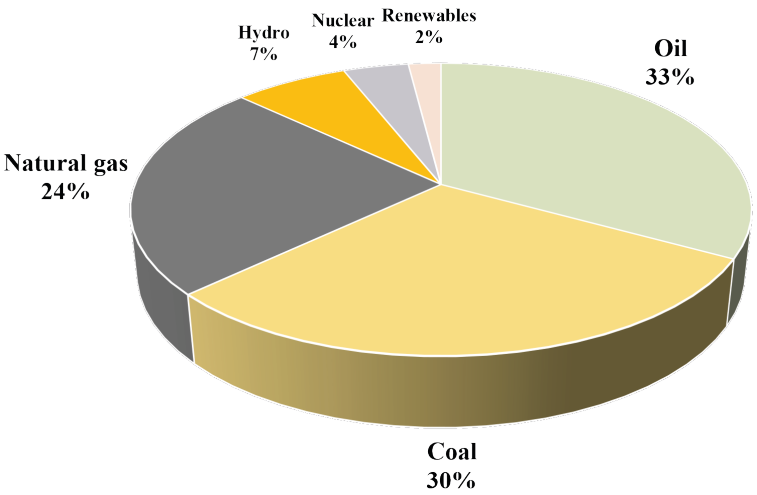

Figure 1.1: World supply of energy demand(BP, 2019a)

Moreover, high CO_2 emission rises concerns on environmental issues. Aforementioned position paper (Weitze, 2018) summarized global CO_2 cycle according to Figure 1.3. 450 Gigatonnes of CO_2 converted to organics per year by photosynthesis (green arrow) corresponding to 95% of natural CO_2 emission through respiration (blue arrow). The rest is provided by non-photosynthetic processes (thin arrow). 32 gigatonnes of CO_2 is emitted per year through combustion of fossil fuels (grey arrow). Some cannot be converted to organics and increase CO_2 amount in atmosphere resulting in climate change. Expected temperature rise of earth surface upon CO_2 emission till 2100 can be seen Figure 1.4. Such temperature changes can be detrimental for humanity.

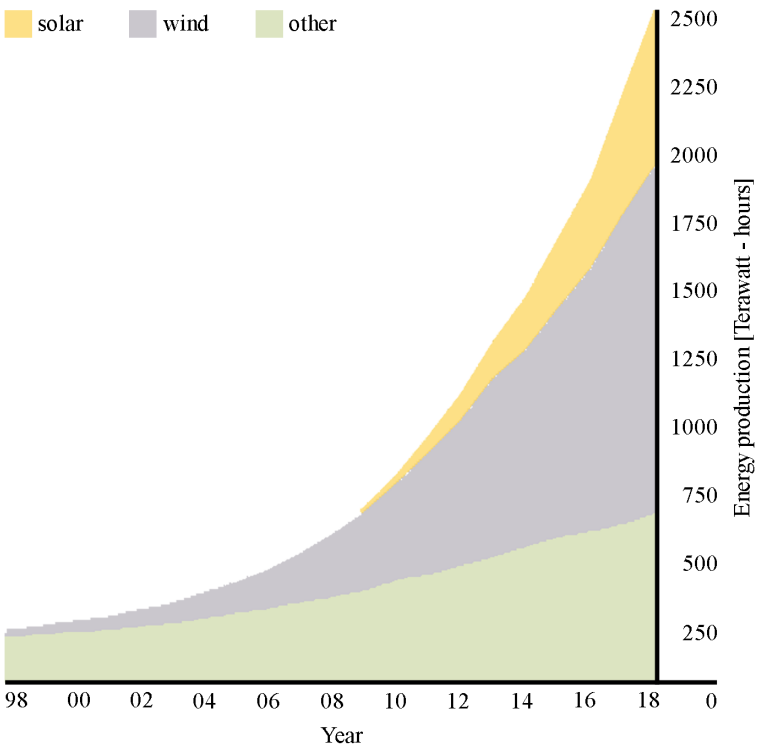

Figure 1.2: Share of power generation by solar energy within renewable sources (BP, 2019b)

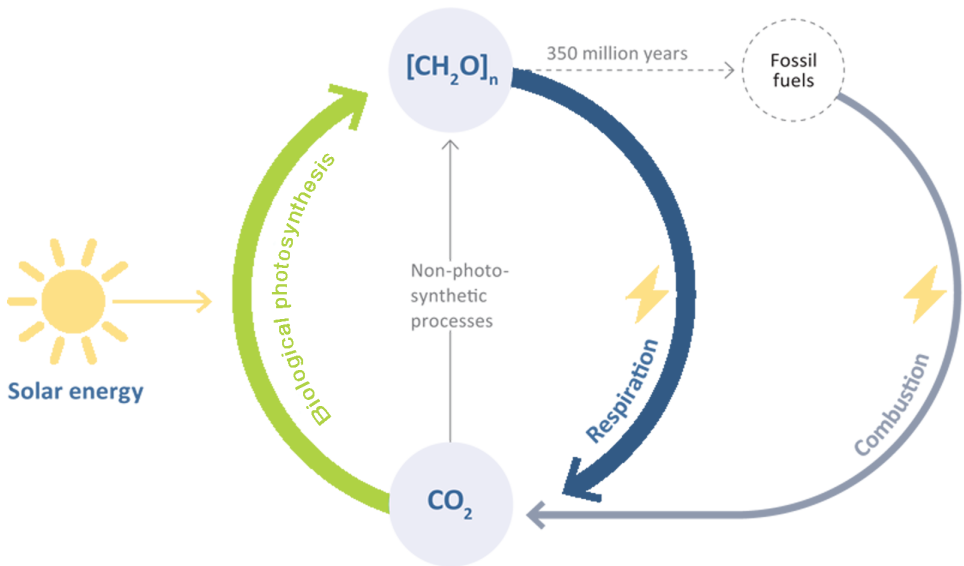

Figure 1.3: Global carbon cycle(Weitze, 2018)

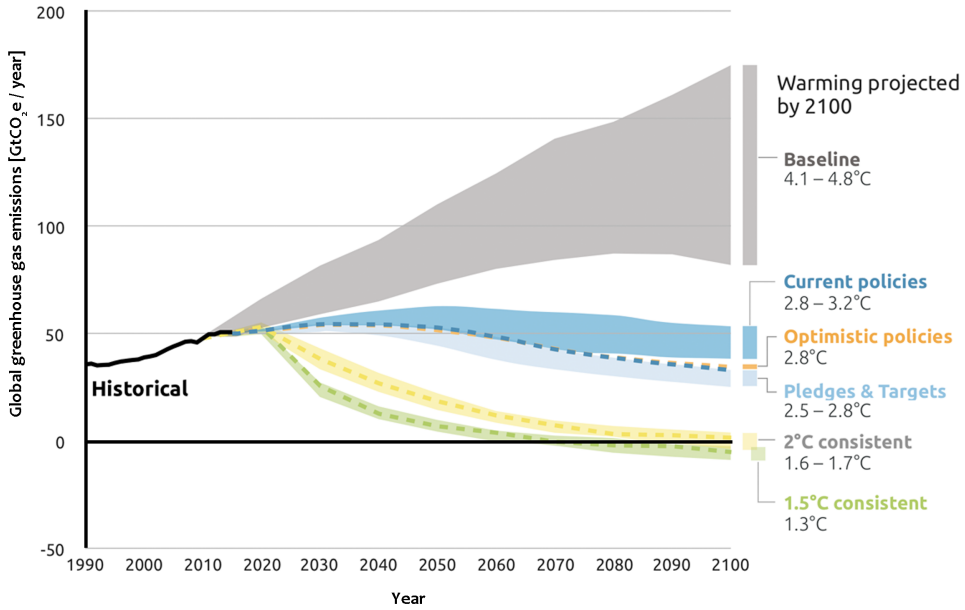

Figure 1.4: Expected warming of earth upon greenhouse gas emissions(Climate Action Tracker, 2019)

As a result, the photocatalytic conversion of CO_2 with H_2O to organics/fuels like methanol at mild conditions using a light absorbing material has become a popular research area in catalysis field to solve problems related with both sustainable energy and CO_2 emission. The phenomena is named as "artificial photosynthesis" and researchers have been concentrated on this topic especially after the sensational achievement of Fujishima and Honda (1972) on photocatalytic water splitting published in Nature in 1972.

1.3 Bottleneck problems of artificial photosynthesis

Advantages of artificial photosynthesis are mentioned above and yet, it has several disadvantages that needs to be overcome for an industrial level application. Review articles Kondratenko, Mul, Baltrusaitis, Larrazábal, and Pérez-Ramírez (2013), Ipek and Uner (2012), (Takanabe, 2019) and (Qureshi & Takanabe, 2017) summarized major problems of artificial photosynthesis and photocatalytic studies as listed below;

- Photocatalytic conversion of CO_2 and H_2O suffers from low reaction rate and efficiency.

- Oxidation and reduction reactions take place on the same catalyst surface, thus interaction of reactants and products can yield lower catalytic rates.
- Charges wandering on the semiconductor surface is in an unregulated fashion; that is, interaction of charges cannot be controlled.
- Only materials with proper band gap for CO_2 reduction and H_2O oxidation can be used. Band gap of the material may not be proper for harvesting solar energy.
- Even C-C bond making is challenging.
- Considering an industrial level operation; CO_2 capture, purification and delivery is not easy and it is costly.
- In terms of research, there is no common ground for experimental methods and interpretation of results.

1.4 Objectives

To understand the bottleneck problems of artificial photosynthesis through photo-induced mechanism, fundamental aspects of artificial photosynthesis were studied by CO_2 and H_2O adsorption isotherms over TiO_2 photocatalyst. Adsorption isotherms and microcalorimetry results were presented to reveal the effect of charge recombination on chemistry. H_2 and CO_2 adsorption isotherms over Pd/TiO_2 were investigated to elucidate the effect of presence of metal on TiO_2 support. Palladium-hydrogen interaction was studied to evaluate hydrogen storage over palladium for CO_2 reduction reaction later.

CHAPTER 2

LITERATURE REVIEW

The study of photocatalytic conversion of CO_2 and H_2O to valuable organics via TiO_2 photocatalyst will be addressed through following aspects:

- Light interaction with a photocatalyst
- Properties of TiO_2
- H_2O splitting reaction
- CO_2 reduction reaction

2.1 Light interaction with the matter

2.1.1 Photocatalysis and heterogeneous photocatalysis phenomena

Photocatalysis is the process where light irradiation promotes reduction and oxidation reactions in the presence of a semiconductor. In heterogeneous photocatalysis, photo-induced events take place on the surface of the photocatalyst. In this study, excitation of substrate (semiconductor) was studied and hence, light absorption ability of the semiconductor defines the efficiency of photo-induced chemistry (Linsebigler, Lu, & Yates, 1995).

2.1.2 Short Historical review

The term "photocatalyst" was first introduced by Plotnikow in 1910 and appeared in the studies of Landou (1913) later (Serpone, Emeline, Horikoshi, Kuznetsov, & Ryabchuk, 2012)(references therein). Light interaction with the catalytic matter was studied by Eibner (1911), Tammann (1920) and Keidel (1929)(Serpone et al., 2012)(references therein); however, the earliest cited study belongs to Renz who observed the color change of TiO_2 upon illumination (Renz, 1921). Great contributions on photochemistry had been made by the studies of Baur (1918-1927), Terenin (1934-1970) and Bard (1975-1985) in the upcoming years. Landou recognized the heterogeneous photocatalyst phenomenon in 1913; but, the concept started developed systematically in the Institut de Catalyse starting from 1970 (Serpone et al., 2012)(references therein). After oil crisis in 1973, the number of studies on the photocatalysis increased immensely and today, more than 40,000 papers are published under the name of photocataysis.

2.1.3 Semiconductor working principle

For a semiconductor, band gap model is valid to understand light absorption by the matter. Proper light energy to excite a semiconductor depends on its band gap. Band gap is the magnitude of forbidden zone between conduction band and valence band of semiconductor. Conduction band represents LUMO (lowest unoccupied molecular orbital) and valence band represents HOMO (highest occupied molecular orbital) of the solid structure (Gaya, 2014). Band gap energies of some semiconductors and reduction/oxidation energies required for some selected reactions can be seen in Figure 2.1. Energy levels define the required illumination energy and also for realization of oxidation and reduction reactions (Uner et al., 2011).

Upon light irradiation, a semiconductor harvests light energy and following processes are expected to occur according to Figure 2.2; (1) electron-hole pair generation (migration of electron from valence band to conduction band), (2) transport of charges in the photocatalyst bulk yielding surface reduction reactions via electrons and surface oxidation reactions in the holes (3), trapping of electrons and holes in the bulk and (4)

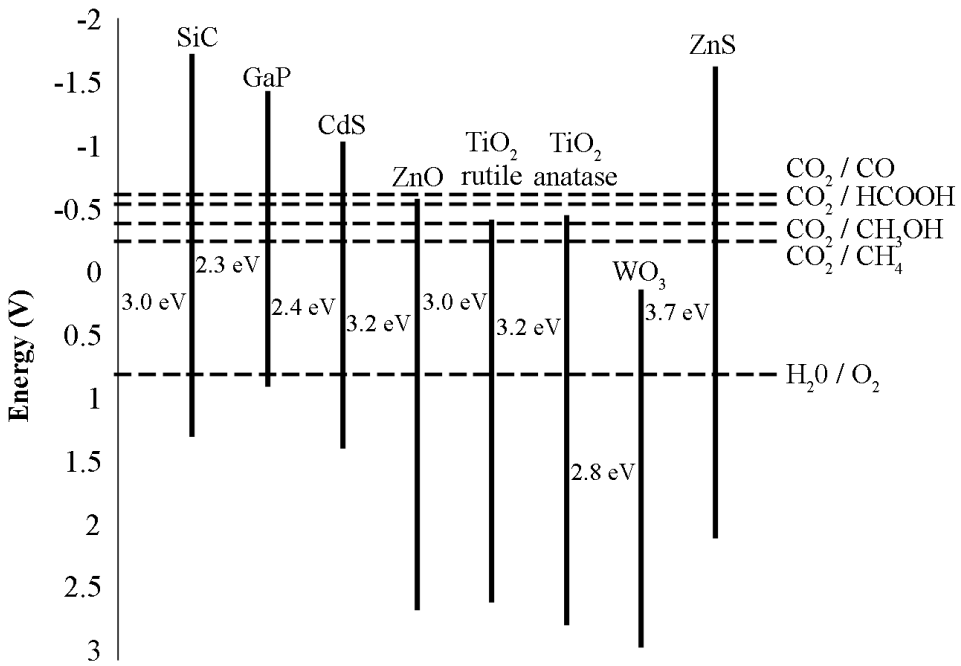

Figure 2.1: Band gap energies of some semiconductors and amount of energy required for selected reactions(Uner et al., 2011)

recombination of electron-hole pairs (Wen et al., 2015),(Hurum, Agrios, Gray, Rajh, & Thurnauer, 2003).

Most of the generated electron hole pairs will recombine immediately (Hurum et al., 2003). Reaction centers will be depleted due to recombination of electron hole pairs. Hence, recombination is often considered as an inhibiting factor to photocatalytic rates (Wen et al., 2015). Hole and electron scavengers can be utilized in photocatalytic systems to lessen recombination event by trapping electrons and holes (Henderson, 2011). Time-resolved absorption spectroscopy (TAS) is usually used to measure dynamics of photo-induced events. Time scale for absorption, trapping and recombination can be seen in Figure 2.3 (Schneider et al., 2014). Surface dynamics and mechanisms will be addressed through illumination intensity and charge recombination in the upcoming sections.

2.1.4 The effects of illumination intensity on photocatalysis

Illumination is a major variable in photocatalysis. Experiments can be carried out at different light intensities to observe effect of increase in the number of charge

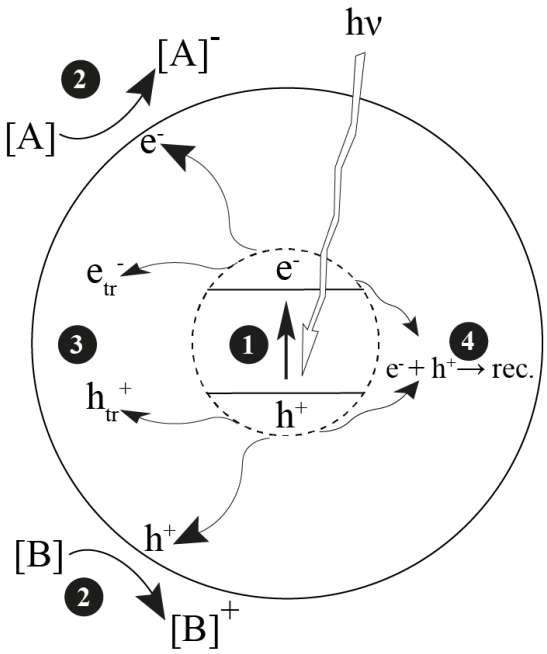

Figure 2.2: Schematic for light interaction with the semiconductor according to band gap model

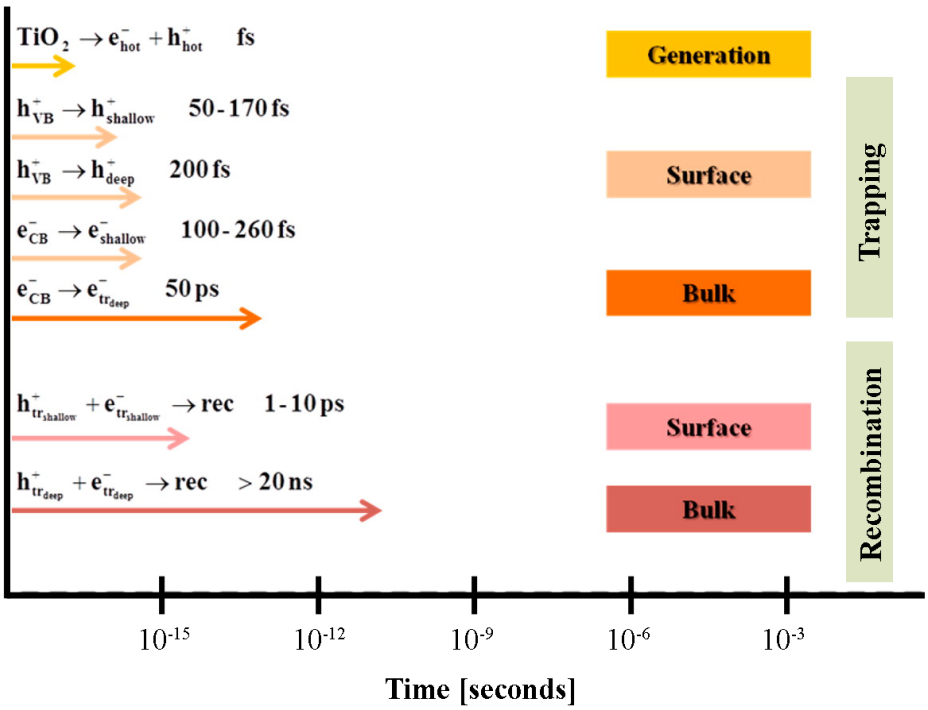

Figure 2.3: Time scales for some of the events occur during illumination(Schneider et al., 2014)

carriers on chemistry. At low intensities, reaction rate depends on the intensity linearly whereas at high intensities, reaction rate changes with square root of intensity (Emeline, Ryabchuk, & Serpone, 2000)(Turchi & Ollis, 1990)(Dilla, Mateblowski, Ristig, & Strunk, 2017). A relatively unified reaction rate-intensity relation is given by Martin, Herrmann, and Hoffmann (1994) as in Table 2.1. The reason for decreasing increase of rates with increasing intensity was stated as increase in the possibility of charge recombination at high intensities (Emeline et al., 2000),(Turchi & Ollis, 1990),(Martin et al., 1994) and (Rabani, Yamashita, Ushida, Stark, & Kira, 1998).

Table 2.1: Dependence of photocatalytic reaction rate on intensity

Intensity	r α I^{β}	Reference
Low	β=1	
High	0 < β < 1	(Martin et al., 1994)
Very High	β =0	

2.1.5 Wildcard of photocatalysis: Charge recombination

As Ohtani (2013) addressed in his critical review, an unexpected result in photocatalytic studies was usually explained by the effect of heat evolution upon enhanced charge carrier recombination and yet no further discussions were made in those studies. The reason is light absorption by the catalyst, charge generation and recombination dynamics are still not well-known even though studies on photocatalysis are beyond measure. A few studies conducted with TiO_2 and water solutions via transient absorption spectroscopy are given Table2.2 (Serpone, Lawless, Khairutdinov, & Pelizzetti, 1995)(Mohamed, Mendive, Dillert, & Bahnemann, 2011)(Shkrob, Sauer, & Gosztola, 2004). Tabulated data suggests neither light absorption nor charge generation processes are one hundred percent efficient. Photon absorption efficiency is highly related with the optical properties of the photocatalyst (Serpone, 1997). In addition, absorbed photons may not result in charge generation (Serpone et al., 1995). As a result, limited knowledge on charge generation results in even more limited knowledge on recombination.

Charge carrier recombination can occur in radiative manner (photoluminescence) or non-radiative manner (heat release) as shown in Equation 2.1 (Fujishima, Zhang, &

Tryk, 2008) in below. Henderson (2011) reported that recombination occurs mostly in non-radiative manner in TiO_2. Depending on the particle medium, particle size, temperature and the pressure of the environment (Serpone et al., 1995),(Berger et al., 2005)(references therein) time scale of recombination can vary from femtosecond to second (Henderson, 2011)(Sieland, Schneider, & Bahnemann, 2017).

$$e^- + h_{tr}^+ \text{ or } e_{tr}^+ + e^+ \text{ or } e^- + h^+ \tag{2.1}$$

Table 2.2: The number of electron hole pair per particle for TiO_2 solutions with different particle sizes and illumination intensities

Diameter size nm	Intensity $J \cdot cm^{-2}$	Intensity photons$\cdot cm^{-2}$	TiO_2 $mol \cdot L^{-1}$	Extinction coefficient $M^{-1} \cdot cm^{-1}$	Electron concentration $mol.L^{-1}$	Absorbed photons per particle	Electron hole pair per particle	Hole scavenger	References
2.1	~0.08 (355nm)	$\sim 1.4 \cdot 10^{17}$	$1.34 \cdot 10^{-3}$	1200 (600 nm adsorption)	$2.8 \cdot 10^{-4}$	0.9	0.2	-	(Serpone et al., 1995)
13.3			$5.26 \cdot 10^{-3}$		$8.3 \cdot 10^{-4}$	225	157		
26.7			$6.51 \cdot 10^{-3}$		$9.8 \cdot 10^{-4}$	1811	1504		
3.0	~9.40 (350nm)	$\sim 1.7 \cdot 10^{19}$	$38.00 \cdot 10^{-3}$	600 (600 nm adsorption)	$5.0\text{-}8.0 \cdot 10^{-4}$	-	6-9	methanol	(Mohamed et al., 2011)
4.6±0.5	0.04 (355nm)	$\sim 6.0 \cdot 10^{16}$	$0.24 \cdot 10^{-3}$	700±50 (800 nm adsorption)	-	-	1-1.2	chemisorbed polyols and carbohydrates	(Shkrob et al., 2004)

Leytner and Hupp (2000) reported that 60% of electron hole pairs recombined in 25 ns corresponding to $\sim$150 kJ/mole heat release for an aqueous TiO_2 solution. For a band to band non-radiative decay heat release would be 310 kJ/mole for TiO_2 (Henderson, 2011) considering to 3.20 eV band gap. Although, thermal effects are not very apparent (Zhao et al., 2019), the results implies possibility of significant energy release due to charge recombination.

Some studies referred to the thermal effects more openly (Henderson, 2011). Dilla, Mateblowski, et al. (2017) studied CO_2 reduction on TiO_2 where increase in the rate constants due to the local heating (Arrhenius type temperature dependence) upon charge recombination was discussed. No CH_4 production was observed when the experiment was repeated at a higher temperature (60°C) in dark and thus, the effect of local heating on the reaction rate was dismissed. The authors did not perform the experiments for the temperature at which the rate would be similar. The effect of hot spots on chemistry can differ from the effect of thermal catalysis performed on heated bulk. Indeed, a photocatalytic process with photo-induced thermal events is different than solely a thermal catalytic process even though similar temperature conditions were provided (Zhao et al., 2018).

Mendive, Hansmann, Bredow, and Bahnemann (2011) studied isolated aqueous TiO_2 solution under UV illumination. De-aggregation of TiO_2 particles was justified by heat release due to recombination. Increase in the adsorption capacity upon de-aggregation of particles was referred as the positive effect of charge recombination.

Neither Dilla, Mateblowski, et al. (2017) nor Mendive et al. (2011) reported temperature measurement upon heat release by charge carrier recombination. It is not easy to estimate temperature increase due to hot spots. It might be very high and immeasurable by standard thermal sensors (Zhao et al., 2019). On the other hand, Berger, Diwald, Knözinger, Sterrer, and Yates Jr (2006) reported a local temperature rise of 25K based on Curie plot upon excitation of TiO_2 nanocrystals with an intensity more than 1.55mW·cm^{-2} ($\sim 10^{15}$ photons·cm^{-2}·s) reporting possibility of photo-induced thermal chemistry.

2.2 TiO_2 semiconductor surface properties

2.2.1 TiO_2 crystal structure

TiO_2 is a photocatalyst with excellent properties such as nontoxicity, cheapness, availability, durability and eco-friendliness. Hence, it is the most commonly used photocatalyst in heterogeneous photocatalysis (De Angelis, Di Valentin, Fantacci, Vittadini, & Selloni, 2014)(references therein). The main drawback in usage of TiO_2 is its inability to harvest sunlight efficiently. TiO_2 can be activated with UV light and only 4% of sunlight radiates in UV-range (Li, Peng, & Peng, 2016).

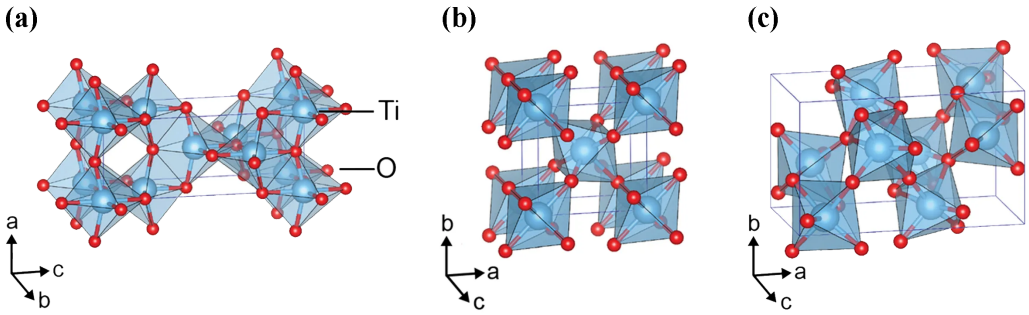

Figure 2.4: Crystal structures of TiO_2 (a) anatase(tetragonal, I41/amd) (b) rutile (tetragonal, P42/mmm), (c) brookite (orthorhombic, Pbca) (Haggerty et al., 2017)

Table 2.3: Comparison of rutile, anatase and brookite phases

	Rutile	Anatase	Brookite
Crystal structure (Gupta & Tripathi, 2011)	Tetragonal	Tetragonal	Orthorhombic
Density (g/cm^3) (Gupta & Tripathi, 2011)	4.13	3.79	3.99
Electron band gap (eV) (Reyes-Coronado et al., 2008)	3.01	3.20	3.13

TiO_2 is a transition metal oxide where anatase, rutile and brookite are the most known phases of it. Rutile is the most stable phase when surface area is smaller than 7 $m^2/g_{catalyst}$, brookite is the most stable phase for surface areas of 7-40 $m^2/g_{catalyst}$ and anatase phase is the most stable phase for higher surface areas (Ranade et al., 2002). Although, rutile phase exhibits higher stability than the other phases in gen-

eral, anatase phase is preferred in solar systems due to its higher electron mobility, lower relative permittivity with less dense structure. Anatase and rutile phases perform a better photocatalytic activity together than the pure phases due to enhanced charge separation (Hurum et al., 2003),(Gupta & Tripathi, 2011). Hence, TiO_2 P25 which is composed of anatase and rutile with ratio of 3:1(Ohno, Sarukawa, Tokieda, & Matsumura, 2001) is a commercialized mixed phase product. Brookite phase is the least favorable phase due to its more complicated structure and rare existence in nature (Gupta & Tripathi, 2011)(De Angelis et al., 2014). There are even less known polymorphs of TiO_2 such as baddeleyte, fluorite and hollandite (De Angelis et al., 2014).Ball and stick representation of selected crystal structures of rutile, anatase and brookite phases can be seen in Figure 2.4. Table2.3 shows a short comparison for these three phases.

2.2.2 The role of oxygen vacancies

There are several defect types in TiO_2 surface and bulk (Table2.4) Among several defect types, both bulk and surface oxygen vacancies is the most investigated and discussed one. (Figure 2.5).

Table 2.4: Defect types in TiO_2(Diebold, 2003)

Bulk defects	Surface defects
Oxygen vacancies	Oxygen vacancies
Ti^{3+},Ti^{4+} intersitials	Step edges Impurities Line defects
Planar defects (i.e. CSP)	Planar defects (i.e. CSP)

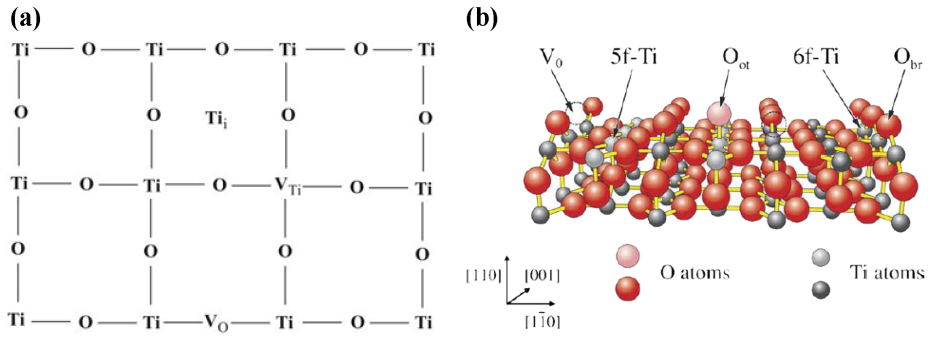

Figure 2.5: (a)Schematic representation of oxygen vacancies and Ti interstitials in the bulk(Gaya, 2014) (b) Schematic representation of oxygen vacancies on TiO_2 (110) surface(Wendt et al., 2005)

TiO_2 can have oxygen deficiencies (5-10% for rutile phase and less for anatase phase) on its surface formed during preparation (De Angelis et al., 2014) which results in negative charge accumulation on surface (n-type semiconductor) (Stevanovic & Yates, 2013). Surface characterization techniques such as STM and AFM can be used to detect and measure oxygen vacancies on surface (Figure 2.6) (Diebold, 2003).

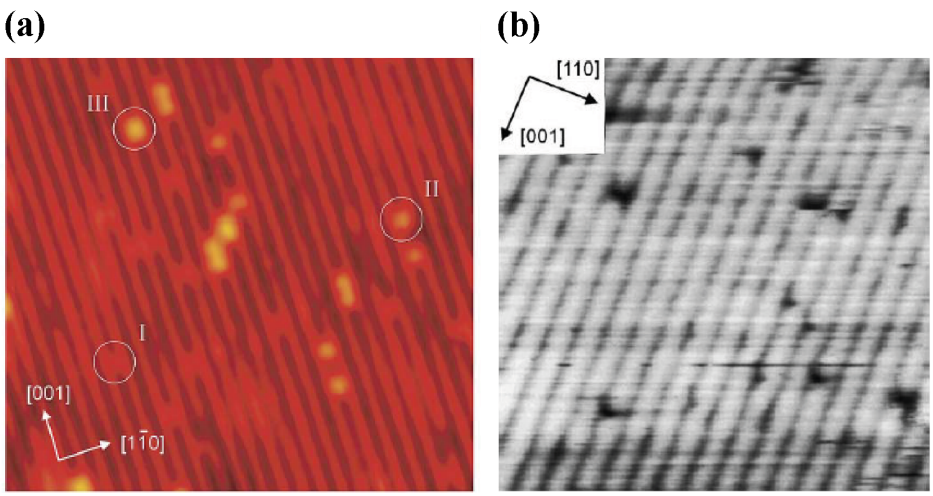

Figure 2.6: (a)STM images of clean, reduced TiO_2(110)- defects of I(vacancies), II(bridging hydroxyls), III(pairs of bridging hydroxyls)(Wendt et al., 2005) (b) Non-contact AFM image of the TiO_2 (110) - black dots are assigned as oxygen vacancies(Diebold, 2003)(references therein)

Oxygen vacancies can also be formed intentionally on an already prepared sample via thermal annealing or electron bombardment (De Angelis et al., 2014)(Diebold,

2003). Previously, UV irradiation was proposed to create oxygen vacancies on TiO_2 surface (Rong et al., 1997)(Wang et al., 1998). However, the hypothesis was rejected later by the studies of other groups summarized in the referred articles; Thompson and Yates (2006)Yates (2009).

Oxygen vacancies affect the electronic structure acting as an electron donor. In addition, they affect adsorbent-adsorbate interactions acting as a adsorption site (Wendt et al., 2005). Reducibility of the metal oxide; that is, ability to exchange oxygen, is critical for reactions progressing for example with Mars-van Krevelen mechanism (Ruiz Puigdollers, Schlexer, Tosoni, & Pacchioni, 2017). Reducibility of the metal oxide influences chemical reactivity (Ruiz Puigdollers et al., 2017); hence, understanding and controlling of oxygen vacancies are essential for an enhanced reaction activity. Lastly, oxygen vacancies can be healed by O_2 dissociation on surface (Stevanovic et al., 2012).

2.2.3 The effects of illumination on TiO_2 surface

Abovementioned, TiO_2 has oxygen vacancies on its surface causing negative charge accumulation on its surface. (n-type semiconductor) This unbalanced charge results in upward bending (increase of electronic potential energy) of TiO_2 band near surface. Band bending is important to understand charge transfer in a semiconductor. For a n-type semiconductor, band bending means extending of depletion layer. Yates group did several studies with photoluminescence spectroscopy to investigate band bending phenomena. For an intrinsic semiconductor, the bands are flat since there is no charge transfer between the bulk and the surface. On the other hand, for a n-type semiconductor, Fermi level (highest occupied level) of bulk is closer to conduction band. As a result, for this type semiconductor, Fermi level of bulk is higher than Fermi level of surface when it is away from equilibrium conditions. Bands bend upward by transferring electrons from bulk to surface until equilibrium is established. Surface is rich with electron charge carriers. Because of more effective electric field in this part, electron-hole pair recombination lags. Downward band bending occurs for a p-type semiconductor. Figure 2.7 summarizes band bending phenomena (Z. Zhang & Yates, 2012). Upon UV light exposure, electron transfers from surface to bulk. For an n-type

and p-type semiconductor, bands flatten as can be seen in Figure 2.8.(Stevanovic & Yates, 2013)(Stevanovic et al., 2012) This causes photon accessible defects for e^-/H^+ pair recombination (Stevanovic et al., 2012).

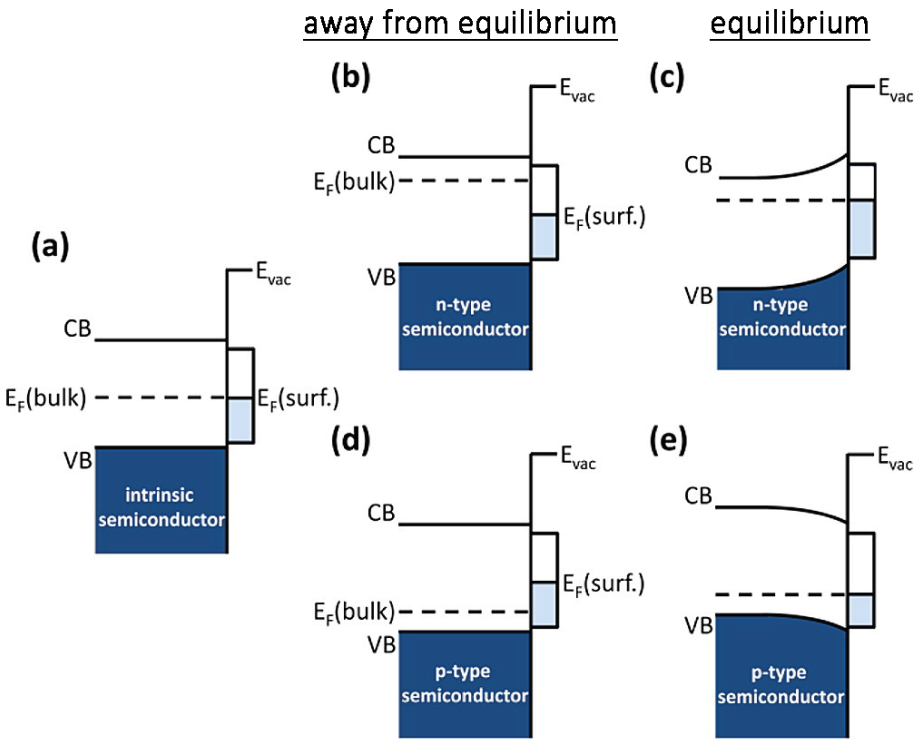

Figure 2.7: Schematics for band bending phenomena (a)flat band position (b)n-type semiconductor at away from equilibrium (c) n-type semiconductor at equilibrium with upward band-bending (d) p-type semiconductor at away from equilibrium (e) p-type semiconductor at equilibrium with downward band bending STM images of clean (Z. Zhang & Yates, 2012)

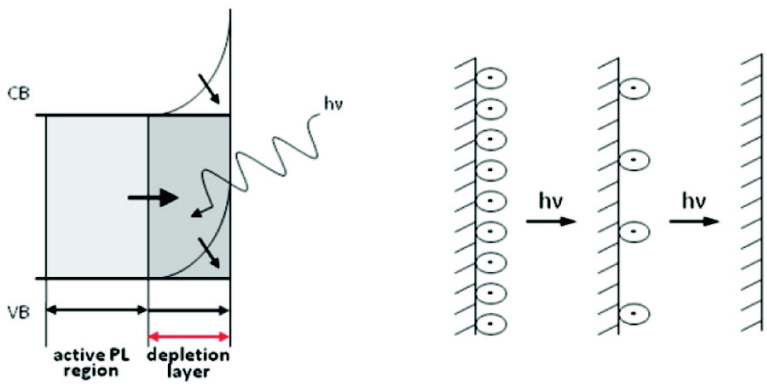

Figure 2.8: Schematics for downward band bending of n-type semiconductor with upward band bending upon illumination due to redistribution charges on surface(Stevanovic et al., 2012)

2.2.4 The effects of adsorption on TiO_2 surface

Adsorption of donor molecules like H_2O(Z. Zhang & Yates, 2012), NH_3(Stevanovic & Yates, 2012) and CO(Stevanovic & Yates, 2012) results in flattening of band for a n-type semiconductor due to formation of positively charged species on surface (Figure 2.9).

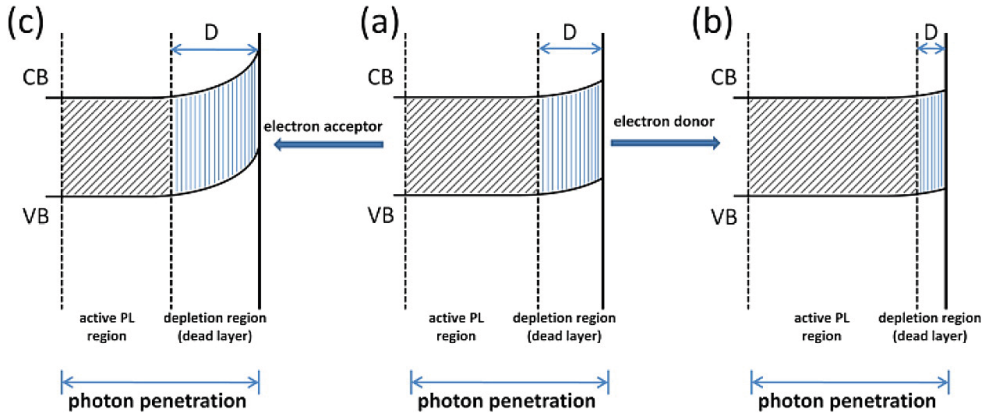

Figure 2.9: Schematics of band position shifting to (a) downward after exposure of an electron donor (b) upward after exposure of an electron acceptor for a n-type semiconductor with upward band bending (Z. Zhang & Yates, 2012)

This yields increase in recombination due to increase in photon accessible defects (Z. Zhang & Yates, 2012). However, if the surface is already illuminated then flat band shifts to downward band upon adsorption of donor molecules (Figure 2.10). This time, recombination lags because of spatially separated charges (Stevanovic et al., 2012).

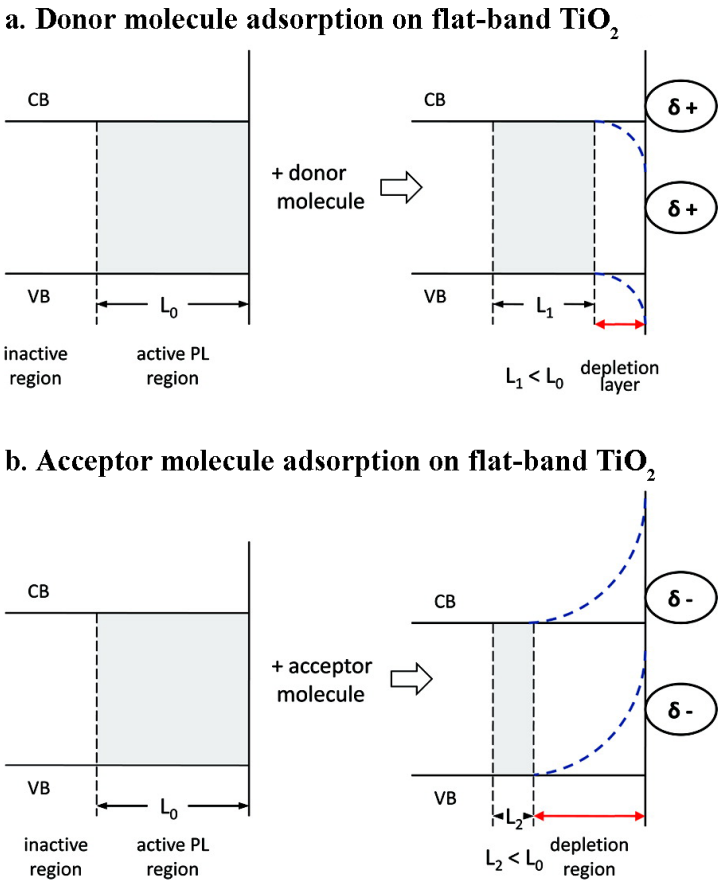

Figure 2.10: Schematics of band position shifting to (a) downward after exposure of an electron donor (b) upward after exposure of an electron acceptor for a n-type semiconductor with flat band bending (Stevanovic et al., 2012)

2.2.5 The effects of metal doping on semiconductor surface

Metal loading on metal oxide surface affects both photocatalytic and catalytic activity of the catalyst (Zhu et al., 2017)(references therein). Upon noble metal loading, surface properties of semiconductor changes. For example, for a n-type semiconductor like TiO_2, metal and semiconductor have different Fermi levels. If the work function of the metal is higher than the semiconductor, electrons from semiconductor flows to the metal until their Fermi levels are at equilibrium. Upward band bending occurs due to this electron transfer and a barrier is formed in the interface called Schottky barrier (Figure 2.11). This barrier can induce electron trapping yielding suppression of charge recombination. Besides, metal itself is a catalytic material and therefore, it enhances catalytic activity of the material (Linsebigler et al., 1995).

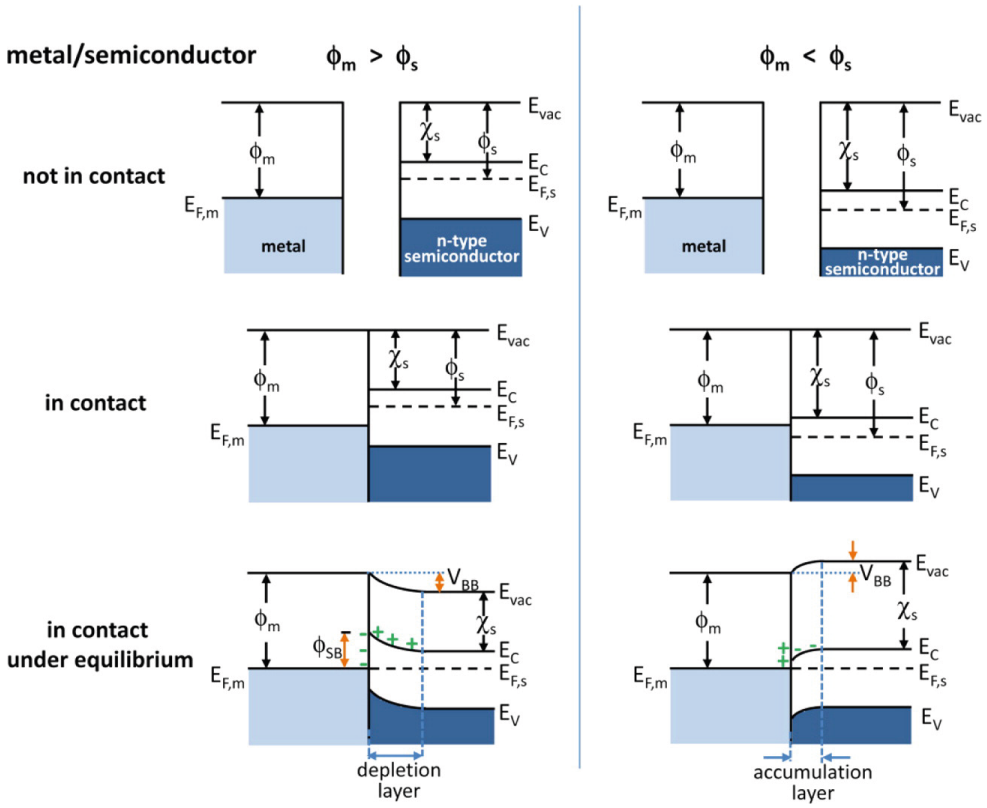

Figure 2.11: Formation of Schottky barrier at the metal/semiconductor interface for $\phi_M > \phi_S$ and $\phi_M < \phi_S$ conditions (Z. Zhang & Yates, 2012)

2.3 H_2O splitting on TiO_2 : H_2 source for reduction

One channel of artificial photosynthesis is water splitting in which water breaks into its molecules as hydrogen and oxygen. It is an uphill reaction ($H_2O \rightarrow H_2 + 1/2O_2$, ΔG^o_{rxn} = 228.57kJ/mol H_2O) but several hydrogen production processes have been developing since it is an attractive energy source with its advantageous properties like high energy efficiency. Unfortunately, many of these processes are either demand fossil fuel sources and tough operation conditions (i.e. steam reforming, coal gasification) or require further development to become economically feasible (i.e. biomass pyrolysis). Water splitting via solar energy utilization is one of the possible routes. Photocatalytic water splitting stands out among others with comparatively fewer problems on yield, scale up, and financial (Jafari et al., 2016). Photocatalytic water splitting method offers not only hydrogen production from renewable energy source but also mild operating conditions. Although, the photocatalytic water splitting processes need serious enhancements, it is an essential step considering mimick-

ing nature's photosynthesis.

TiO_2 has been utilizing in water splitting due to its above-mentioned properties (Jafari et al., 2016). Table2.5 shows hydrogen production rate via water splitting for bare TiO_2 in a gas-liquid-solid and gas-solid system. It can be seen that the amount of H_2 produced even after several hours is quite small. On an atomic level, H_2O adsorption behavior can differ from facet to facet for TiO_2 surface. Molecular adsorption vs. dissociative adsorption of H_2O is investigated by many. Dissociative water adsorption is very little or none on a defect free rutile TiO_2 (110) surface according to HREELS and TPD experiments (Henderson, 1996a). Water can dissociate on defects such as steps and vacancies where H_2O can bind to two Ti^{3+} around oxygen vacancy (Lu, Linsebigler, & Yates, 1994). On the other hand, rutile TiO_2 (100) surface is more active for water dissociation due to proximity of Ti^{4+} sites and bridging oxygen (O^{2-}) sites in (100) surface compared to (110) surface (Henderson, 1996b). For anatase surface, theoretical studies are usually carried out to investigate H_2O adsorption on a catalyst surface. For a defect free anatase surface (101), water adsorbs molecularly on Ti^{4+} and bridging O^{2-} sites (Tilocca & Selloni, 2004)(references therein) similar to rutile surface. Dissociation is possible in the presence of defects (Tilocca & Selloni, 2003). Different than rutile, defects form on subsurface of anatase (Cheng & Selloni, 2009) leading to more stable interaction of water with defects (Aschauer et al., 2010).

Table 2.5: H_2 production rate over TiO_2

Catalyst	Experimental conditions					Production rate ($\mu mol \cdot g^{-1}_{catalyst} \cdot h^{-1}$)	References
	T (°C)	P (bar)	I ($mW \cdot cm^{-2}$)	Flow rate	Additional information	H_2	
TiO_2 P25 suspended in water and ethanol	7	-	-	-	300 W Xe arc lamp (simulated solar light)	10.20	(Zhu, Liu, & Meng, 2014)
TiO_2 P25 suspended in water	-	-	40	-	250 W Hg lamp (UV light region)	1.20	(Tian et al., 2018)
TiO_2 powder	50	-	150	Saturated water vapor (T=50°C) in Ar with 2mL/min flow rate	500 W Hg lamp	6.10	(L. Zhang et al., 2017)
	85					8.70	
	100					9.10	
	150					12.00	

2.4 CO_2 reduction on TiO_2

CO_2 reduction to valuable organic chemicals with one or two carbons like CO, CH_4, CH_3OH, and C_2H_5OH is an attractive way to solve CO_2 and energy related problems (Li et al., 2016). CO_2 as the reactant and TiO_2 as the photocatalyst offer formation of profitable photocatalytic system; however, production yield is very low for industrial level operation even with material enhancement of the catalyst (Dilla, Schlögl, & Strunk, 2017)(Dilla, Mateblowski, et al., 2017). Additionally, apart from insufficiency of TiO_2 or any other photocatalyst for practical applications, CO_2 reduction is problematic due to lack of knowledge on reaction route (Dilla, Mateblowski, et al., 2017) and relatively stable nature of CO_2 itself (Freund & Roberts, 1996).

Adsorption of CO_2 on TiO_2 is the crucial step for photocatalytic CO_2 reduction (Acharya et al., 2011). Hence, atomic level investigation is provided by many to develop a better strategy for CO_2 reduction reaction (Acharya et al., 2011)(Mino et al., 2014). CO_2 can bind to TiO_2 surface in several geometries (Figure 2.12) usually observed by IR studies (Taifan, Boily, & Baltrusaitis, 2016). CO_2 can be physisorbed, chemisorbed or dissociate on a metal oxide surface. CO_2 can interact with adsorption sites like metal, oxygen or oxygen vacancies of the metal oxide. It can form physisorbed CO_2, chemisorbed CO_2^- or carbonate (CO_2^-). Direct dissociation of CO_2 to C or CO is unlikely(Burghaus, 2014). CO_2 adsorption on Ti^{4+} (Ti_{5f}) sites and oxygen vacancies on clean TiO_2 surface were monitored through TPD (Henderson, 1998)(Thompson, Diwald, & Yates, 2003) and STM (Acharya et al., 2011)(X. Lin, Wang, Lyubinetsky, Kay, & Dohnálek, 2013) experiments (Figure 2.13). Theoretical binding energy of CO_2 on defect free TiO_2 (110) surface was calculated as 65 kJ/mole, and reported as 48.5 kJ/mol experimentally. Difference is attributed to strong CO_2-CO_2 repulsion. The repulsion was not strong for TiO_2 surface with oxygen vacancies where the spatial separation of adsorbed CO_2 was suggested as the reason (Thompson et al., 2003)(references therein). The studies on TiO_2 (110) indicate that oxygen vacancies offer more stable adsorption sites than Ti^{4+} (Ti_{5f}) sites as shown by TPD experiments (Henderson, 1998). For a reduced surface where oxygen vacancies are dominant, CO_2 preferentially adsorbed on these sites. However, for a O_2 treated surface, CO_2 adsorbed on Ti^{4+} (Ti_{5f}) sites (Acharya et al., 2011)(Markovits, Fahmi,

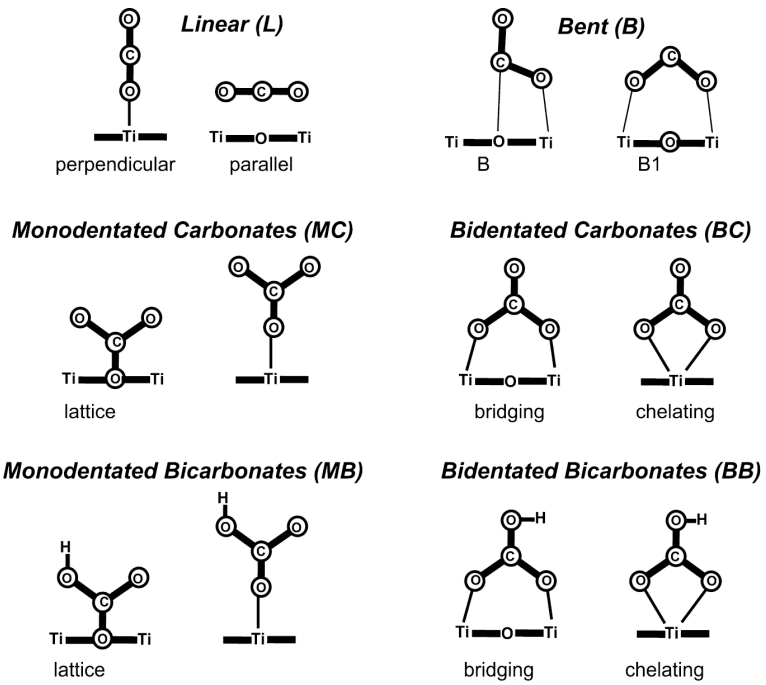

Figure 2.12: Possible CO_2 adsorption geometries on TiO_2 surface (Mino et al., 2014)

& Minot, 1996). Moreover, CO_2 is mobile on Ti^{4+} (Ti_{5f}) sites and can diffuse slowly between Ti^{4+} (Ti_{5f}) rows. Diffusion from vacancies is possible also (X. Lin et al., 2013)(Lee, Liao, Tsai, Huang, & Wu, 2013). However, diffusion of CO_2 between Ti^{4+} (Ti_{5f}) and vacancy sites is not observed implying these adsorption sites are spatially separated (Acharya et al., 2011). Diffusion rate of CO_2 between Ti^{4+} (Ti_{5f}) sites increases as coverage increases in line with CO_2-CO_2 repulsion forces (Acharya et al., 2011) where adsorbate-adsorbate interaction prevails (Markovits et al., 1996). No CO_2 dissociation to CO was detected and linear adsorption of CO_2 detected through HREELS (High resolution electron energy loss spectrometry) (Henderson, 1998).

Reported production rate results for photocatalytic CO_2 reduction with water in a gas-solid system can be seen in Table2.6. Similar to Table2.5 for H_2O splitting reaction, the rates are very low for CO_2 reduction with water also. Material enhancement is a key factor for enhanced rates and yet results are still away from industrial level production (Kondratenko et al., 2013). Aside from material enhancement, feeding strategy is critical. Henderson (1998) reported that upon dosing of CO_2 and H_2O one after another, a reaction does not take place. CO_2 adsorption blocked by H_2O or adsorbed CO_2 is displaced by H_2O. Only, dosing of CO_2 and H_2O together on TiO_2 with oxygen vacancies resulted in HCO_3^- formation. In addition, reactor design is

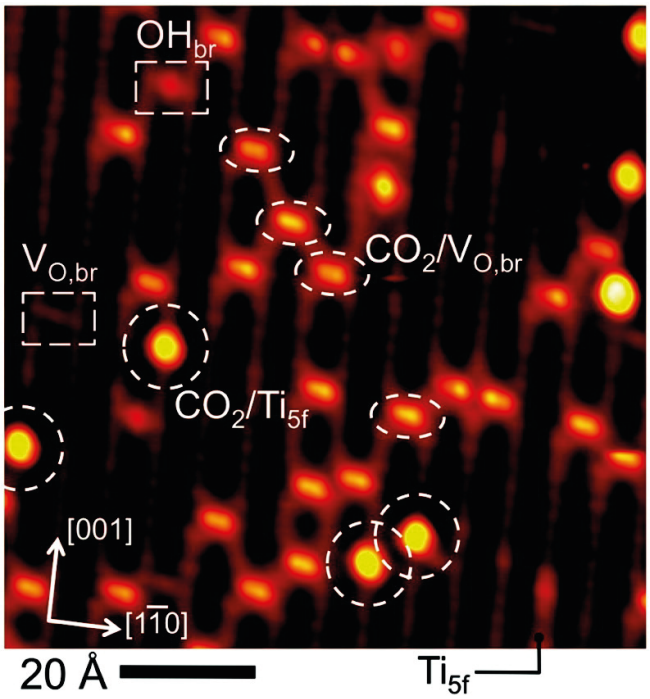

Figure 2.13: STM image of Possible CO_2 adsorption geometries on TiO_2 surface (Acharya et al., 2011)

strategic. Lee et al. (2013) designed a twin reactor to be able to spatially separate H_2O splitting and CO_2 reduction and claimed better catalytic performance. Enhanced CO_2 reduction rate are observed for photo-thermal processes under light source (concentrated) yielding elevated temperatures (Hoch et al., 2014). Similarly, Guan, Kida, Harada, Isayama, and Yoshida (2003) and Guan, Kida, and Yoshida (2003) used a combined catalyst (one of them is a photocatalyst) for photocatalytic H_2O splitting and CO_2 hydrogenation at elevated temperatures utilizing concentrated solar energy.

Table 2.6: CO and CH_4 production rate over TiO_2

Catalyst	Experimental conditions					Production rate ($\mu mol \cdot g^{-1}_{catalyst} \cdot h^{-1}$)		References
	T (°C)	P (bar)	I ($mW \cdot cm^{-2}$)	Flow rate	Additional information	CO	CH_4	
TiO_2 P25 powder	-	1.50	755.0	15000 ppm CO_2 in He 6000 ppm H_2O	Calcination @400°C for 3 h 10 W 365 nm LED	-	0.78	(Dilla et al., 2019)
TiO_2 P25 powder	-	-	180.0	7000 ppm CO_2 in He (1700 nmol/min) 100 ppm H_2O (24 nmol/min)	Calcination @400°C for 3 h 200 W Hg/Xe lamp (UV+Visible light region)	-	0.09	(Dilla, Mateblowski, et al., 2017)
TiO_2 P25 thin film	-	-	-	CO_2 and H_2O vapor mixture formed by reaction of $NaHCO_3$ (0.12 g) and HCl aqueous solution (0.25 mL, 4M),	300 W simulated solar Xe arc lamp	-	0.38	(Yu, Low, Xiao, Zhou, & Jaroniec, 2014)
TiO_2 powder	20	0.71	20.5	P_{H_2O}=0.023 bar (T=20°C)	300 W Xe lamp (UV light region)	0.64	0.22	(Xiong et al., 2017)
TiO_2 powder	100	1.20	40 .0	P_{H_2O}=0.042 bar P_{CO_2}=0.02 bar	500 W Hg lamp (365nm)	31.00	46.00	(Tahir & Amin, 2015)

CHAPTER 3

MATERIALS AND METHODS

3.1 Materials

TiO_2 P25 (Aeroxide®) was used mainly in the experiments. The properties of commercial TiO_2 and details of BET analysis are given in Appendix A.

Pd/TiO_2 samples with three different metal loadings (0.5%, 1.0% and 2.0% (w/w)) were prepared by incipient wetness impregnation method using palladium(II)nitrate solution ($Pd(NO_3)_2.xH_2O$) and TiO_2 P25 (Aeroxide®) as support. Calculation for intended metal loadings can be seen in Appendix B. Moreover, ICP-OES (Perkin Elmer Optima 4300DV) analysis was done to measure actual palladium loadings. Comparison of intended and reported palladium loadings by ICP-OES is given in Table 3.1.

Table 3.1: Comparison of intended palladium loadings and reported palladium loading by ICP-OES analysis

	Intended palladium loadings (%)	Palladium loadings reported by ICP-OES analysis (%)
1	0.5	0.77
2	1.0	1.50
3	2.0	2.80

γ-Al_2O_3 (AlfaAesar) was used for comparison with CO_2 adsorption isotherm over TiO_2 P25. BET analysis of γ-Al_2O_3 is given in Appendix A.

Lastly, ZnO and Fe_2O_3 were used during direct heat measurements via microcalorimeter for comparison with TiO_2 P25.

3.2 Experimental set-up

3.2.1 Volumetric chemisorption manifolds

Experiments were done with two home-built volumetric chemisorption manifolds mainly. Ace glass stopcocks were placed as gas inlet-outlet valves and sample cell valve. One of the manifold was connected to a Setaram C80 microcalorimeter (Figure 3.1). The other manifold has space to illuminate sample cell via 100W UV lamp (Blak-Ray B-100A 365nm)(Figure 3.2). Gas pressure was monitored by a pressure gauge (MKS Baratron Capacitance Manometer) and a digital reader (MKS PR4000B). A turbomolecular vacuum pump station (Pfeiffer HiCube 80 Eco) was used to empty the gas inside the manifold up to 10^{-5} Torr before each experiments.

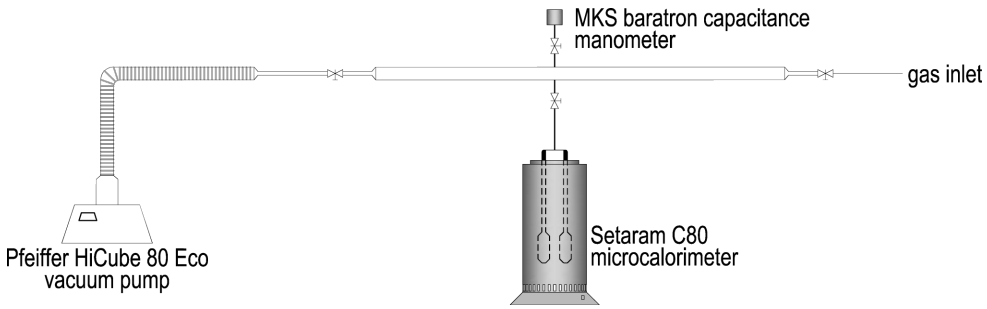

Figure 3.1: Chemisorption manifold connected to a microcalorimeter

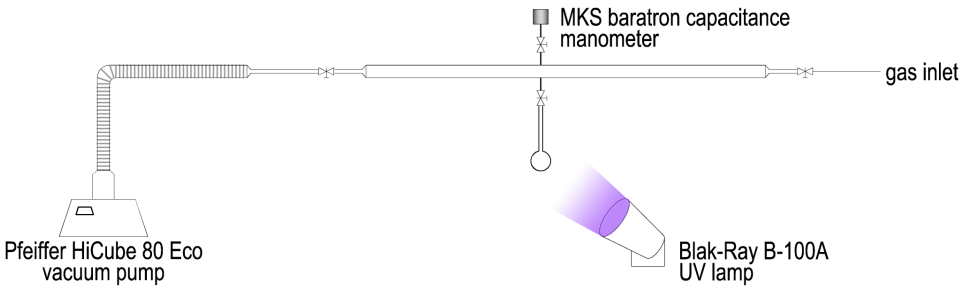

Figure 3.2: Chemisorption manifold with UV illumination source

3.2.2 Configurations with microcalorimeter and light source

Four different configurations were arranged with microcalorimeter and different light sources as can be seen in Figure 3.3(a-d).

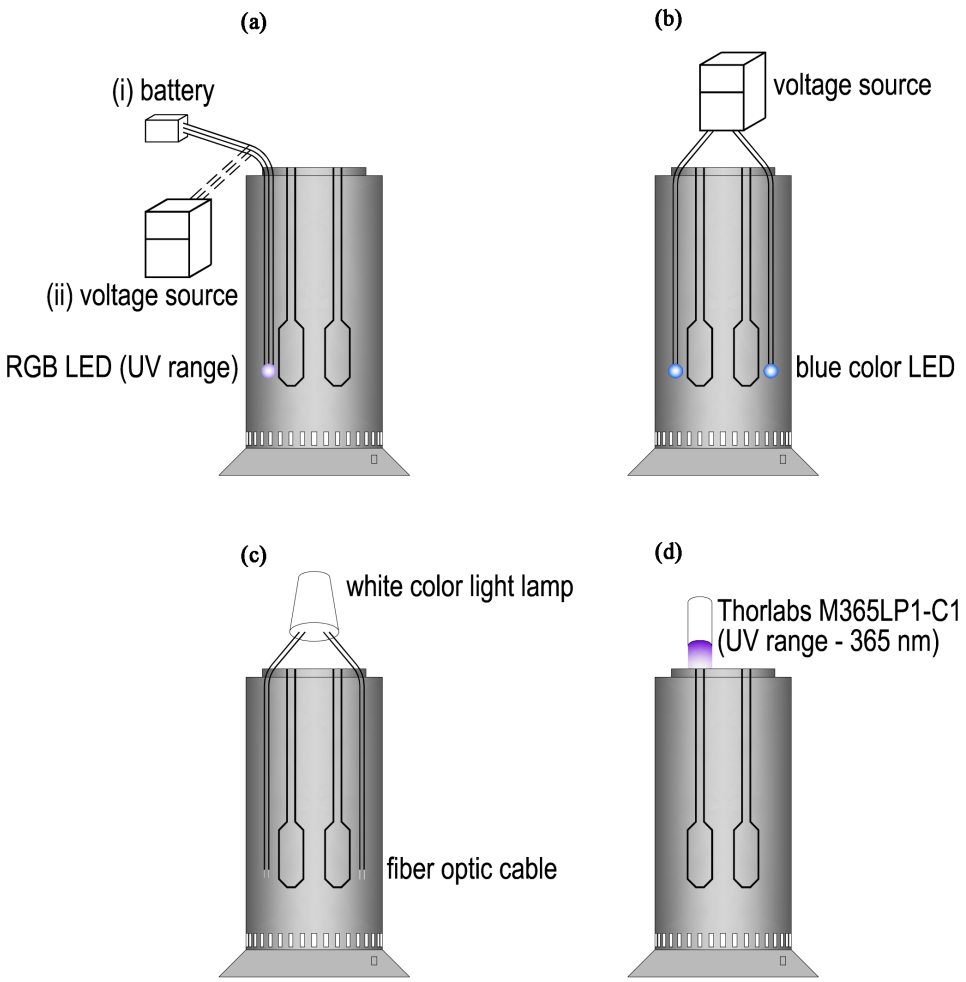

Figure 3.3: Light source and microcalorimeter arrangements (a) RGB LED in UV range connected to (i) a battery (ii) a voltage source (b) Blue color LEDS connected to a voltage source (c) Fiber optice cables connected to a white light lamp (d) Thorlabs M365LP1-C1 LED lamp illuminates the microcalorimeter cavity in UV range (365nm)

3.2.3 TPR set-up

Micromeritics Chemisorb 2720 equipment was used for H_2 reduction over Pd/TiO_2 sample via temperature programmed reduction. The samples were placed in U-shaped quartz reactor where adsorption or desorption signal was obtained by a thermal conductivity detector (TCD) connected to the system. He was used as carrier gas. 10% H_2-Ar gas was used for reduction. The samples were heated to 900°C with 5°C/min heating rate. The experiment was conducted at atmospheric pressure.

3.2.4 TEM and HRTEM analysis

TEM and high-resolution TEM (HRTEM) images were obtained via Jem Jeol 2100F 200kV HRTEM equipment with FEG electron gun.

3.3 Experimental procedure for adsorption studies in the manifold

Adsorption isotherms were obtained according to manual given in Appendix C. Collected data (equilibrium pressure) was interpreted into the amount of adsorbed gas parameter by assuming validity of ideal gas law at experimental conditions.

3.4 Experiment parameters for adsorption studies in the manifold

Adsorption isotherms were obtained at several different conditions with different experiment sequels. Experiment parameters are tabulated for the experiments with TiO_2 P25, Pd/TiO_2 and γ-Al_2O_3 as can be seen in Appendix D.

CHAPTER 4

RESULTS AND DISCUSSION

4.1 A brief discussion on artificial photosynthesis

Artificial photosynthesis is the general terminology used for chemical synthesis performed using CO_2 and H_2O to produce hydrocarbons under illumination. The reaction involves direct interaction of the relevant molecules on the surface. The highly endothermic nature of the direct chemical conversion of CO_2 and H_2O is the major bottleneck. Gibbs free energies of the selected reactions are given in Table 4.1 where the reactions are not spontaneous apparently. In the same table, the crossover temperatures, the lowest temperature at which the Gibbs free energy of the reaction is equal to zero ($T_{crossover}=\Delta H/\Delta S$) are given. Very high crossover temperatures indicate that CO_2 reduction with H_2O is not feasible at all. Only with H_2 as a reducing agent, CO_2 reduction path becomes favorable ($\Delta G^o_{rxn}<0$) for methane and formic acid formation where the crossover temperature is still high for carbon monoxide formation (Table 4.2). Hence, current approaches towards realization of artificial photosynthesis need to be reassessed.

Table 4.1: Comparison of ΔH^o_{rxn}, ΔG^o_{rxn}, ΔS^o_{rxn} and $T_{crossover}$ of CO_2 reduction with H_2O for gas phase reaction (Data taken from Koretsky (2013) and NIST (2018))

No	Reaction	ΔH^o_{rxn} (kJ/mol CO_2)	ΔG^o_{rxn} (kJ/mol CO_2)	ΔS^o_{rxn} (kJ/mol $CO_2 \cdot K$)	$T_{crossover}$ (K)
1	$CO_2 + 2H_2O \rightarrow CH_4 + 2O_2$	802.34	800.78	$5.23 \cdot 10^{-3}$	153411
2	$CO_2 \rightarrow CO + 0.5O_2$	282.98	257.19	0.09	3144
3	$CO_2 + H_2O \rightarrow HCOOH + 0.5O_2$	256.73	170.22	0.29	885

Table 4.2: ΔH^o_{rxn}, ΔG^o_{rxn}, ΔS^o_{rxn} and $T_{crossover}$ of CO_2 reduction with H_2 for gas phase reaction (Data taken from Koretsky (2013) and NIST (2018))

No	Reaction	ΔH^o_{rxn} (kJ/mol CO_2)	ΔG^o_{rxn} (kJ/mol CO_2)	ΔS^o_{rxn} (kJ/mol $CO_2 \cdot K$)	$T_{crossover}$ (K)
1	$CO_2 + 4H_2 \rightarrow CH_4 + 2H_2O$	-164.94	-113.50	-0.11	Spontaneous
2	$CO_2 + H_2 \rightarrow CO + H_2O$	41.16	28.62	0.04	1029
3	$CO_2 + H_2 \rightarrow HCOOH$	14.91	-58.35	0.25	Spontaneous

4.2 CO_2 adsorption isotherms on TiO_2 P25

4.2.1 Adsorption isotherms obtained in dark by utilizing microcalorimeter

Three consecutive CO_2 adsorption experiments were conducted at 50°C in dark. At first, CO_2 adsorption isotherm on fresh TiO_2 P25 was obtained. Then, the system was heated to 220°C during the evacuation and the second adsorption isotherm was obtained after the system was cooled down to 50°C. Lastly, the system was heated to 250°C during the evacuation and the third adsorption isotherm was obtained after the system was cooled down to 50°C again. Adsorption isotherms are given in Figure 4.1. 40 µmol/$g_{catalyst}$ CO_2 adsorbed on surface at 50°C in dark. Adsorbed amount was increased to ∼102 µmol/$g_{catalyst}$ on average after the heat treatments. Increase in the adsorption amount can be related to removal of contamination from the surface after the heat treatments. Carbon impurities on surface may reacted with CO_2 yielding decomposition of C residues (Yang, Yu, van der Linden, Wu, & Mul, 2010). Indeed, presence of carboxylic acids on TiO_2 surface due to adsorption from air was noticed in a recent study published in Science (Balajka et al., 2018).

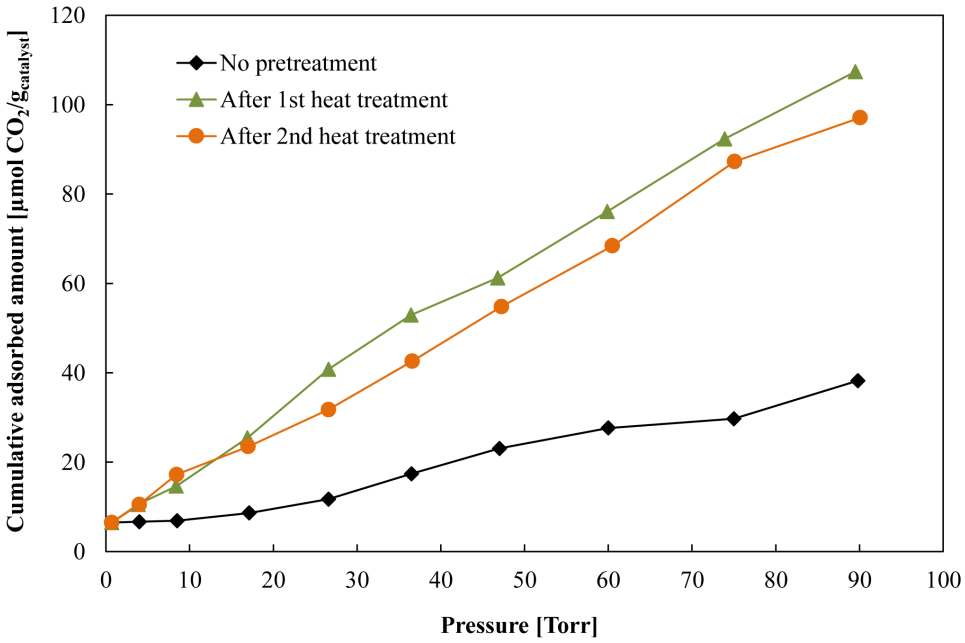

Figure 4.1: CO_2 adsorption isotherms on fresh and heat treated TiO_2 P25 obtained in dark at 50°C

Change of differential heat of adsorption values with respect to cumulative adsorbed

amounts curves are given in Figure 4.2. Differential heat of adsorption values for the adsorption isotherm on fresh TiO_2 surface show a very high initial heat of adsorption values indicating a different surface event which is the interaction or exchange of CO_2 with the surface contamination, possibly. On the other hand, differential heat of adsorption values for the adsorption isotherms obtained after the heat treatments look very similar to each other with relatively low values. It can be clearly seen that after 40 μmol/$g_{catalyst}$, differential heat of adsorption values for the second and third adsorption isotherms stay around 25 kJ/mole corresponding to heat of condensation of CO_2. This means one CO_2 adsorbs on another instead of other available sites on catalyst surface. 40 μmol/$g_{catalyst}$ corresponds to 5% of reported BET surface area indicating weak adsorption of CO_2 and low surface coverage in line with literature (Linsebigler et al., 1995).

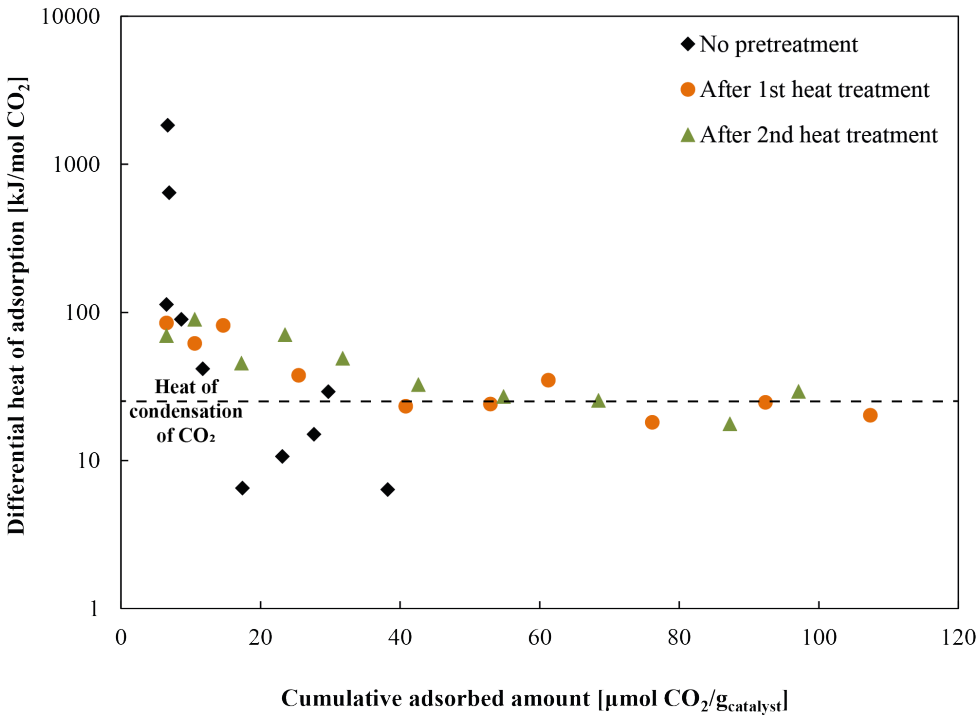

Figure 4.2: Differential heat of adsorption values in logarithmic scale with respect to cumulative adsorbed amount of CO_2 on fresh and heat treated TiO_2 P25 in dark at 50°C

Moreover, Figure 4.3 shows CO_2 adsorption isotherm on a H_2 pretreated TiO_2 P25 at 50°C in dark where pressure was as high as atmospheric pressure. Adsorption isotherm started with negative values indicating desorption at the beginning. This is related with adsorbed H_2 that could not be removed during the evacuation period.

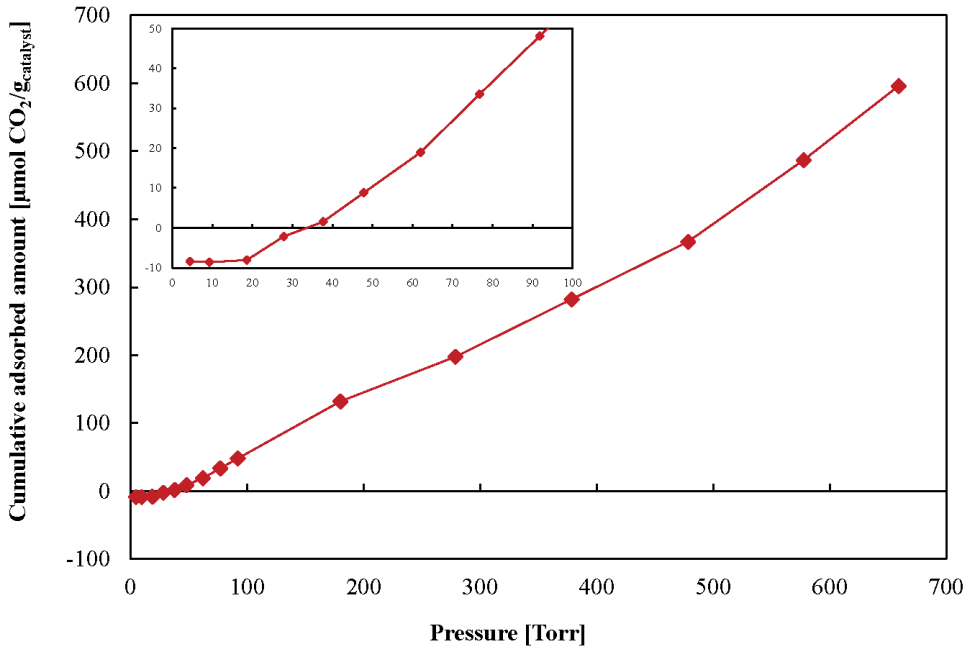

Figure 4.3: CO_2 adsorption isotherm on H_2 pretreated TiO_2 P25 surface obtained in dark at 50°C

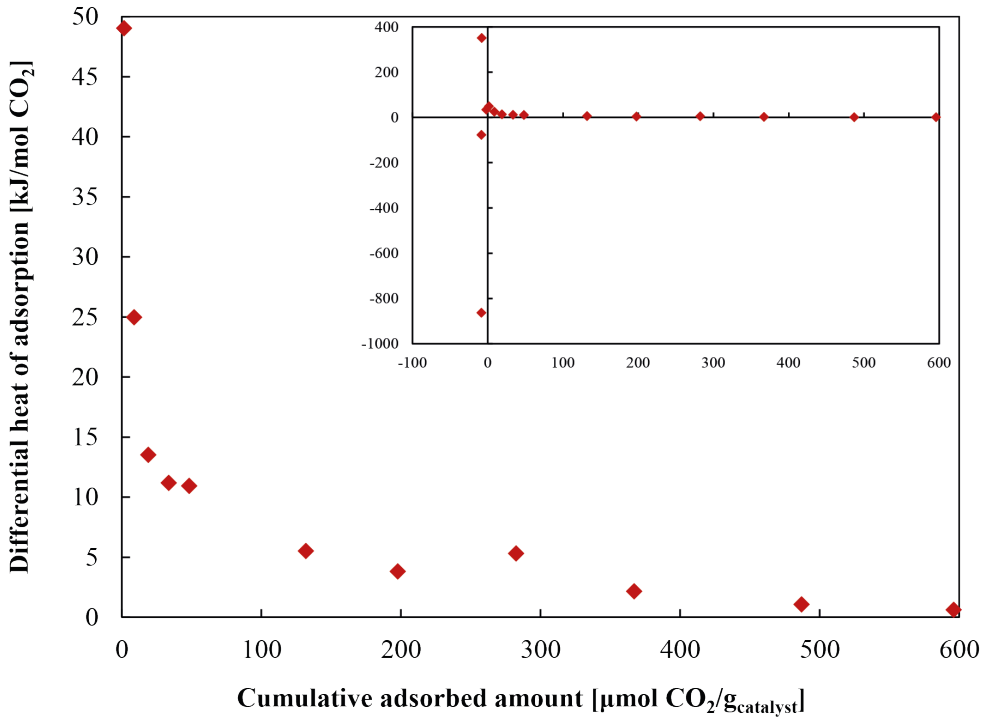

Figure 4.4: Differential heat of adsorption values with respect to cumulative adsorbed amount of CO_2 on H_2 pretreated TiO_2 P25 obtained in dark at 50°C

Furthermore, negative differential heat of adsorption values at the beginning are due to observed desorption at the beginning (Figure 4.4). This behavior emphasizes the

importance of surface cleanliness one more time to obtain reliable results. Besides, only 600 μmol/$g_{catalyst}$ CO_2 adsorbed on surface at atmospheric pressure. During the adsorption, differential heat of adsorption values dropped to very low values (5-15 kJ/mol) suggesting weak interaction of CO_2 with the surface.

4.2.2 CO_2 adsorption isotherms with and without illumination

After concluding weak adsorption of CO_2 on TiO_2 surface, the effect of illumination on adsorption isotherm was investigated. At first, CO_2 adsorption isotherm on fresh TiO_2 P25 was obtained at room temperature, then under UV light after evacuation consecutively (Figure 4.5). Only 55 μmol/$g_{catalyst}$ CO_2 adsorbed in dark at room temperature at equilibrium pressure (∼93 Torr) on fresh TiO_2. Negative values (-50 μmol/$g_{catalyst}$ at ∼93 Torr equilibrium pressure) were obtained under UV illumination at room temperature indicating desorption of CO_2 molecules from the surface. CO_2 might interacted with impurities on the surface as deduced before; hence, the same experiment was repeated three times in a cyclic manner on clean TiO_2 P25 surface (catalyst was pretreated with O_2 under UV illumination for 30 minutes) (Figure 4.6(a)).

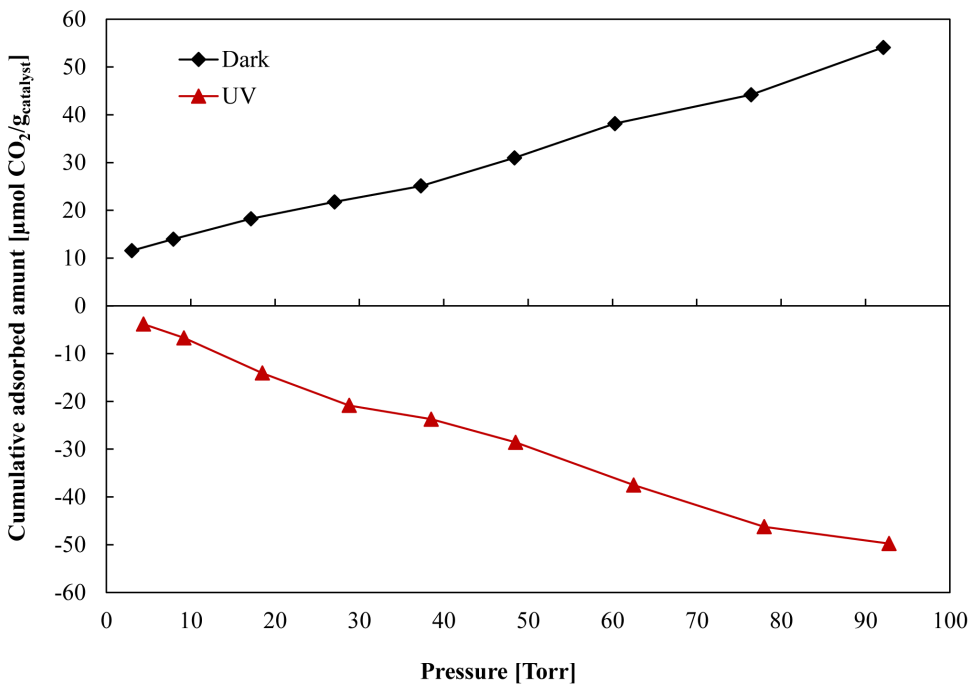

Figure 4.5: CO_2 adsorption isotherms on fresh TiO_2 P25 obtained in dark and under UV illumination consecutively at room temperature

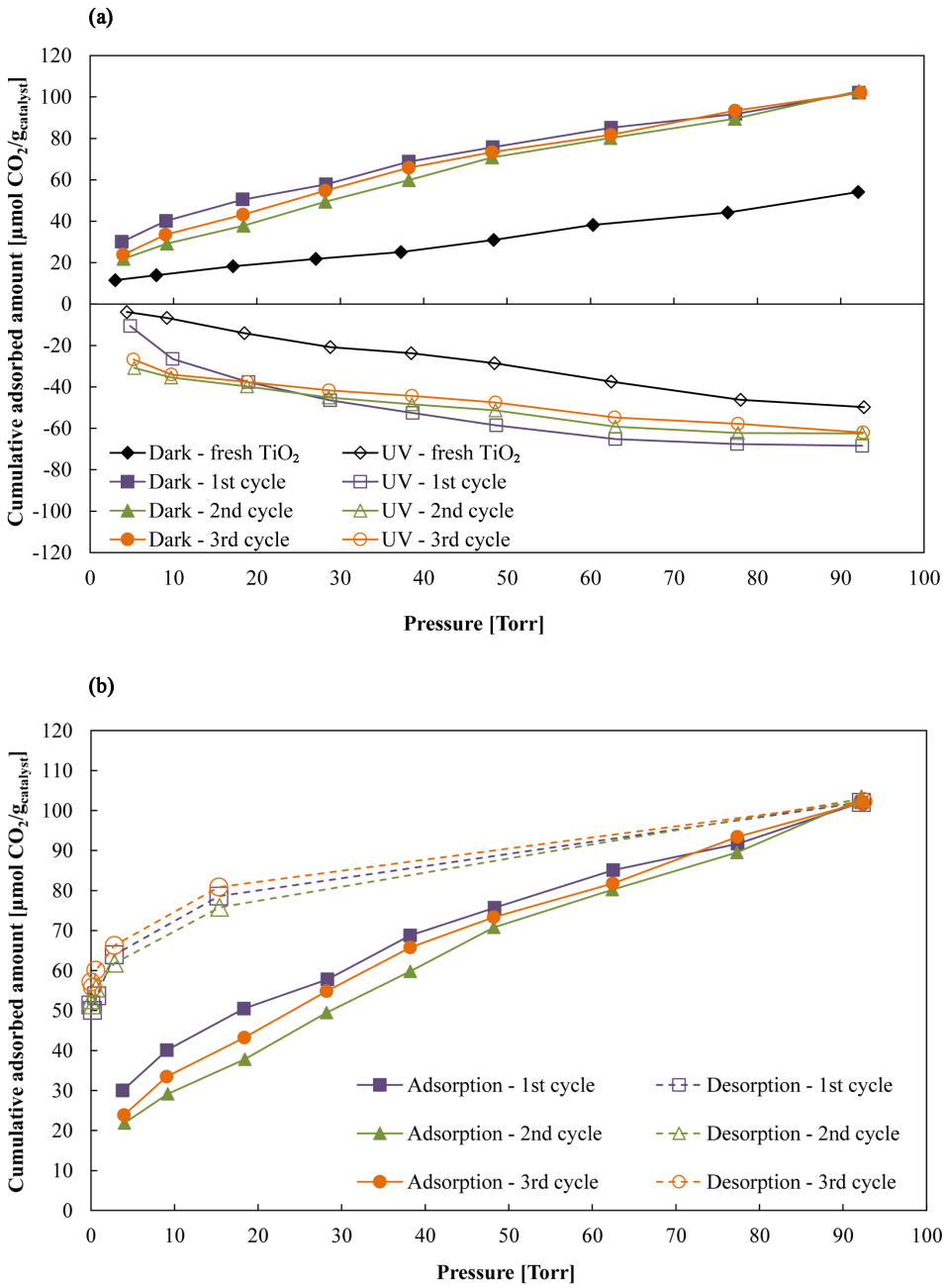

Figure 4.6: (a) CO_2 adsorption isotherms on fresh and pretreated TiO_2 P25 in dark and under UV illumination at room temperature (b) Desorption isotherms obtained on pretreated TiO_2 P25 in dark at room temperature

Adsorbed amount increased twofold and reached to 102 µmol $CO_2/g_{catalyst}$ in dark suggesting cleaner surface. The behavior under UV illumination remained even with clean surface. Only, desorption amount observed under UV illumination increased to -66 µmol/$g_{catalyst}$ on average. Hence, the behavior under illumination is not related to impurities on the TiO_2 surface. Another point worth mentinoning is for the cycling

experiments, desorption isotherms were also obtained (Figure 4.6(b)). Intercept of desorption isotherms with y-axis is determined as 50 µmol $CO_2/g_{catalyst}$. This result is in line with microcalorimeter results where 50 µmol $CO_2/g_{catalyst}$ can be considered as the amount of strongly bound molecules on TiO_2. It was already mentioned in the literature review that CO_2 can be adsorbed on either oxygen vacancy sites or Ti^{4+}. These sites are actually the weak Lewis acid base sites of the TiO_2 (Mino, Cesano, Scarano, Spoto, & Martra, 2019)(Martra, 2000). Since, CO_2 is able to adsorbed on only these sites, the amount of CO_2 adsorption amount can be considered as an indirect indication of the oxygen vacancy concentration of the TiO_2 surface.

CO_2 adsorption on a similar surface (commercial γ-Al_2O_3) was investigated to evaluate reliability of the measurements. Lewis acid base sites of γ-Al_2O_3 are also known (Lahousse, Maugé, Bachelier, & Lavalley, 1995). CO_2 adsorption isotherms were found similar for both of the surfaces. 125 µmol $CO_2/g_{catalyst}$ adsorbed on γ-Al_2O_3 and 100 µmol $CO_2/g_{catalyst}$ adsorbed on TiO_2 P25. Interception of desorption isotherm of γ-Al_2O_3 with y-axis is around 25 µmol $CO_2/g_{catalyst}$ but it is around 50 µmol $CO_2/g_{catalyst}$ for TiO_2 P25.

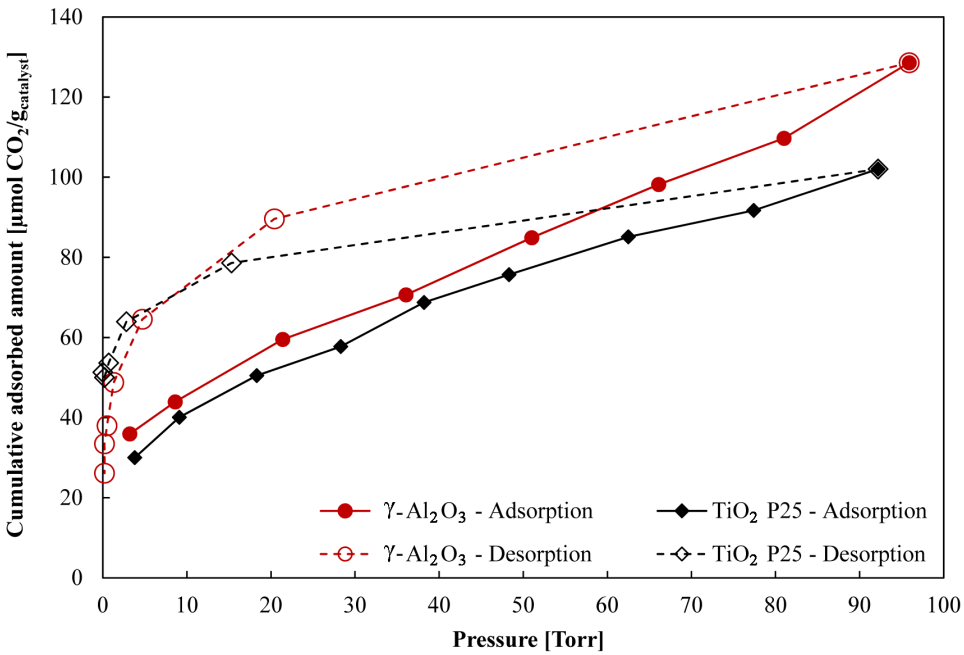

Figure 4.7: CO_2 adsorption isotherms on fresh γ-Al_2O_3 and clean TiO_2 P25 surfaces in dark at room temperature

Moreover, reliability of the measurements is provided by literature (Ras et al., 2013)

(Figure 4.8). Adsorption isotherm was obtained at 40°C in literature data. Since adsorption is an exothermic process, the adsorbed amounts decrease as the temperature increases. Hence, adsorption isotherm is slightly below the adsorption isotherm obtained in this study at room temperature.

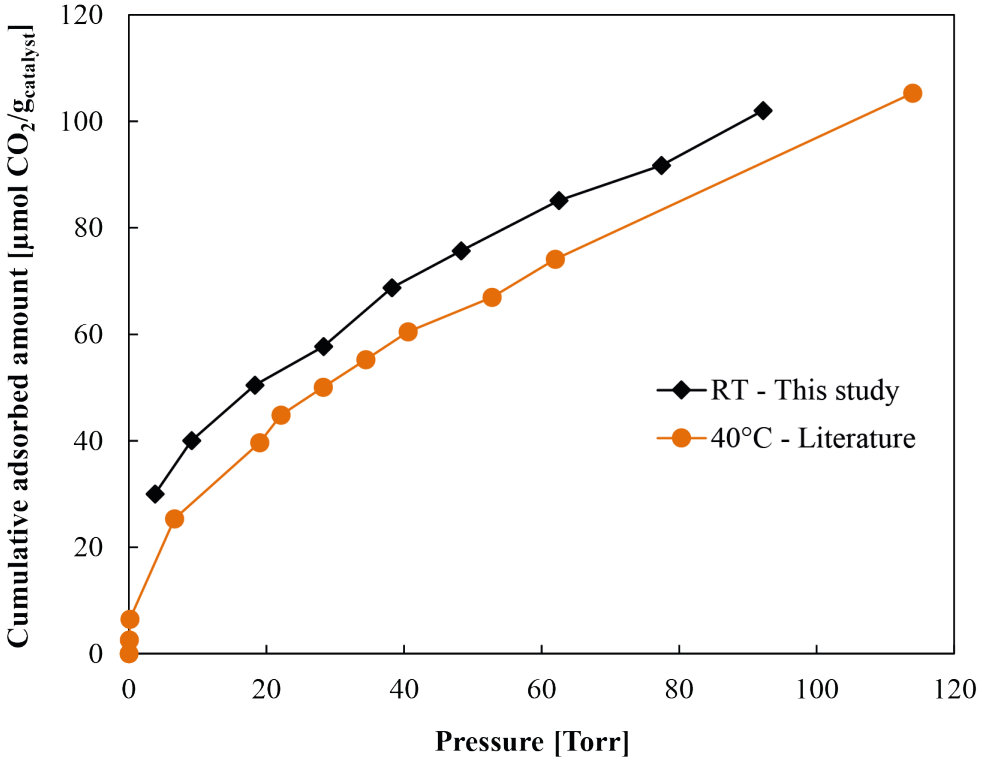

Figure 4.8: Comparison of CO_2 adsorption isotherm on clean TiO_2 P25 surface with literature data (Ras et al., 2013)

Finally, CO_2 measurements are assured to be reliable. The observed desorption under illumination during CO_2 adsorption on TiO_2 is not due to removal of impurities since the surface was clean. The heating of catalyst bulk due to the heating of ambient with the light source (Appendix E) cannot also result in observed desorption. However, local temperature rise due to heat release upon charge recombination can justify the observed behaviour under UV illumination. Assuming only the gas in the sample cell was heated, calculation on adsorption amount under UV illumination was repeated where details can be found in Appendix F. When the adjusted cell temperature was 160°C, a reasonable isotherm is obtained (adsorption isotherm is in the positive side of the graph). The adjusted isotherm is similar to adsorption isotherm in dark which can be considered as a reference, an isotherm that is shown reliable (Figure 4.9). Hence, the evidences indicate local temperature rise upon charge recombination is

present under illumination. This temperature rise have affected the chemistry in such a way that heating of gas in cell to 160°C would have affected it.

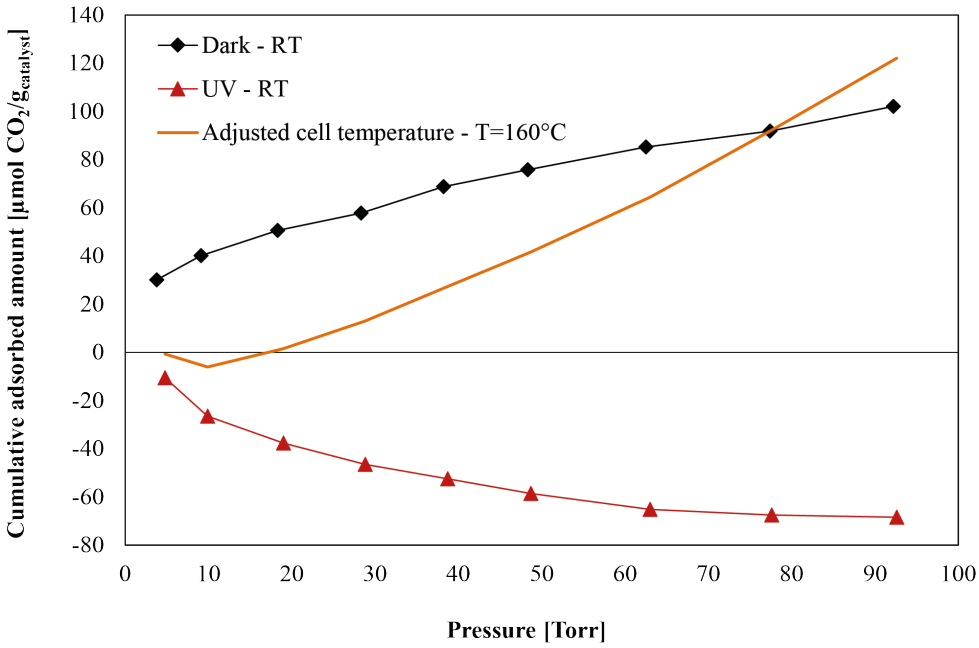

Figure 4.9: CO_2 adsorption isotherms on clean TiO_2 P25 in dark, under UV illumination at room temperature and adsorption isotherm obtained according to adjusted cell temperatures under UV illumination

4.3 H_2O adsorption isotherms on TiO_2 P25

4.3.1 H_2O adsorption isotherms with and without illumination

At first, H_2O adsorption isotherm obtained on TiO_2 P25 in dark at room temperature. Desorption isotherm was also obtained just after adsorption experiment finished. After the evacuation for an overnight, adsorption isotherm was obtained under UV illumination at room temperature (Figure 4.10(a)). Before the experiments, the surface was exposed to CO_2 and evacuated for a long period. Thus, the surface was considered clean. The experiments were repeated with clean surface where pretreatment was done with O_2 under UV illumination for 30 minutes. Adsorption isotherms in the first set of experiment and the repeated ones coincide with each other assuring clean surface during the experiments.

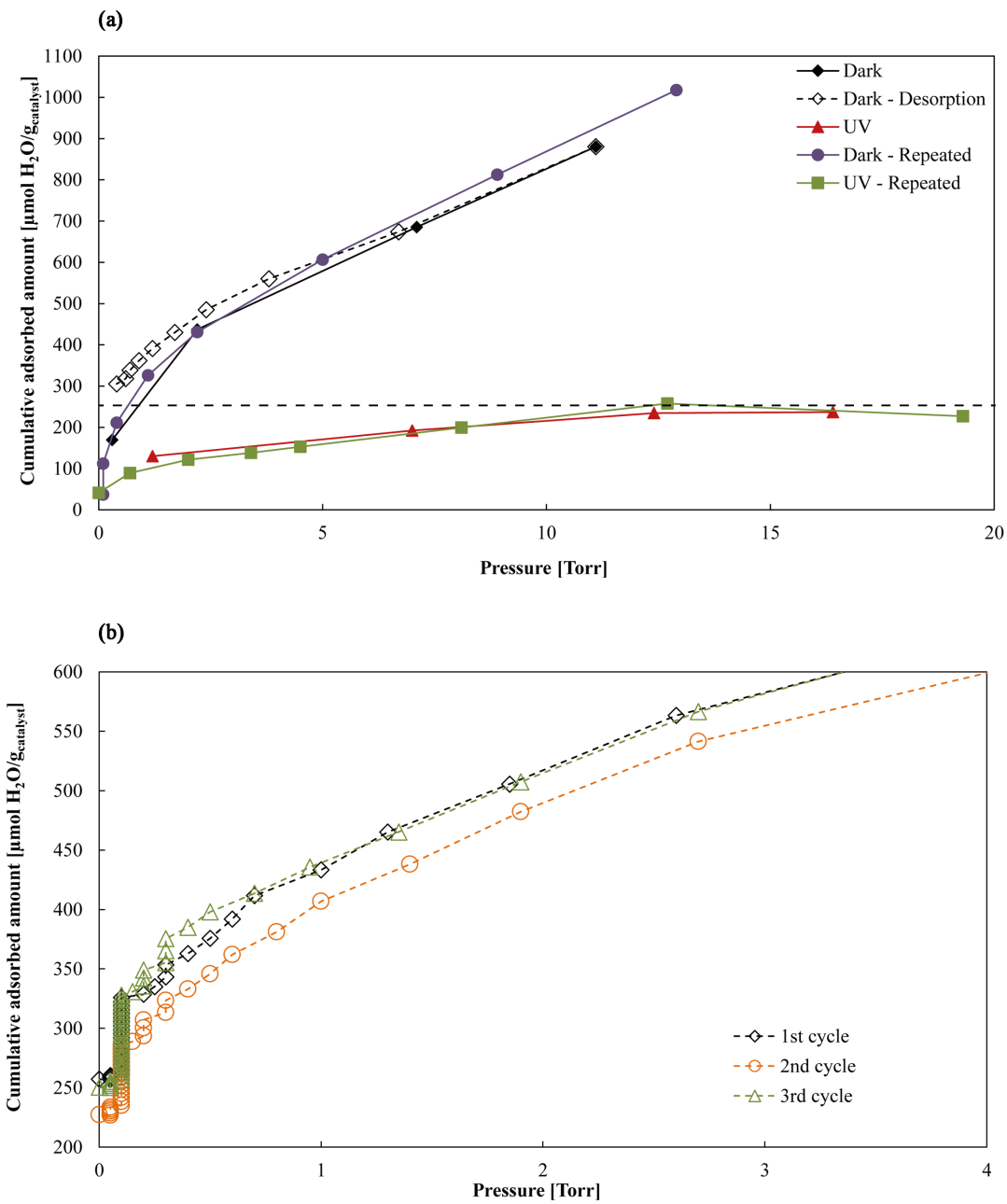

Figure 4.10: (a) H_2O adsorption isotherms on TiO_2 P25 at room temperature (the surface was exposed to CO_2 at first and long evacuation period later) (b) Desorption isotherms on TiO_2 P25 at room temperature - Close look

880 μmol $H_2O/g_{catalyst}$ adsorbed in dark and around 240 μmol $H_2O/g_{catalyst}$ adsorbed under UV illumination at the same equilibrium pressure, ∼11 Torr. A substantial decrease in the adsorption amount, 640 μmol $H_2O/g_{catalyst}$, was observed for the illuminated case where isotherm look like a Langmuir type of adsorption isotherm. Desorption isotherm obtained after H_2O adsorption in dark intercepts y-axis around

250 μmol/$g_{catalyst}$. This amount is pretty much at the same level with H_2O saturation amount under UV illumination.

Another set of experiment where H_2O adsorption and desorption isotherms were obtained on a clean TiO_2 surface in a cycling manner in dark at room temperature is also consistent with the previous H_2O experiments. Desorption isotherms obtained in the cyclic experiments (Figure 4.10(b)) intercept y-axis around 250 μmol $H_2O/g_{catalyst}$ also. This amount can be considered as the amount of strongly bound H_2O molecules on TiO_2 surface.

4.3.2 H_2O adsorption isotherms at elevated temperatures

Strong adsorption capacity (multilayer adsorption) of H_2O on TiO_2 surface is known (Yamamoto et al., 2008). Hence, we were able to carry out H_2O adsorption experiments on TiO_2 P25 surface in dark at elevated temperatures (50, 100 and 150°C) with the chemisorption set-up connected to the microcalorimeter. Comparison of adsorption isotherms with the previous ones executed at room temperature are given in Figure 4.11. Since adsorption is an exothermic process, the adsorbed amounts decreased as the temperature of sample cell increased as expected. The adsorption isotherm obtained in dark at 150°C is almost identical to adsorption isotherm obtained under UV illumination at room temperature.

Differential heat of adsorption values for the experiments performed at elevated temperatures are given in Figure 4.12. For adsorption isotherm at 150°C, differential heat of adsorption values decreased to ∼40 kJ/mol (heat of condensation value of water) at saturation point of the surface (250 μmol $H_2O/g_{catalyst}$) indicating monolayer capacity. For the other two adsorption isotherms at 50°C and 100°C, differential heat of adsorption values stay around 40 kJ/mol after 250 μmol $H_2O/g_{catalyst}$ adsorbed amount implying multilayer formation. Lastly, H_2O adsorption isotherm data at room temperature, 50, 100, 150°C were fitted to Temkin isotherm in agreement with strong adsorption of water on heterogeneous surface (Appendix H).

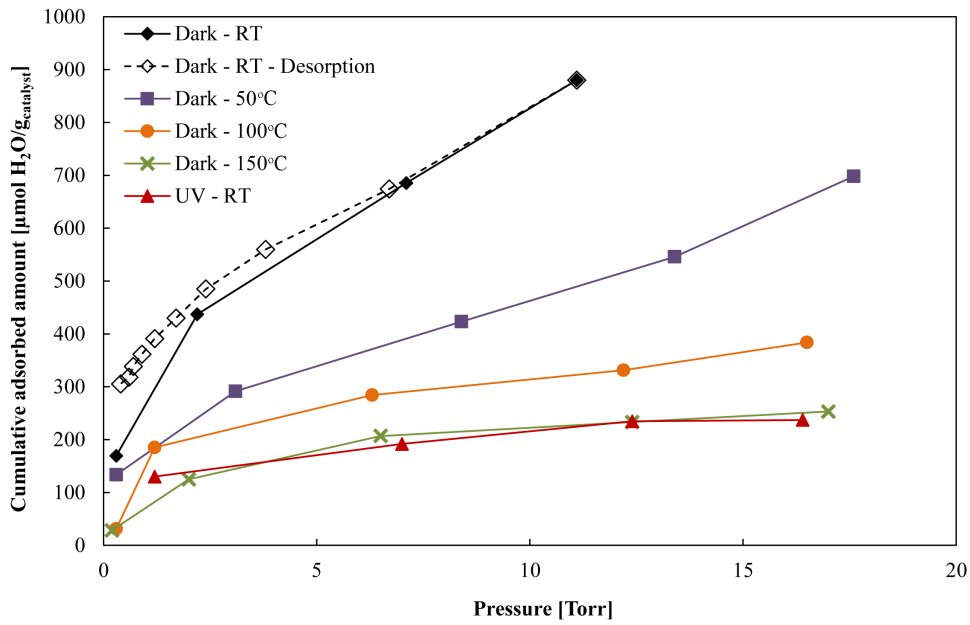

Figure 4.11: H_2O adsorption isotherms on fresh TiO_2 P25 obtained in dark at room temperature, 50, 100 and 150°C and under UV illumination at room temperature

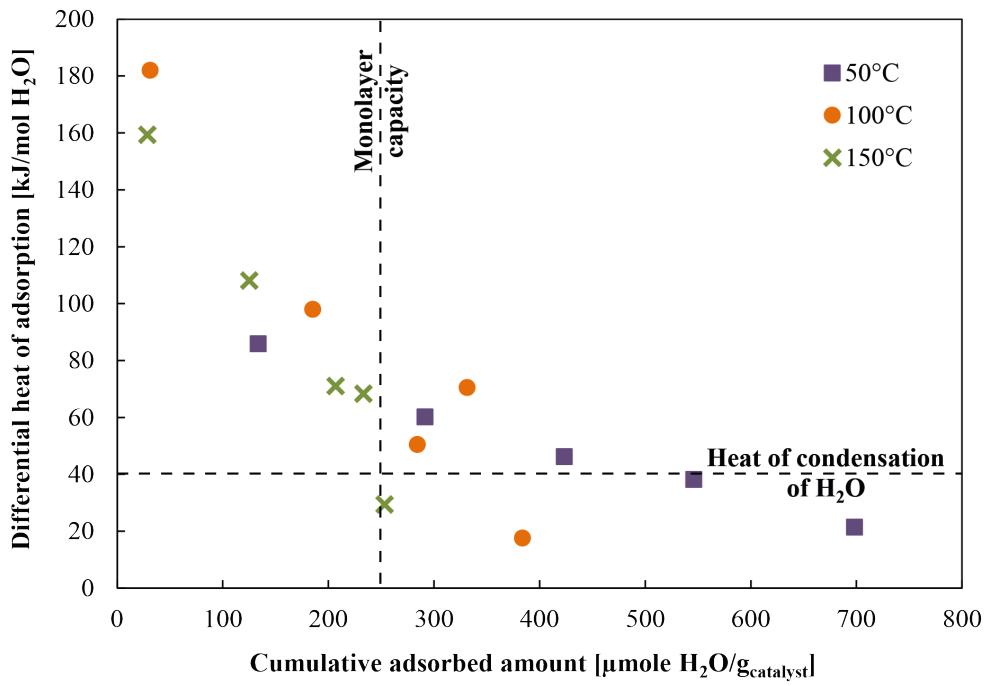

Figure 4.12: Differential heat of adsorption values for H_2O adsorption isotherms on fresh TiO_2 P25 obtained in dark 50, 100 and 150°C

4.3.3 Total and weak H_2O adsorption isotherms

Last evidence on amount of strongly bound H_2O molecules on TiO_2 came from total and weak water adsorption isotherms obtained at room temperature in dark (Figure 4.13). After obtaining total adsorption isotherm at room temperature in dark, the system was evacuated for 5 minutes and another adsorption isotherm was obtained at the same conditions. The procedure was repeated with 15 minutes evacuation. 5 and 15 minutes evacuation periods are an estimation that is considered enough to remove all weakly adsorbed molecules from the surface. Total adsorption isotherm shows 1060 µmol $H_2O/g_{catalyst}$ adsorption amount at 15 Torr equilibrium pressure and weak adsorption isotherms show 860 µmol $H_2O/g_{catalyst}$ adsorption amount on average at the same pressure. In addition, considering intercepts of linear part of adsorption isotherms with y-axis, adsorption amount of strongly bound molecules was determined as ∼230 µmol $H_2O/g_{catalyst}$ in line with monolayer capacity deduced from desorption isotherms and microcalorimeter results.

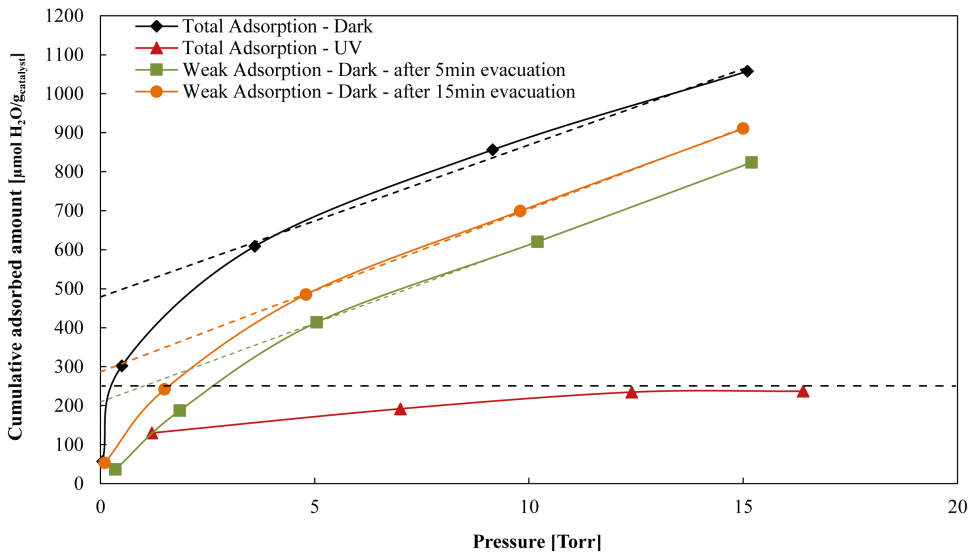

Figure 4.13: Total and weak H_2O adsorption isotherms on fresh TiO_2 P25 obtained in dark at room temperature and comparison with H_2O adsorption isotherm under illumination at room temperature

All the evidences point out 230-250 µmol $H_2O/g_{catalyst}$ as the monolayer capacity for H_2O on TiO_2. Therefore, only strongly bound molecules remained on TiO_2 surface for adsorption isotherm obtained at 150°C. Similarly, only strongly bound molecules

remained on TiO_2 surface under illumination also. There are several possibilities for desorption of molecules under UV illumination. Firstly, possibility of water splitting reaction and desorption of products from the surface subsequently. However, it is not likely considering low H_2 production rates. Secondly, the surface modification under UV illumination is an option. Since, duration of UV illumination was short during the experiments (∼4h), surface modification through defect formation under illumination is not possible. Since, the surface was clean, photo-oxidation and desorption of unintentionally exist hydrophobic molecules (carbon contaminants) from the surface was not possible also. Thirdly, heating of bulk catalyst due to the heating of ambient with light source is not the case since the catalyst was heated to only 40°C as shown in the Appendix E. Lastly, H_2O adsorption under illumination results in downward band bending in TiO_2 in theory yielding lagging of recombination event. Yet, charge recombination is highly common and lagging cannot prevent the inevitable recombination. However, local temperature rise due to heat release upon charge recombination can facilitate desorption of weakly bonded water molecules. According to the results, local temperature rise on the catalyst upon charge recombination is claimed to have an effect on the chemistry in such a way that 150°C cell temperature have affected it during the adsorption experiment.

4.4 Direct measurement of heat release upon charge recombination via microcalorimeter

After collecting indirect evidences on local temperature rise due to heat release upon charge recombination, attempts have been made to measure heat release directly via microcalorimeter. Four different configurations were arranged with microcalorimeter and different light sources. In all of these configurations, TiO_2 was exposed to air unless stated otherwise. The cell temperature was kept at 50°C. Light on/off experiments performed where heat evolution (exothermic heat flow) upon illumination was recorded. The points where light was turned off are shown with arrows in the Figures.

At first, a LED in UV range was obtained via RGB cables connected to a cell battery. LED and the cables were put into sample cavity of the microcalorimeter where TiO_2 powder was placed in a glass tube which was in the sample cavity. An identical

empty glass tube was put into reference cavity (Figure 3.3(a)(i)). Upon illumination peaks/shifts with different heights in exothermic heat flow direction were observed (Figure 4.14). Shift to baseline was observed each time when the light was turned off. In another experiment, empty tubes were placed in both of the cavities to measure heat formation upon illumination of an empty tube. Height of the peaks obtained upon illumination of TiO_2 were greater than the peaks obtained upon illumination of empty glass tube.

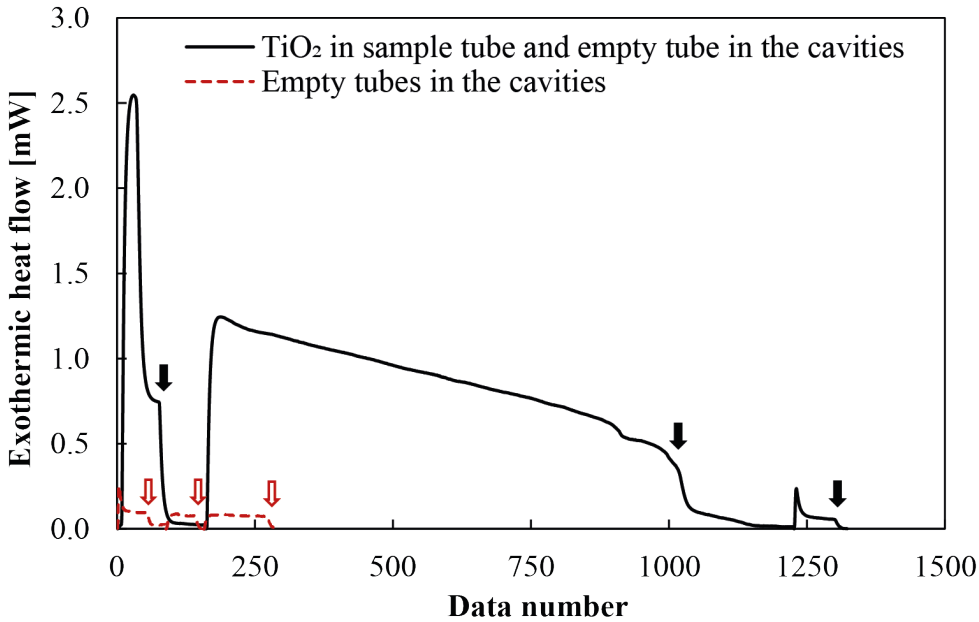

Figure 4.14: Heat formation upon illumination of TiO_2 sample in glass tube in the sample cavity (empty tube in the reference cavity) and illumination of empty tube in the sample cavity (empty tube in the reference cavity). UV range RGB LED connected to a cell battery was used. Arrows shows the points when light was turned off.

However, these experiments were not reproducible. Hence, the observed difference in heat evolution cannot be attributed to heat release upon charge recombination. The changes in the placement of the LED, fluctuations due to battery and heat release from cable resistances were suspected as the possible reasons for failure during the reproduction of the experiments. Hence, to eliminate fluctuations due to battery, the RGB cables were connected to a voltage source (Figure 3.3(a)(ii)). This time, the experiments were carried out at different voltages and hence, intensities. ZnO and Fe_2O_3 were also used to see the effect of change of material on heat formation. Identical shifts in heat formation upon illumination was found when the same voltage value

was used (Figure 4.15). Heat formation increased when the voltage was increased also. Heat formation was found neither a function of the material nor its amount. It was concluded that heat release due to cable resistances was recorded during these experiments explaining increase in heat release with increase in voltage.

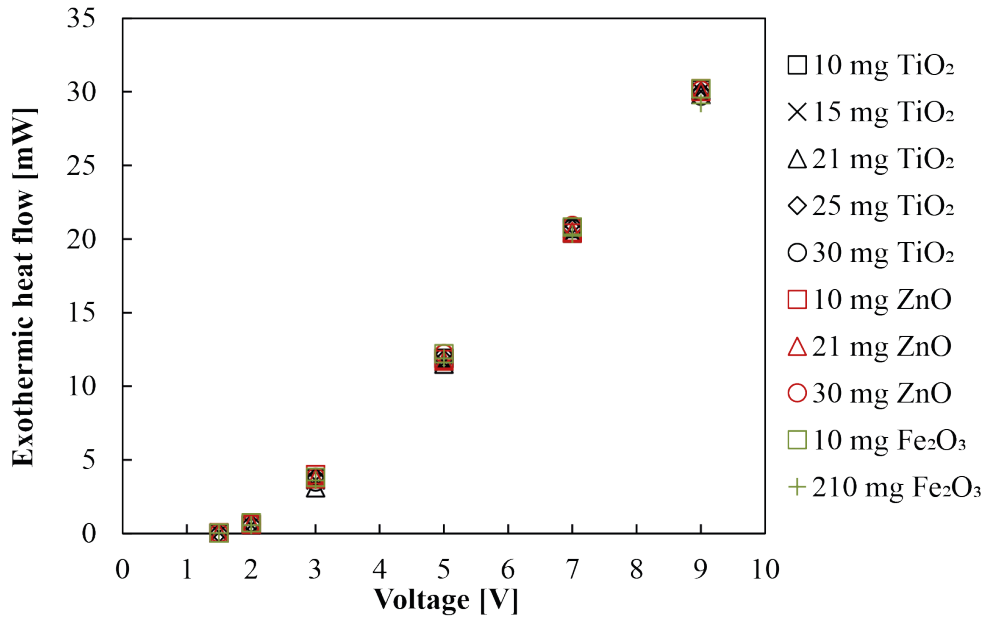

Figure 4.15: Heat formation upon illumination of TiO_2, ZnO and Fe_2O_3 samples in glass tube in the sample cavity (empty tube in the reference cavity) at different voltages. UV range RGB LED connected to a voltage source was used.

To eliminate cable resistance factor, two blue color LEDs were connected to the same voltage source were used. They were placed into both of the microcalorimeter cavities (Figure 3.3(b)). Peaks are observed upon illumination of both TiO_2 in glass tube in the sample cavity and empty tube in the reference cavity. However, the placement of the LEDs was not as delicate as it should be even when the LEDs were put into cavities without any glass tubes. Therefore, heat release due to resistances were still recorded (Figure 4.16). Heat formation in both of the cavities did not cancel each other. Endothermic values are related with working principle of microcalorimeter.

To eliminate cable resistance factor all together, fiber optic cables, allow only white light, were used (Figure 3.3(c))). Heat formation was observed again even though the values are extremely small (Figure 4.17). Observed differences in heat values are due to failure in the exactly same placement of the cables identical to each other in both of the cavities. Endothermic values are related with working principle of

microcalorimeter again.

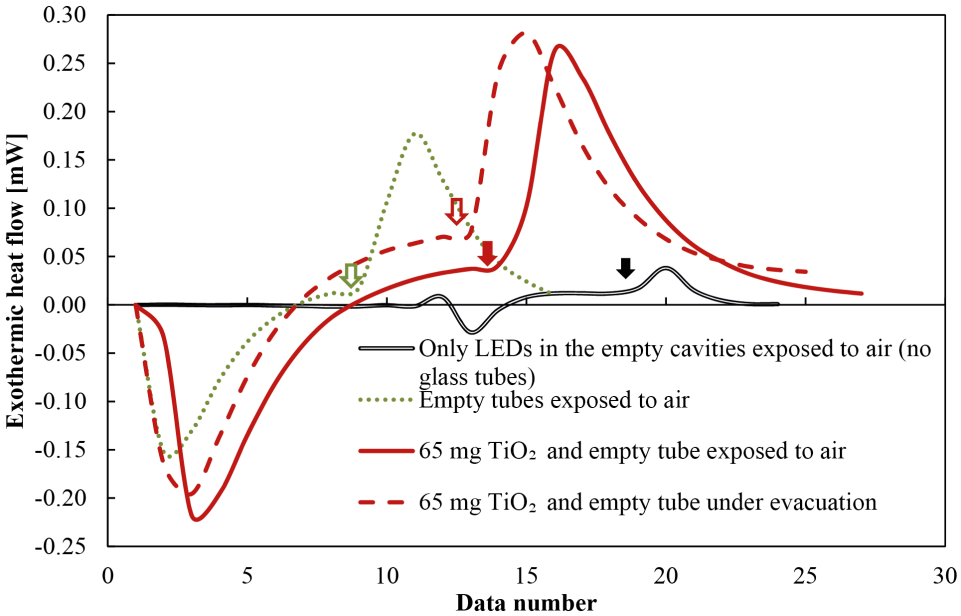

Figure 4.16: Heat formation upon illumination of (i) empty cavities (ii) empty tubes in the cavities (iii) 65 mg TiO_2 sample in glass tube in the sample cavity and empty tube in the reference cavity and (iv) same as (iii) but both of the glass tubes were under evacuation. Blue color LEDs connected to a voltage source was used. Arrows shows the points when light was turned off.

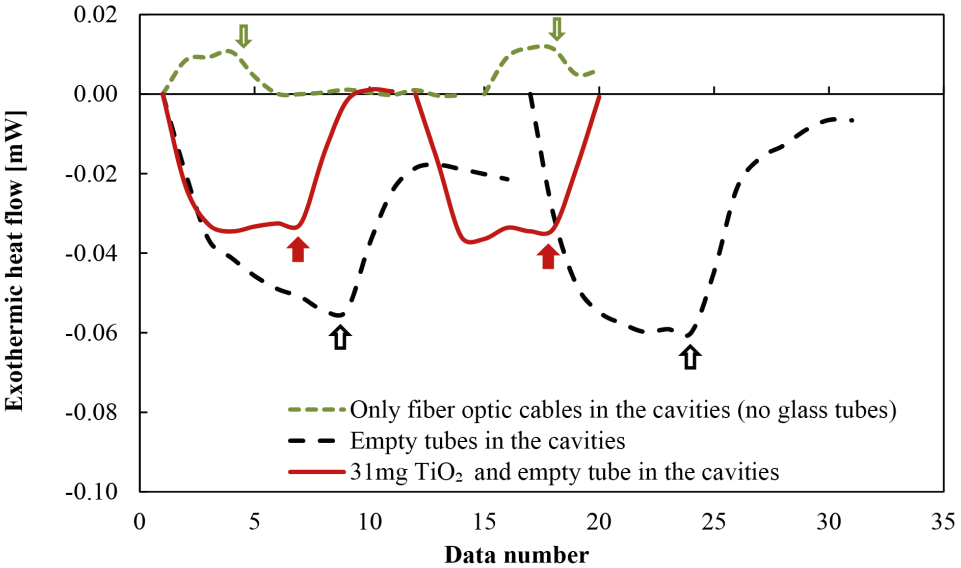

Figure 4.17: Heat formation upon illumination of (i) empty cavities (ii) empty tubes in the cavities (iii) TiO_2 sample in glass tube in the sample cavity and empty tube in the reference cavity. Fiber optic cables to a white light lamp was used. Arrows shows the points when light was turned off.

Finally, a UV LED lamp (Thorlabs M365LP1-C1 (365nm)) was used to illuminate cavity from above (Figure 3.3(d)). Only one of the cavity was illuminated each time. Different intensities were used. Heat formation increased with intensity as expected. However, no difference was detected between empty tube illumination, sample tube illumination or reference tube illumination at the same intensity value (Figure 4.18). Heat formation was observed due to light absorption by the wall of the cavity, glass tube and air in the cavity. The studies will be continue by preventing light absorption by the walls of the cavities in the microcalorimeter via reflecting layer on the cavity.

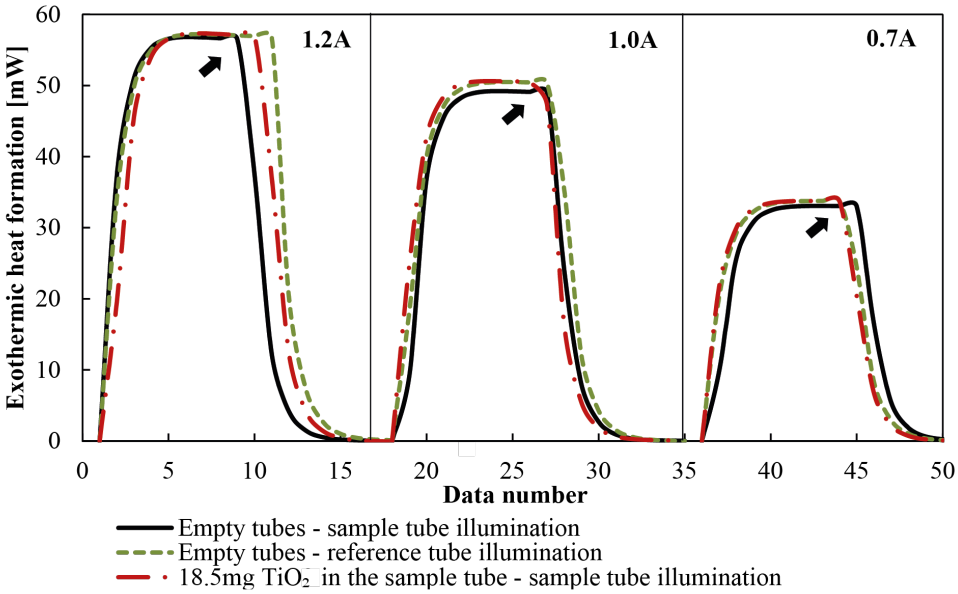

Figure 4.18: Heat formation upon illumination of (i) empty sample tube in sample cavity (empty tube in the reference cavity) (ii) empty tube reference in reference cavity (empty tube in the sample cavity) (iii) TiO_2 sample in glass tube in the sample cavity (empty tube in the reference cavity). UV LED lamp was used. Arrows shows the points when light was turned off.

4.5 H_2 and CO_2 adsorption isotherms on Pd/TiO_2

Pd/TiO_2 catalyst was chosen for investigation of metal-hydrogen systems on metal oxide support. Palladium-hydrogen interaction is strong, easily established and well studied. Additionally, palladium can be reduced at low temperatures and decreases the reduction temperature of TiO_2 where mild temperature conditions are very advantageous in adsorption studies via microcalorimetry.

4.5.1 TEM and HRTEM images of Pd/TiO_2

To investigate surface morphology of 0.5%, 1.0% and 2.0% Pd/TiO_2, TEM and HRTEM images of the surfaces were analyzed at 500, 200, 100 and 10nm distances (Figure 4.19-4.21). Darker points in the images correspond to palladium particles. As can be deduced from these three Figures, there are palladium aggregations on each catalyst resulting in wide range of particle size where particle size greater than 10nm can be observed. We can talk about relatively well distribution of palladium onto surface for 0.5% Pd/TiO_2. Aggregations are more obvious for 1.0% and 2.0% cases. For 1.0% Pd/TiO_2, poor dispersion of palladium on support can be clearly seen. Due to aggregations, sphericity of flatness of particles are hard to judge.

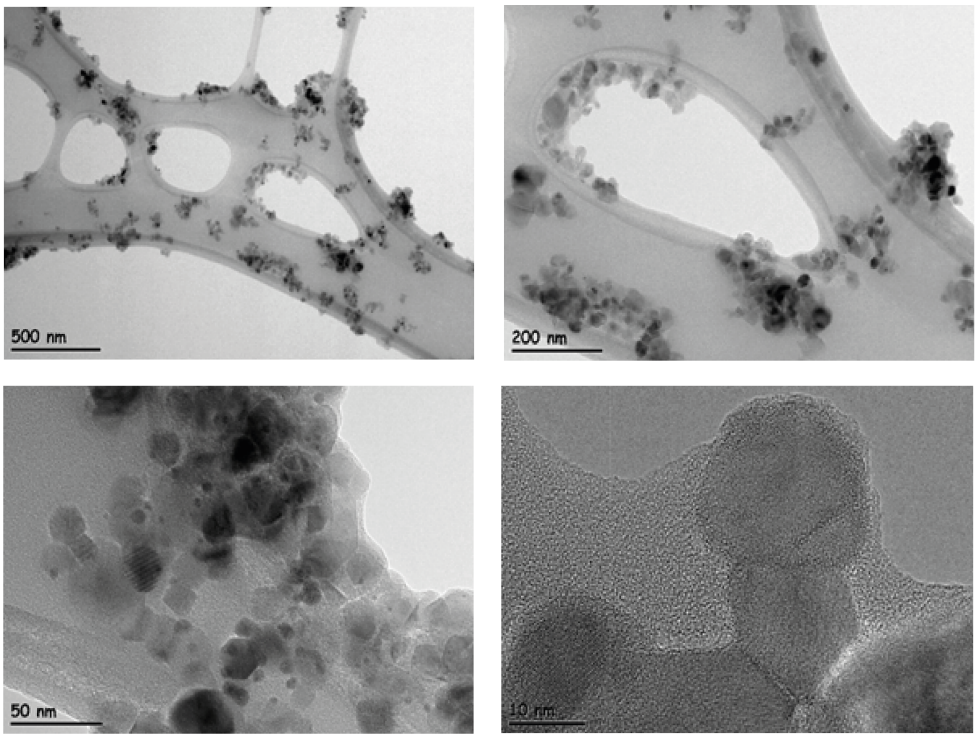

Figure 4.19: TEM and HRTEM images of 0.5% Pd/TiO_2

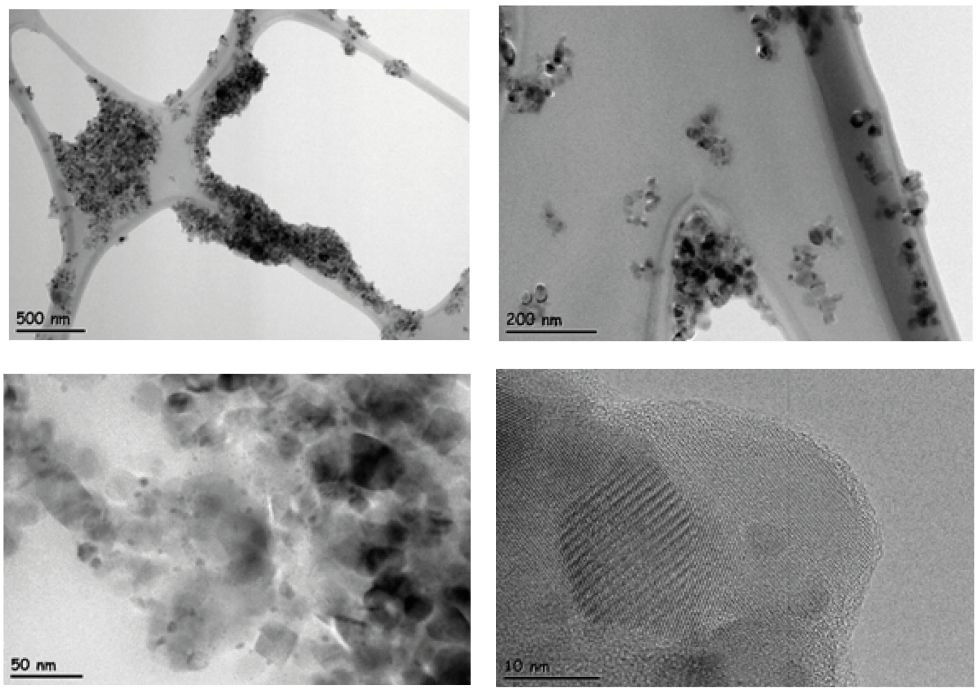

Figure 4.20: TEM and HRTEM images of 1.0% Pd/TiO_2

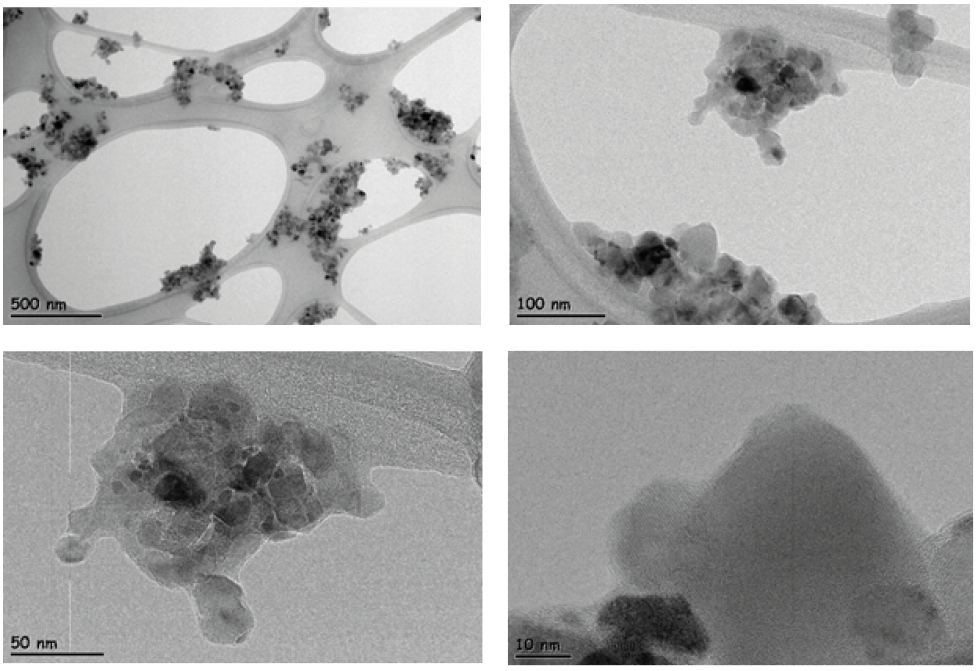

Figure 4.21: TEM and HRTEM images of 2.0% Pd/TiO_2

4.5.2 H_2-TPR on Pd/TiO_2

Temperature programmed reduction profiles of 0.5%, 1.0% and 2.0% Pd/TiO_2 were obtained with H_2 as the reducing agent Figure 4.22.

The first peak is around 68°C for all three samples. This peak is attributed to decomposition of β-PdH related to large particles according to literature (Babu, Lingaiah, Pasha, Kumar, & Prasad, 2009)(references therein). PdH can be formed easily at low temperatures (W. Lin et al., 2005) during the H_2 flow at the beginning of TPR experiment. As palladium weight percentage increases, this peak formed slightly at lower temperatures with a larger area under the curve. Palladium particle with a larger size has higher H_2 storage capacity and decompose at a lower temperature (Bhogeswararao & Srinivas, 2015). Therefore, order of palladium particle size from largest to smallest is 2.0%, 1.0% and 0.5% Pd/TiO_2 apparently.

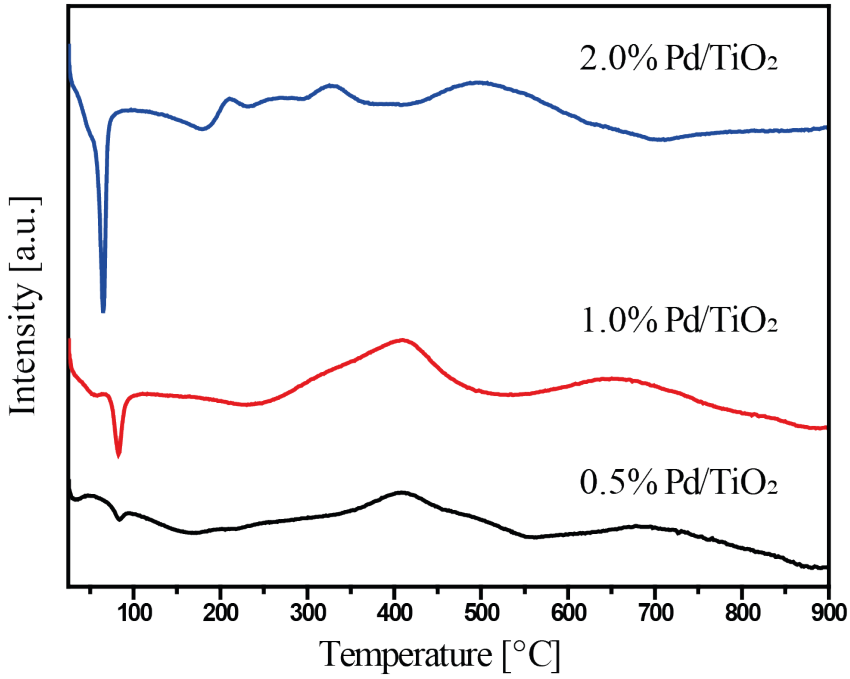

Figure 4.22: H_2 TPR of Pd/TiO_2

The large peaks can bee seen around 400°C and 650-700°C for 0.5% and 1.0% Pd/TiO_2. Surface oxygen of bare TiO_2 is removed by H_2 around 550°C. In the presence of palladium and spillover effect, temperature for surface oxygen removal decreases to ~350°C (González, Ardila, Montes de Correa, Martínez, & Fuentes-Zurita, 2007) where spilled hydrogen from palladium facilitates reduction of support. Hence, the peaks at 400°C belongs to the surface reduction of TiO_2. The peaks at 650-700°C can be attributed to bulk reduction of TiO_2 (Hwang, Ihm, Park, & Park, 2013).

For 2.0% Pd/TiO_2, there are two small peaks at 200 and 350°C and a large peak at 500°C. Considering palladium particle size, spillover effect due to palladium is unlikely. Therefore, the peaks at lower temperatures cannot be attributed to reduction of the support. However, presence of stronger interaction of bulk PdO species with support are detected in literature where its reduction to Pd^0 is around 200-300° (Huang, Ye, Huang, Zhang, & Leung, 2013)(Ferrer et al., 2005). This could be the reason for the peaks at lower temperatures indicating presence of bulk palladium for 2.0% case. As a result, the peak at 500°C can be the surface oxygen removal of TiO_2 similar to bare TiO_2.

4.5.3 Monitoring of surface reduction with H_2 on 0.5% and 2.0% Pd/TiO_2

Surface reduction was monitored in chemisorption manifold over 0.5% and 2.0% Pd/TiO_2 (Figure 4.23). For 2.0% Pd/TiO_2, no adsorption was seen after 8 Torr where H_2 amount stayed around 400 μmol/$g_{catalyst}$. Considering H_2O formation reaction ($H_2 + 1/2O_2 \rightarrow H_2O$) where 1 mol of H_2O leaves upon reaction of 1 mol of H_2, observing no change in adsorption amount is reasonable. In addition, heat of adsorption values indicate surface reduction by forming water since the heat values start around 250 kJ/mol H_2 which is the heat of formation of water (Figure 4.24). The differential heat values decreases to lower values because of fluctuations around 400 μmol/$g_{catalyst}$ rather than the change in absolute heat values during H_2 adsorption over 2.0% Pd/TiO_2. On the other hand, 0.5% Pd/TiO_2 adsorbed H_2 continually. Differential heat values stayed in between 160-80 kJ/mol H_2 during the continual H_2 uptake. One of the reason for this interesting behavior could be H_2 spillover from palladium to support in line with H_2-TPR result.

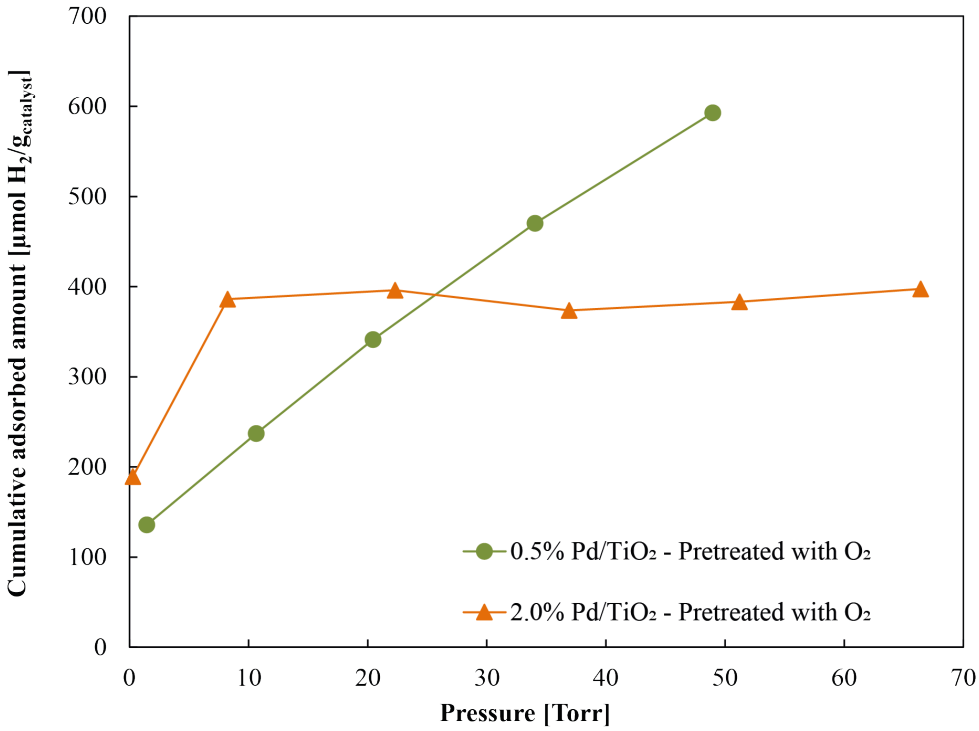

Figure 4.23: Monitoring of surface reduction via H_2 exposure of 0.5% and 2.0% Pd/TiO_2

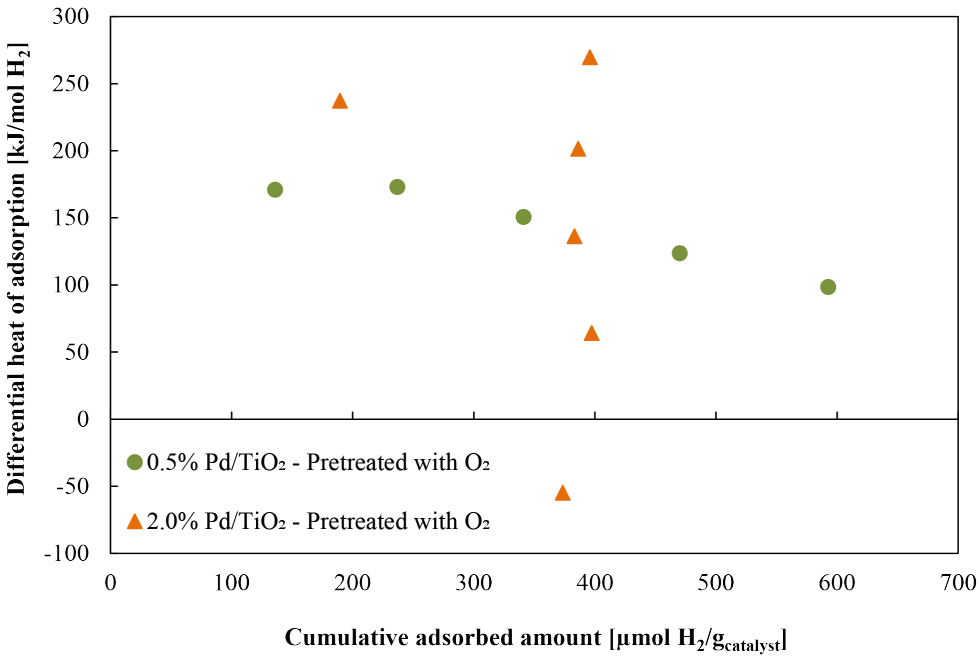

Figure 4.24: Differential heat of adsorption values with respect to cumulative adsorbed amounts during H_2 exposure of 0.5% and 2.0% Pd/TiO_2

4.5.4 H_2 adsorption isotherms on Pd/TiO_2

Further investigation on PdH formation was done by H_2 adsorption experiments on 0.5, 1.0 and 2.0% Pd/TiO_2. As can be seen from Figure 4.25, hydrogen uptake is very high for 1.0% where ~600μmol/$g_{catalyst}$ H_2 adsorbed on surface at ~80 Torr equilibrium pressure. 2.0% Pd/TiO_2 follows this with ~300μmol/$g_{catalyst}$ H_2 adsorbed on surface at ~80 Torr equilibrium pressure. Finally, only ~100μmol/$g_{catalyst}$ H_2 adsorbed on surface at ~80 Torr equilibrium pressure over 0.5% Pd/TiO_2.

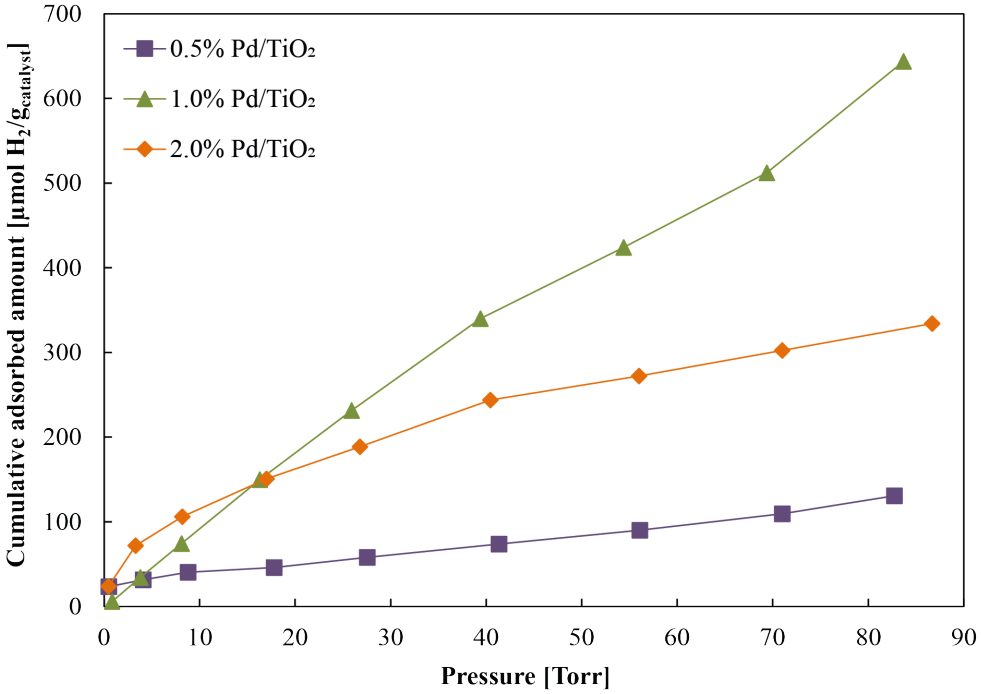

Figure 4.25: H_2 adsorption isotherms on reduced Pd/TiO_2 in dark at 50°C

Adsorption isotherm for 2.0% Pd/TiO_2 seems like reaching a saturation point. Differential heat of adsorption values for 2.0% Pd/TiO_2 decreases to 40 kJ/mol H_2 at this saturation point (Figure 4.26). Interestingly, for 1.0% Pd/TiO_2, the heat values stayed around 40 kJ/mol H_2 after this saturation point also indicating surface coverage. For 0.5% Pd/TiO_2, differential heat of adsorption values drops to 40 kJ/mol H_2 again from 120 kJ/mol H_2. ~40 kJ/mol H_2 is the heat of 'absorption' value for palladium-hydrogen system (Jewell & Davis, 2006)(references therein). Hence, we might be observing H_2 diffusion into palladium bulk and absorption of H_2 in palladium interstitials consecutively.

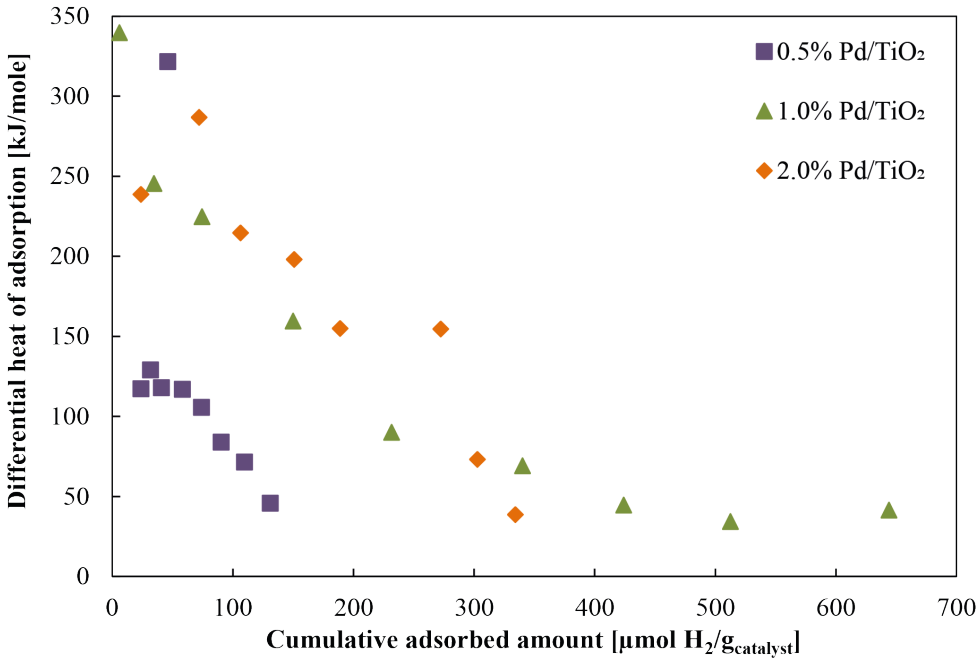

Figure 4.26: Differential heat of adsorption values with respect to cumulative adsorbed amounts of H_2 on reduced Pd/TiO_2 in dark at 50°C

Smaller amount of adsorption of 0.5% Pd/TiO_2 is in line with previous conclusions from TEM and H_2-TPR results that is relatively well dispersed palladium on support. SMSI effect is known for Pd/TiO_2 which hinders H_2 adsorption; however, reduction temperature in this study is low even for low temperature induced SMSI effect (Sá, Bernardi, & Anderson, 2007). Hence, SMSI effect is unlikely. Additionally, presence of palladium bulk was already deduced for 2.0% Pd/TiO_2, hence higher adsorption amount compared to 0.5% Pd/TiO_2 is reasonable. On the other hand, different conclusions have been made on 1.0% Pd/TiO_2. Poor dispersion was seen in TEM but similar TPR profiles to 0.5% Pd/TiO_2 was observed also. Hence, 1.0% Pd/TiO_2 needs further characterization.

4.5.5 CO_2 adsorption isotherms on Pd/TiO_2

Finally, CO_2 adsorbed on Pd/TiO_2 surfaces which were pretreated with O_2 (or air) to study oxidized surface and H_2 to study reduced surface (Figure 4.27).

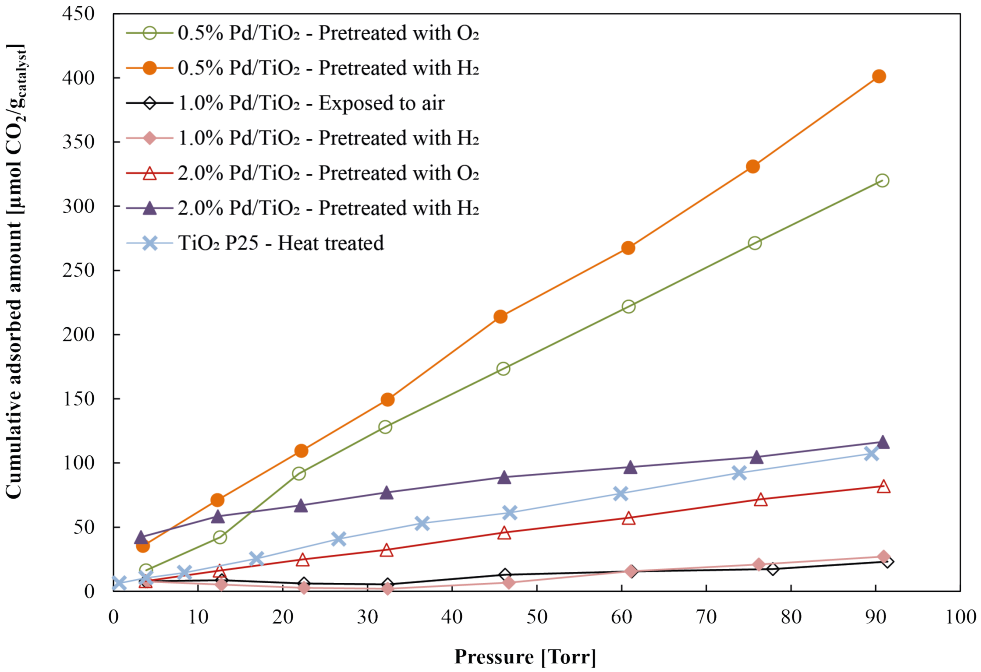

Figure 4.27: CO_2 adsorption isotherms on Pd/TiO_2 and TiO_2 P25 (for comparison) obtained in dark at 50°C

$\sim$400 µmol/$g_{catalyst}$ CO_2 adsorption amount was observed for 0.5% Pd/TiO_2 at $\sim$90 Torr equilibrium pressure. This value is 3 times higher than CO_2 adsorption amount on heat treated TiO_2. H_2 exposure on palladium can facilitate reduction of surface through spillover and yield formation of oxygen vacancies. Since oxygen vacancies are the main adsorption sites for CO_2, increase in their concentration results in higher adsorption amount of CO_2. CO_2 adsorption amount on oxidized 0.5% Pd/TiO_2 surface is also much higher than CO_2 adsorption on bare TiO_2. Palladium itself offer adsorption sites for CO_2. Moreover, palladium redispersion in the presence of O_2 is known (Newton, Belver-Coldeira, Martínez-Arias, & Fernández-García, 2007) and this can enhance CO_2 adsorption on oxidized 0.5% Pd/TiO_2.

For 2.0% Pd/TiO_2, CO_2 adsorption amount is in the same range with bare TiO_2. Presence of palladium bulk did not enhance CO_2 adsorption capacity. For 1.0% Pd/TiO_2, very small amounts of CO_2 adsorbed on surface. Differential heat of adsorption values for 1.0% Pd/TiO_2 show very high initial heat of adsorption values indicating a different surface event (Figure 4.28). During the evacuation period before the CO_2 adsorption experiment, H_2 on surface may not be removed totally. Hence, interaction of CO_2 with H_2 is highly possible. However, considering arguable results for

1.0% Pd/TiO_2 mentioned previously, the situation should be handled carefully where further investigations are needed.

1.0% Pd/TiO_2 attracts attention with high H_2 storage capacity but the CO_2 adsorption on its surface was very low. On the other hand, 0.5% Pd/TiO_2 stands out among others with relatively well dispersion and enhanced CO_2 adsorption capacity, however; CO_2 adsorption was weak on this surface also. Indeed, differential heat of adsorption values for all of the CO_2 adsorption isotherms over Pd/TiO_2 intensify around 25 kJ/mol corresponding to heat of condensation of CO_2 (Figure 4.28). After ~90 µmol $CO_2/g_{catalyst}$, heat values stay around 5-10 kJ/mol CO_2 for 0.5% Pd/TiO_2 indicating weak adsorption. Overall, CO_2 adsorption was weak on any surface within this study where isotherms fitted to Freundlich isotherm indicating weak adsorption on heterogeneous surface (Appendix G). Both of 0.5% Pd/TiO_2 and 1.0% Pd/TiO_2 need further investigation.

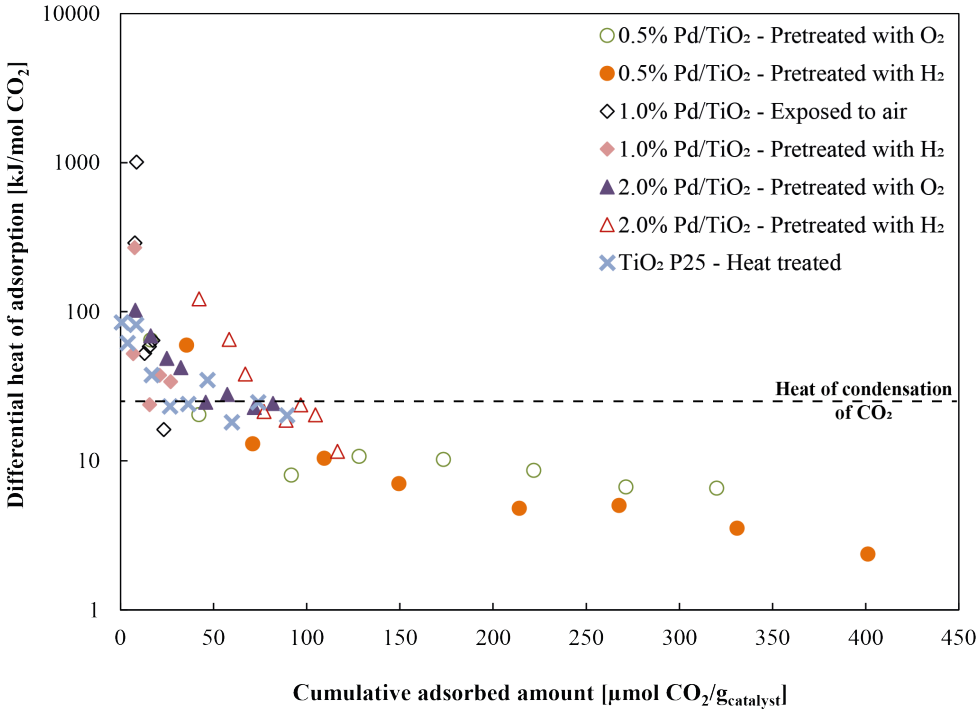

Figure 4.28: Differential heat of adsorption values in logarithmic scale with respect to cumulative adsorbed amount of CO_2 on Pd/TiO_2 and TiO_2 P25 (for comparison) obtained in dark at 50°C

CHAPTER 5

CONCLUSIONS

To elucidate the bottleneck problems of artificial photosynthesis, CO_2 and H_2O adsorption isotherms on TiO_2 P25 with and without illumination were obtained. Indirect evidences were collected on local temperature rise on the surface. CO_2 adsorption isotherms showed desorption under UV illumination at room temperature. Assuming temperature increase only in the sample cell (160°C estimated), calculation of adsorbed amounts yielded reasonable isotherm similar to CO_2 adsorption in dark. H_2O adsorption isotherms on TiO_2 P25 under illumination showed Langmuir type of adsorption isotherm indicating presence of only strongly bound molecules in accordance with the adsorption isotherm obtained at 150°C, desorption isotherms and total-weak adsorption isotherms. Local temperature rise due to heat release upon charge recombination explains the desorption of weakly adsorbed H_2O molecules. Direct measurement of heat release upon charge recombination was tried to be measured where set-up configurations and problems related with the measurements were explained. Additionally, weak adsorption of CO_2 experimentally observed and fitted to Freundlich isotherm. Direct relation with CO_2 adsorbed amount on TiO_2 and oxygen vacancy concentration is suspected. Strong adsorption of H_2O on heterogeneous surface was shown through experimetal data fitting to Temkin isotherm.

Presence of bulk palladium was shown for 2.0% Pd/TiO_2 through TEM and H_2-TPR analysis and H_2 adsorption isotherm. Consecutively, well dispersion of palladium and spillover effect was shown for 0.5% Pd/TiO_2. 1.0% Pd/TiO_2 showed high H_2 storage capacity. However, it showed very low CO_2 adsorption capacity due to issues related with surface cleanliness possibly. Metal-hydrogen systems are promising for developing strategies for enhanced reduction of CO_2 with H_2.

REFERENCES

Acharya, D. P., Camillone, N., & Sutter, P. (2011). Co2 adsorption, diffusion, and electron-induced chemistry on rutile tio2(110): A low-temperature scanning tunneling microscopy study. *The Journal of Physical Chemistry C*, *115*(24), 12095-12105. doi: 10.1021/jp202476v

Aschauer, U., He, Y., Cheng, H., Li, S.-C., Diebold, U., & Selloni, A. (2010). Influence of subsurface defects on the surface reactivity of tio2: Water on anatase (101). *The Journal of Physical Chemistry C*, *114*(2), 1278-1284. doi: 10.1021/jp910492b

Babu, N. S., Lingaiah, N., Pasha, N., Kumar, J. V., & Prasad, P. S. (2009). Influence of particle size and nature of pd species on the hydrodechlorination of chloroaromatics: Studies on pd/tio2 catalysts in chlorobenzene conversion. *Catalysis Today*, *141*(1), 120 - 124. doi: 10.1016/j.cattod.2008.03.018

Balajka, J., Hines, M. A., DeBenedetti, W. J. I., Komora, M., Pavelec, J., Schmid, M., & Diebold, U. (2018). High-affinity adsorption leads to molecularly ordered interfaces on tio2 in air and solution. *Science*, *361*(6404), 786–789. doi: 10.1126/science.aat6752

Berger, T., Diwald, O., Knözinger, E., Sterrer, M., & Yates Jr, J. T. (2006). Uv induced local heating effects in tio2 nanocrystals. *Phys. Chem. Chem. Phys.*, *8*, 1822-1826. doi: 10.1039/B517107E

Berger, T., Sterrer, M., Diwald, O., Knözinger, E., Panayotov, D., Thompson, T. L., & Yates, J. T. (2005). Light-induced charge separation in anatase tio2 particles. *The Journal of Physical Chemistry B*, *109*(13), 6061-6068. doi: 10.1021/jp0404293

Bhogeswararao, S., & Srinivas, D. (2015). Catalytic conversion of furfural to industrial chemicals over supported pt and pd catalysts. *Journal of Catalysis*, *327*, 65 - 77. doi: 10.1016/j.jcat.2015.04.018

BP. (2019a). *Bp energy outlook.* Retrieved from `https://www.bp.com/content/dam/bp/business-sites/en/global/corporate/`

pdfs/energy-economics/energy-outlook/bp-energy-outlook-2019.pdf

BP. (2019b). *Bp statistical review of world energy* (68th ed.). Retrieved from https://www.bp.com/content/dam/bp/business-sites/en/global/corporate/pdfs/energy-economics/energy-outlook/bp-energy-outlook-2019.pdf

Burghaus, U. (2014). Surface chemistry of co2 – adsorption of carbon dioxide on clean surfaces at ultrahigh vacuum. *Progress in Surface Science*, *89*(2), 161 - 217. doi: 10.1016/j.progsurf.2014.03.002

Cheng, H., & Selloni, A. (2009). Surface and subsurface oxygen vacancies in anatase tio2 and differences with rutile. *Phys. Rev. B*, *79*, 092101. doi: 10.1103/PhysRevB.79.092101

Climate Action Tracker. (2019). *Global temperatures - 2100 warming projections.* Retrieved from https://climateactiontracker.org/global/temperatures/

De Angelis, F., Di Valentin, C., Fantacci, S., Vittadini, A., & Selloni, A. (2014). Theoretical studies on anatase and less common tio2 phases: Bulk, surfaces, and nanomaterials. *Chemical Reviews*, *114*(19), 9708-9753. doi: 10.1021/cr500055q

Diebold, U. (2003). The surface science of titanium dioxide. *Surface Science Reports*, *48*(5), 53 - 229. doi: 10.1016/S0167-5729(02)00100-0

Dilla, M., Mateblowski, A., Ristig, S., & Strunk, J. (2017). Photocatalytic co2 reduction under continuous flow high-purity conditions: Influence of light intensity and h2o concentration. *ChemCatChem*, *9*(23), 4345-4352. doi: 10.1002/cctc.201701189

Dilla, M., Moustakas, N. G., Becerikli, A. E., Peppel, T., Springer, A., Schlögl, R., ... Ristig, S. (2019). Judging the feasibility of tio2 as photocatalyst for chemical energy conversion by quantitative reactivity determinants. *Phys. Chem. Chem. Phys.*, *21*, 13144-13150. doi: 10.1039/C9CP00981G

Dilla, M., Schlögl, R., & Strunk, J. (2017). Photocatalytic co2 reduction under continuous flow high-purity conditions: Quantitative evaluation of ch4 formation in the steady-state. *ChemCatChem*, *9*(4), 696-704. doi: 10.1002/cctc.201601218

Emeline, A. V., Ryabchuk, V., & Serpone, N. (2000). Factors affecting the efficiency

of a photocatalyzed process in aqueous metal-oxide dispersions: Prospect of distinguishing between two kinetic models. *Journal of Photochemistry and Photobiology A: Chemistry*, *133*(1), 89 - 97. doi: 10.1016/S1010-6030(00) 00225-2

Evonik. (2019). Product information - aeroxide tio2 p25 titanium dioxide. , 1-2.

Ferrer, V., Moronta, A., Sanchez, J., Solano, R., Bernal, S., & Finol, D. (2005, 10). Effect of the reduction temperature on the catalytic activity of pd-supported catalysts. *Catalysis Today*, *107*, 487-492. doi: 10.1016/j.cattod.2005.07.059

Freund, H.-J., & Roberts, M. (1996). Surface chemistry of carbon dioxide. *Surface Science Reports*, *25*(8), 225 - 273. doi: 10.1016/S0167-5729(96)00007-6

Fujishima, A., & Honda, K. (1972). Electrochemical photolysis of water at a semiconductor electrode. *Nature*, *238*, 37-38. doi: 10.1038/238037a0

Fujishima, A., Zhang, X., & Tryk, D. A. (2008). Tio2 photocatalysis and related surface phenomena. *Surface Science Reports*, *63*(12), 515 - 582. doi: 10.1016/ j.surfrep.2008.10.001

Gaya, U. I. (2014). *Heterogeneous photocatalysis using inorganic semiconductor solids*. Springer, Dordrecht. doi: 10.1007/978-94-007-7775-0

González, C. A., Ardila, A. N., Montes de Correa, C., Martínez, M. A., & Fuentes-Zurita, G. (2007). Pd/tio2 washcoated cordierite minimonoliths for hydrodechlorination of light organochlorinated compounds. *Industrial & Engineering Chemistry Research*, *46*(24), 7961-7969. doi: 10.1021/ie070713r

Guan, G., Kida, T., Harada, T., Isayama, M., & Yoshida, A. (2003). Photoreduction of carbon dioxide with water over k2ti6o13 photocatalyst combined with cu/zno catalyst under concentrated sunlight. *Applied Catalysis A: General*, *249*, 11–18. doi: 10.1016/S0926-860X(03)00205-9

Guan, G., Kida, T., & Yoshida, A. (2003). Reduction of carbon dioxide with water under concentrated sunlight using photocatalyst combined with fe-based catalyst. *Applied Catalysis B: Environmental*, *41*, 387–396. doi: 10.1016/ S0926-3373(02)00174-1

Gupta, S. M., & Tripathi, M. (2011). A review of tio2 nanoparticles. *Chinese Science Bulletin*, *56*(16), 1639. doi: 10.1007/s11434-011-4476-1

Haggerty, J. E., Schelhas, L. T., Kitchaev, D. A., Mangum, J. S., Garten, L. M., Sun, W., … Tate, J. (2017). High-fraction brookite films from amorphous

precursors. *Scientific Reports*, *7*, 15232. doi: 10.1038/s41598-017-15364-y

Henderson, M. A. (1996a). An hreels and tpd study of water on tio2(110): the extent of molecular versus dissociative adsorption. *Surface Science*, *355*(1), 151 - 166. doi: 10.1016/0039-6028(95)01357-1

Henderson, M. A. (1996b). Structural sensitivity in the dissociation of water on tio2 single-crystal surfaces. *Langmuir*, *12*(21), 5093-5098. doi: 10.1021/la960360t

Henderson, M. A. (1998). Evidence for bicarbonate formation on vacuum annealed tio2(110) resulting from a precursor-mediated interaction between co2 and h2o. *Surface Science*, *400*(1), 203 - 219. doi: 10.1016/S0039-6028(97)00863-7

Henderson, M. A. (2011). A surface science perspective on tio2 photocatalysis. *Surface Science Reports*, *66*(6), 185 - 297. doi: 10.1016/j.surfrep.2011.01.001

Hoch, L. B., Wood, T. E., O'Brien, P. G., Liao, K., Reyes, L. M., Mims, C. A., & Ozin, G. A. (2014). The rational design of a single-component photocatalyst for gas-phase co2 reduction using both uv and visible light. *Advanced Science*, *1*(1), 1400013. doi: 10.1002/advs.201400013

Huang, H., Ye, X., Huang, H., Zhang, L., & Leung, D. Y. (2013). Mechanistic study on formaldehyde removal over pd/tio2 catalysts: Oxygen transfer and role of water vapor. *Chemical Engineering Journal*, *230*, 73 - 79. doi: 10.1016/j.cej.2013.06.035

Hurum, D. C., Agrios, A. G., Gray, K. A., Rajh, T., & Thurnauer, M. C. (2003). Explaining the enhanced photocatalytic activity of degussa p25 mixed-phase tio2 using epr. *The Journal of Physical Chemistry B*, *107*(19), 4545-4549. doi: 10.1021/jp0273934

Hwang, K.-R., Ihm, S.-K., Park, S.-C., & Park, J.-S. (2013). Pt/zro2 catalyst for a single-stage water-gas shift reaction: Ti addition effect. *International Journal of Hydrogen Energy*, *38*(14), 6044 - 6051. doi: 10.1016/j.ijhydene.2013.01.101

Ipek, B., & Uner, D. (2012). *Artificial photosynthesis from a chemical engineering perspective* (M. M. Najafpour, Ed.). doi: 10.5772/26909

Jafari, T., Moharreri, E., Amin, A. S., Miao, R., Song, W., & Suib, S. L. (2016). Photocatalytic water splitting - the untamed dream: A review of recent advances. *Molecules*, *21*(7). doi: 10.3390/molecules21070900

Jewell, L. L., & Davis, B. H. (2006). Review of absorption and adsorption in the

hydrogen–palladium system. *Applied Catalysis A: General*, *310*, 1 - 15. doi: 10.1016/j.apcata.2006.05.012

Kondratenko, E. V., Mul, G., Baltrusaitis, J., Larrazábal, G. O., & Pérez-Ramírez, J. (2013). Status and perspectives of co2 conversion into fuels and chemicals by catalytic, photocatalytic and electrocatalytic processes. *Energy Environ. Sci.*, *6*, 3112-3135. doi: 10.1039/C3EE41272E

Koretsky, M. D. (2013). *Engineering and chemical thermodynamics*. Wiley.

Lahousse, C., Maugé, F., Bachelier, J., & Lavalley, J.-C. (1995). Acidic and basic properties of titania–alumina mixed oxides; active sites for propan-2-ol dehydration. *J. Chem. Soc., Faraday Trans.*, *91*, 2907-2912. doi: 10.1039/FT9959102907

Lee, W.-H., Liao, C.-H., Tsai, M.-F., Huang, C.-W., & Wu, J. C. (2013). A novel twin reactor for co2 photoreduction to mimic artificial photosynthesis. *Applied Catalysis B: Environmental*, *132-133*, 445 - 451. doi: 10.1016/j.apcatb.2012.12.024

Leytner, S., & Hupp, J. T. (2000). Evaluation of the energetics of electron trap states at the nanocrystalline titanium dioxide/aqueous solution interface via time-resolved photoacoustic spectroscopy. *Chemical Physics Letters*, *330*(3), 231 - 236. doi: 10.1016/S0009-2614(00)01112-X

Li, K., Peng, B., & Peng, T. (2016). Recent advances in heterogeneous photocatalytic co2 conversion to solar fuels. *ACS Catalysis*, *6*(11), 7485-7527. doi: 10.1021/acscatal.6b02089

Lin, W., Lin, L., Zhu, Y., Xie, Y., Scheurell, K., & Kemnitz, E. (2005). Novel pd/tio2–zro2 catalysts for methane total oxidation at low temperature and their 18o-isotope exchange behavior. *Journal of Molecular Catalysis A: Chemical*, *226*(2), 263 - 268. doi: 10.1016/j.molcata.2004.10.048

Lin, X., Wang, Z. T., Lyubinetsky, I., Kay, B. D., & Dohnálek, Z. (2013). Interaction of co2 with oxygen adatoms on rutile tio2(110). *Physical Chemistry Chemical Physics*, *15*(17), 6190–6195. doi: 10.1039/c3cp44040k

Linsebigler, A. L., Lu, G., & Yates, J. T. (1995). Photocatalysis on tio2 surfaces: Principles, mechanisms, and selected results. *Chemical Reviews*, *95*(3), 735-758. doi: 10.1021/cr00035a013

Lu, G., Linsebigler, A., & Yates, J. T. (1994). Ti3+ defect sites on tio2(110): Produc-

tion and chemical detection of active sites. *The Journal of Physical Chemistry*, *98*(45), 11733-11738. doi: 10.1021/j100096a017

Markovits, A., Fahmi, A., & Minot, C. (1996). A theoretical study of co2 adsorption on tio2. *Journal of Molecular Structure: THEOCHEM*, *371*, 219 - 235. doi: 10.1016/S0166-1280(96)04696-9

Martin, S. T., Herrmann, H., & Hoffmann, M. R. (1994). Time-resolved microwave conductivity. part 2.—quantum-sized tio2 and the effect of adsorbates and light intensity on charge-carrier dynamics. *J. Chem. Soc., Faraday Trans.*, *90*, 3323-3330. doi: 10.1039/FT9949003323

Martra, G. (2000). Lewis acid and base sites at the surface of microcrystalline tio2 anatase: relationships between surface morphology and chemical behaviour. *Applied Catalysis A: General*, *200*(1), 275 - 285. doi: 10.1016/S0926-860X(00)00641-4

Mendive, C. B., Hansmann, D., Bredow, T., & Bahnemann, D. (2011). New insights into the mechanism of tio2 photocatalysis: Thermal processes beyond the electron–hole creation. *The Journal of Physical Chemistry C*, *115*(40), 19676-19685. doi: 10.1021/jp112243q

Mino, L., Cesano, F., Scarano, D., Spoto, G., & Martra, G. (2019). Molecules and heterostructures at tio2 surface: the cases of h2o, co2, and organic and inorganic sensitizers. *Research on Chemical Intermediates*, *45*(12), 5801-5829. doi: 10.1007/s11164-019-04003-y

Mino, L., Spoto, G., & Ferrari, A. M. (2014). Co2 capture by tio2 anatase surfaces: A combined dft and ftir study. *The Journal of Physical Chemistry C*, *118*(43), 25016-25026. doi: 10.1021/jp507443k

Mohamed, H. H., Mendive, C. B., Dillert, R., & Bahnemann, D. W. (2011). Kinetic and mechanistic investigations of multielectron transfer reactions induced by stored electrons in tio2 nanoparticles: A stopped flow study. *The Journal of Physical Chemistry A*, *115*(11), 2139-2147. doi: 10.1021/jp108958w

Newton, M., Belver-Coldeira, C., Martínez-Arias, A., & Fernández-García, M. (2007). "oxidationless" promotion of rapid palladium redispersion by oxygen during redox co/(no+o2) cycling. *Angewandte Chemie International Edition*, *46*(45), 8629-8631. doi: 10.1002/anie.200702134

NIST. (2018). *Nist chemistry webbook standard reference database number 69.* Re-

trieved 2019-12-19, from `https://webbook.nist.gov/chemistry/` doi: https://doi.org/10.18434/T4D303

Ohno, T., Sarukawa, K., Tokieda, K., & Matsumura, M. (2001). Morphology of a tio2 photocatalyst (degussa, p-25) consisting of anatase and rutile crystalline phases. *Journal of Catalysis*, *203*(1), 82 - 86. doi: 10.1006/jcat.2001.3316

Ohtani, B. (2013). Titania photocatalysis beyond recombination: A critical review. *Catalysts*, *3*(4), 942–953. doi: 10.3390/catal3040942

Pickl, M. J. (2019). The renewable energy strategies of oil majors – from oil to energy? *Energy Strategy Reviews*, *26*, 100370. doi: 10.1016/j.esr.2019.100370

Qureshi, M., & Takanabe, K. (2017). Insights on measuring and reporting heterogeneous photocatalysis: Efficiency definitions and setup examples. *Chemistry of Materials*, *29*(1), 158-167. doi: 10.1021/acs.chemmater.6b02907

Rabani, J., Yamashita, K., Ushida, K., Stark, J., & Kira, A. (1998). Fundamental reactions in illuminated titanium dioxide nanocrystallite layers studied by pulsed laser. *The Journal of Physical Chemistry B*, *102*(10), 1689-1695. doi: 10.1021/jp973411j

Ranade, M. R., Navrotsky, A., Zhang, H. Z., Banfield, J. F., Elder, S. H., Zaban, A., ... Whitfield, H. J. (2002). Energetics of nanocrystalline tio2. *Proceedings of the National Academy of Sciences*, *99*(suppl 2), 6476-6481. doi: 10.1073/pnas.251534898

Ras, E.-J., Louwerse, M. J., Mittelmeijer-Hazeleger, M. C., & Rothenberg, G. (2013). Predicting adsorption on metals: simple yet effective descriptors for surface catalysis. *Phys. Chem. Chem. Phys.*, *15*, 4436-4443. doi: 10.1039/C3CP42965B

Renz, C. (1921). Lichtreaktionen der oxyde des titans, cers und der erdsäuren. *Helvetica Chimica Acta*, *4*(1), 961-968. doi: 10.1002/hlca.192100401101

Reyes-Coronado, D., Rodríguez-Gattorno, G., Espinosa-Pesqueira, M. E., Cab, C., de Coss, R., & Oskam, G. (2008). Phase-pure tio2nanoparticles: anatase, brookite and rutile. *Nanotechnology*, *19*(14), 145605. doi: 10.1088/0957-4484/19/14/145605

Rong, W., Kazuhito, H., Akira, F., Makoto, C., Eiichi, K., Astushi, K., ... Toshiya, W. (1997). Light-induced amphiphilic surfaces. *Nature*, *338*, 431-432. doi: 10.1038/41233

Ruiz Puigdollers, A., Schlexer, P., Tosoni, S., & Pacchioni, G. (2017). Increasing oxide reducibility: The role of metal/oxide interfaces in the formation of oxygen vacancies. *ACS Catalysis*, *7*(10), 6493-6513. doi: 10.1021/acscatal.7b01913

Sá, J., Bernardi, J., & Anderson, J. A. (2007). Imaging of low temperature induced smsi on pd/tio2 catalysts. *Catalysis Letters*, *114*, 91-95. doi: 10.1007/s10562-007-9049-1

Schneider, J., Bahnemann, D., Ye, J., Li Puma, G., & Dionysiou, D. D. (Eds.). (2016). *Photocatalysis*. The Royal Society of Chemistry. doi: 10.1039/9781782622338

Schneider, J., Matsuoka, M., Takeuchi, M., Zhang, J., Horiuchi, Y., Anpo, M., & Bahnemann, D. W. (2014). Understanding tio2 photocatalysis: Mechanisms and materials. *Chemical Reviews*, *114*(19), 9919-9986. doi: 10.1021/cr5001892

Serpone, N. (1997). Relative photonic efficiencies and quantum yields in heterogeneous photocatalysis. *Journal of Photochemistry and Photobiology A: Chemistry*, *104*(1), 1 - 12. doi: 10.1016/S1010-6030(96)04538-8

Serpone, N., Emeline, A. V., Horikoshi, S., Kuznetsov, V. N., & Ryabchuk, V. K. (2012). On the genesis of heterogeneous photocatalysis: a brief historical perspective in the period 1910 to the mid-1980s. *Photochem. Photobiol. Sci.*, *11*, 1121-1150. doi: 10.1039/C2PP25026H

Serpone, N., Lawless, D., Khairutdinov, R., & Pelizzetti, E. (1995). Subnanosecond relaxation dynamics in tio2 colloidal sols (particle sizes rp = 1.0-13.4 nm). relevance to heterogeneous photocatalysis. *The Journal of Physical Chemistry*, *99*(45), 16655-16661. doi: 10.1021/j100045a027

Shkrob, I. A., Sauer, M. C., & Gosztola, D. (2004). Efficient, rapid photooxidation of chemisorbed polyhydroxyl alcohols and carbohydrates by tio2 nanoparticles in an aqueous solution. *The Journal of Physical Chemistry B*, *108*(33), 12512-12517. doi: 10.1021/jp0477351

Sieland, F., Schneider, J., & Bahnemann, D. W. (2017). Fractal charge carrier kinetics in tio2. *The Journal of Physical Chemistry C*, *121*(43), 24282-24291. doi: 10.1021/acs.jpcc.7b07087

Stevanovic, A., Büttner, M., Zhang, Z., & Yates, J. T. (2012). Photoluminescence of tio2: Effect of uv light and adsorbed molecules on surface band structure. *Journal of the American Chemical Society*, *134*(1), 324-332. doi: 10.1021/

ja2072737

Stevanovic, A., & Yates, J. T. (2012). Probe of nh3 and co adsorption on the very outermost surface of a porous tio2 adsorbent using photoluminescence spectroscopy. *Langmuir*, *28*(13), 5652-5659. doi: 10.1021/la205032j

Stevanovic, A., & Yates, J. T. (2013). Electron hopping through tio2 powder: A study by photoluminescence spectroscopy. *The Journal of Physical Chemistry C*, *117*(46), 24189-24195. doi: 10.1021/jp407765r

Tahir, M., & Amin, N. S. (2015). Indium-doped tio2 nanoparticles for photocatalytic co2 reduction with h2o vapors to ch4. *Applied Catalysis B: Environmental*, *162*, 98 - 109. doi: 10.1016/j.apcatb.2014.06.037

Taifan, W., Boily, J.-F., & Baltrusaitis, J. (2016). Surface chemistry of carbon dioxide revisited. *Surface Science Reports*, *71*(4), 595 - 671. doi: 10.1016/j.surfrep .2016.09.001

Takanabe, K. (2019). Addressing fundamental experimental aspects of photocatalysis studies. *Journal of Catalysis*, *370*, 480-484. doi: 10.1016/j.jcat.2018.10.006

Thompson, T. L., Diwald, O., & Yates, J. T. (2003). Co2 as a probe for monitoring the surface defects on tio2(110)temperature-programmed desorption. *The Journal of Physical Chemistry B*, *107*(42), 11700-11704. doi: 10.1021/jp030430m

Thompson, T. L., & Yates, J. T. (2006). Surface science studies of the photoactivation of tio2 - new photochemical processes. *Chemical Reviews*, *106*(10), 4428-4453. doi: 10.1021/cr050172k

Tian, B., Lei, Q., Tian, B., Zhang, W., Cui, Y., & Tian, Y. (2018). Uv-driven overall water splitting using unsupported gold nanoparticles as photocatalysts. *Chem. Commun.*, *54*, 1845-1848. doi: 10.1039/C7CC09770K

Tilocca, A., & Selloni, A. (2003). Reaction pathway and free energy barrier for defect-induced water dissociation on the (101) surface of tio2-anatase. *The Journal of Chemical Physics*, *119*(14), 7445-7450. doi: 10.1063/1.1607306

Tilocca, A., & Selloni, A. (2004). Vertical and lateral order in adsorbed water layers on anatase tio2(101). *Langmuir*, *20*(19), 8379-8384. doi: 10.1021/la048937r

Turchi, C. S., & Ollis, D. F. (1990). Photocatalytic degradation of organic water contaminants: Mechanisms involving hydroxyl radical attack. *Journal of Catalysis*, *122*(1), 178 - 192. doi: 10.1016/0021-9517(90)90269-P

Uner, D., Oymak, M. M., & Ipek, B. (2011). Co2 utilisation by photocatalytic con-

version to methane and methanol. *International Journal of Global Warming*, *3*(1/2), 142. doi: 10.1504/IJGW.2011.038376

Wang, R., Hashimoto, K., Fujishima, A., Chikuni, M., Kojima, E., Kitamura, A., ... Watanabe, T. (1998). Photogeneration of highly amphiphilic tio2 surfaces. *Advanced Materials*, *10*(2), 135-138. doi: 10.1002/(SICI)1521-4095(199801)10:2<135::AID-ADMA135>3.0.CO;2-M

Weitze, M.-D. (Ed.). (2018). Artificial photosynthesis. state of research, scientific-technological challenges and perspectives. Retrieved from `https://en.acatech.de/publication/artificial-photosynthesis-state-of-research-scientific-technological-challenges-and-perspectives/`

Wen, J., Li, X., Liu, W., Fang, Y., Xie, J., & Xu, Y. (2015). Photocatalysis fundamentals and surface modification of tio2 nanomaterials. *Chinese Journal of Catalysis*, *36*(12), 2049 - 2070. doi: 10.1016/S1872-2067(15)60999-8

Wendt, S., Schaub, R., Matthiesen, J., Vestergaard, E., Wahlström, E., Rasmussen, M., ... Besenbacher, F. (2005). Oxygen vacancies on tio2(110) and their interaction with h2o and o2: A combined high-resolution stm and dft study. *Surface Science*, *598*(1), 226 - 245. doi: 10.1016/j.susc.2005.08.041

Xiong, Z., Lei, Z., Kuang, C.-C., Chen, X., Gong, B., Zhao, Y., ... Wu, J. C. (2017). Selective photocatalytic reduction of co2 into ch4 over pt-cu2o tio2 nanocrystals: The interaction between pt and cu2o cocatalysts. *Applied Catalysis B: Environmental*, *202*, 695 - 703. doi: 10.1016/j.apcatb.2016.10.001

Yamamoto, S., Bluhm, H., Andersson, K., Ketteler, G., Ogasawara, H., Salmeron, M., & Nilsson, A. (2008). In situ x-ray photoelectron spectroscopy studies of water on metals and oxides at ambient conditions. *Journal of Physics: Condensed Matter*, *20*(18), 184025. doi: 10.1088/0953-8984/20/18/184025

Yang, C.-C., Yu, Y.-H., van der Linden, B., Wu, J. C. S., & Mul, G. (2010). Artificial photosynthesis over crystalline tio2-based catalysts: Fact or fiction? *Journal of the American Chemical Society*, *132*(24), 8398-8406. doi: 10.1021/ja101318k

Yates, J. T. (2009). Photochemistry on tio2: Mechanisms behind the surface chemistry. *Surface Science*, *603*(10), 1605 - 1612. doi: 10.1016/j.susc.2008.11.052

Yu, J., Low, J., Xiao, W., Zhou, P., & Jaroniec, M. (2014). Enhanced photocatalytic co2-reduction activity of anatase tio2 by coexposed 001 and 101

facets. *Journal of the American Chemical Society*, *136*(25), 8839-8842. doi: 10.1021/ja5044787

Zhang, L., Kong, G., Meng, Y., Tian, J., Zhang, L., Wan, S., … Wang, Y. (2017). Direct coupling of thermo- and photocatalysis for conversion of co2–h2o into fuels. *ChemSusChem*, *10*(23), 4709-4714. doi: 10.1002/cssc.201701472

Zhang, Z., & Yates, J. T. (2012). Band bending in semiconductors: Chemical and physical consequences at surfaces and interfaces. *Chemical Reviews*, *112*(10), 5520-5551. doi: 10.1021/cr3000626

Zhao, Y., Gao, W., Li, S., Williams, G. R., Mahadi, A. H., & Ma, D. (2019). Solar-versus thermal-driven catalysis for energy conversion. *Joule*, *3*(4), 920 - 937. doi: 10.1016/j.joule.2019.03.003

Zhao, Y., Li, Z., Li, M., Liu, J., Liu, X., Waterhouse, G. I. N., … Zhang, T. (2018). Reductive transformation of layered-double-hydroxide nanosheets to fe-based heterostructures for efficient visible-light photocatalytic hydrogenation of co. *Advanced Materials*, *30*(36), 1803127. doi: 10.1002/adma.201803127

Zhu, Y., Gao, C., Bai, S., Chen, S., Long, R., Song, L., … Xiong, Y. (2017). Hydriding pd cocatalysts: An approach to giant enhancement on photocatalytic co2 reduction into ch4. *Nano Research*, *10*(10), 3396-3406. doi: 10.1007/s12274-017-1552-0

Zhu, Y., Liu, D., & Meng, M. (2014). H2 spillover enhanced hydrogenation capability of tio2 used for photocatalytic splitting of water: a traditional phenomenon for new applications. *Chem. Commun.*, *50*, 6049-6051. doi: 10.1039/C4CC01667J

APPENDIX A

PROPERTIES OF TiO_2 P25 AND γ-Al_2O_3

Table A.1: TiO_2 P25 (Aeroxide®) product information (Evonik, 2019)

Properties	Unit	Value
Specific surface area (BET)	m^2/g	35-65
Tamped density	g/L	100-180
Titanium dioxide	%	$\geq$99.50
Al_2O_3 content	%	$\leq$0.300
SiO_2 content	%	$\leq$0.200
Fe_2O_3 content	%	$\leq$0.010
HCl content	%	$\leq$0.300
Sieve residue	%	$\leq$0.050

BET analysis is done for TiO_2 P25 and γ-Al_2O_3 with Micromeritics TriStar II surface area and porosity equipment by using N_2. The samples degassed for 12h at $\sim$110-115°C.

Table A.2: BET analysis of TiO_2 P25 (Aeroxide®)

Properties	Unit	Value
Specific surface area	m^2/g	49.03
Total pore volume (single point adsorption)	cm^3/g	0.13
Average pore size	nm	10.80

Table A.3: BET analysis of γ-Al_2O_3 (AlsaAesar)

Properties	Unit	Value
Specific surface area	m^2/g	66.50
Total pore volume (single point adsorption)	cm^3/g	0.19
Average pore size	nm	11.56

APPENDIX B

SAMPLE CALCULATION FOR PALLADIUM AMOUNT IN TiO_2

The palladium solution contains ∼10% (w/w) palladium

$$m_{TiO_2} = 2.0015\ g \tag{B.1a}$$

$$Pd(NO_3)_2 \cdot xH_2O = 0.4\ g \tag{B.1b}$$

$$0.4\ g(Pd(NO_3)_2 \cdot xH_2O) \cdot 0.01\ \frac{Pd}{Pd(NO_3)_2 \cdot xH_2O} = 0.04\ g\ Pd \tag{B.1c}$$

$$Total\ catalyst\ weight = 2.0015 + 0.04 = 2.0415\ g \tag{B.1d}$$

$$Pd\ \% = \frac{100 \cdot 0.04\ g}{2.0415\ g} = 2.0\ \% \tag{B.1e}$$

APPENDIX C

EXPERIMENTAL PROCEDURE FOR A CHEMISORPTION EXPERIMENT

A_{in}, A_{out} and A_{cell} are used to denote gas inlet valve, gas outlet valve and sample cell valve. V_1, V_2 and V_{cell} are used to denote volume of manifold when all the valves are closed, volume of the manifold when only sample valve is open and difference between first two volume corresponds to volume of sample cell.

1. All the valves are closed.
2. Weigh your catalyst and put it into sample cell.
3. Connect sample cell to manifold using metal-glass connection parts.
4. Evacuate molecules in V1 by opening A_{out}.
5. Evacuate sample cell also by opening A_{cell}.
6. Closed A_{cell} and then A_{out} when the pressure is read as zero.
7. Open desired gas tube and take gas into the system until A_{in} point.

For a dead volume measurement;

8. Use a gas that does not interact with the sample.
9. Open A_{in} to take desired amount of gas into system.
10. Close A_{in} and take note of the pressure as P1.
11. Open A_{cell} and wait for equilibrium to be established.
12. When equilibrium established (pressure does not change anymore), take note of the pressure as P_2.

13. Close A_{sample} and take note of the pressure as P_3.

For an adsorption measurement;

14. Continue from Step 4 to Step 13 but use a gas that is wanted to be adsorbed on surface.
15. Open A_{in} to take more gas into the system.
16. Continue with the Step 9 until the pressure that is desired.
17. After finishing the experiment, evacuate the manifold by opening Aout.
18. Finally, open A_{cell} to evacuate the adsorbed molecules.

For removal of the sample;

19. Close A_{cell} and A_{out}.
20. Take an inert gas or air to system from A_{in}.
21. Send the gas to sample cell by opening A_{cell}.
22. Close all the valves.
23. Take the sample cell by loosening metal gas connection.

For a desorption procedure;

24. Instead of conducting Step 18, close A_{out} and take note of the pressure (evacuated V1) as P1 that is zero.
25. Open A_{cell} and wait for equilibrium to be established. Take note of the pressure as P2.
26. Close A_{cell} and take note of the pressure as P_3.
27. Open A_{out} to evacuate V_1.
28. Continue with Step 24 until you reach zero pressure as P_2.

APPENDIX D

EXPERIMENTAL PARAMETERS

- Experiments on TiO_2 P25

In adsorption experiments with water, distilled water in a glass tube is connected to manifold. TiO_2 P25 was used as the catalyst. Experimental conditions for H_2O adsorption on TiO_2 P25 are summarized in TableD.1.

In adsorption experiments with CO_2, pressurized CO_2 gas tube connected to manifold was used. Experimental conditions for CO_2 on TiO_2 are summarized in TableD.2.

O_2 adsorption isotherms were obtained on TiO_2 at with the same manner where experimental conditions are tabulated in TableD.3.

- Experiments on Pd/TiO_2

CO_2 and H_2 adsorbed on Pd/TiO_2 with the conditions listed in TableD.4. Also the sequence of the experiments is given in TableD.6.

- Experiments on γ-Al_2O_3

CO_2 adsorbed on commercial γ-Al_2O_3 with the conditions listed in TableD.7.

Table D.1: Experimental conditions during H_2O experiments on TiO_2 P25

	Dark experiments	Illuminated experiments
Set-up	Chemisorption set-up and/or microlarimeter	Chemisorption set-up and light source
Cell temperature during the experiment	Room temperature, 50°C, 100°C, 150°C	Room temperature
Upper limit of pressure in the manifold	up to 20-25 Torr	up to 20-25 Torr
Dead volume measurement gas	He or air	He or air
Pre-treatment	None O_2 treated (under UV light)	None O_2 treated (under UV light)

Table D.2: Experimental conditions during CO_2 experiments on TiO_2 P25

	Dark experiments	Illuminated experiments
Set-up	Chemisorption set-up and/or microlarimeter	Chemisorption set-up and light source
Cell temperature during the experiment	Room temperature or 50°C	Room temperature
Upper limit of pressure in the manifold	usually up to 100 Torr	usually up to 100 Torr
Dead volume measurement gas	He or air	He or air
Pre-treatment	None O_2 treated (under UV light) Heat treated H_2 treated	None O_2 treated (uner UV light) Heat treated H_2 treated

Table D.3: Experimental conditions during O_2 experiments on TiO_2 P25

	Dark experiments	Illuminated experiments
Set-up	Chemisorption set-up and/or microlarimeter	Chemisorption set-up and light source (UV or visible)
Cell temperature during the experiment	Room temperature or 50°C	Room temperature
Upper limit of pressure in the manifold	up to 100 Torr	up to 100 Torr
Dead volume measurement gas	He	He
Pre-treatment	None	None

Table D.4: Experimental conditions during CO_2 and H_2 experiments on Pd/TiO_2

	Dark experiments with CO_2	Dark experiments with H_2
Set-up	Chemisorption set-up and microlarimeter	Chemisorption set-up and microlarimeter
Cell temperature during the experiment	50°C	50°C
Upper limit of pressure in the manifold	up to 100 Torr	up to 100 Torr
Dead volume measurement gas	He or air	He or Air
Pre-treatment	O_2 (or air) treated H_2 treated	O_2 treated H_2 treated

Table D.5: The sequence of H_2 adsorption experiments on Pd/TiO_2 samples

Pd/TiO_2	Step 1	Step 2
0.5%	Reduction with H_2 at 150°C (4 dose of 100 Torr H_2 in 2h)	H_2 adsorbed on sample at 50°C
1.0%	Reduction with H_2 at 150°C (1 dose of 200 Torr and 2 dose of 100 Torr H_2 in 2h)	H_2 adsorbed on sample at 50°C
2.0%	Reduction with H_2 at 150°C (4 dose of 100 Torr H_2 in 2h)	H_2 adsorbed on sample at 50°C

Table D.6: The sequence of CO_2 adsorption experiments on Pd/TiO_2 samples

Pd/TiO_2	Step 1	Step 2	Step 3	Step 4
0.5%	Sample exposed to O_2 at 250°C	CO_2 adsorbed on sample at 50°C	H_2 adsorbed on sample at 50°C	CO_2 adsorbed on sample at 50°C
1.0%	Sample exposed to H_2 twice at 50°C	CO_2 adsorbed on sample at 50°C	Sample exposed to H_2 at 50° first then to air	CO_2 adsorbed on sample at 50°C
2.0%	Sample exposed to O_2 at 250°C	CO_2 adsorbed on sample at 50°C	H_2 adsorbed on sample at 50°C	CO_2 adsorbed on sample at 50°C

Table D.7: Experiment conditions during CO_2 experiments on γ-Al_2O_3

	Dark experiments
Set-up	Chemisorption set-up
Cell temperature during the experiment	Room temperature
Upper limit of pressure in the manifold	up to 100 Torr
Dead volume measurement gas	Air
Pre-treatment	None

APPENDIX E

THE EFFECT OF ILLUMINATION ON AMBIENT TEMPERATURE NEAR THE CATALYST SURFACE

The effect of illumination on ambient temperature near the catalyst surface was investigated since heating of illuminated area (glass tube, catalyst and adsorbate) due to light source is possible in a photocatalytic study. Hence, temperature increase near the surface was recorded during illumination. Temperature increased up to 40°C at most (Figure E.1).

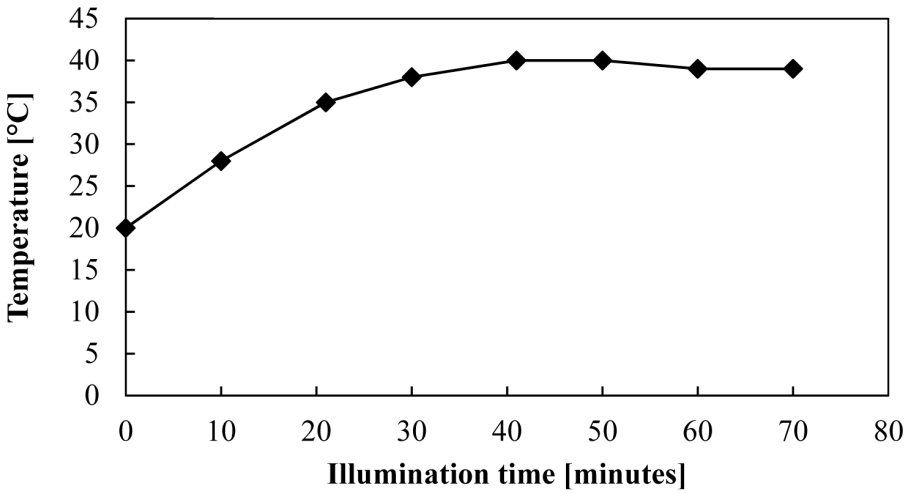

Figure E.1: Temperature profile of ambient temperature near the surface over time during illumination

APPENDIX F

CALCULATION FOR ADJUSTMENT OF CELL TEMPERATURE

Amount of gas in the manifold is calculated as follows assuming all the gas in the system is at cell temperature.

$$N_1 = \frac{P_1 \cdot V_1}{R \cdot T_{cell}} \tag{F.1a}$$

$$N_2 = \frac{P_2 \cdot V_2}{R \cdot T_{cell}} \tag{F.1b}$$

$$N_{cell} = \frac{P_3 \cdot V_3}{R \cdot T_{cell}} \tag{F.1c}$$

Since V_2 is equal to summation of V_1 and V_{cell}. N_2 term can be divided into two terms and cell temperature can be changed independent of temperature of incoming gas.

$$N_1 = \frac{P_1 \cdot V_1}{R \cdot T_{cell}} \tag{F.2a}$$

$$N_2 = \frac{P_1 \cdot V_1}{R \cdot T_{cell}} + \frac{P_3 \cdot V_3}{R \cdot T_{cell,new}} \tag{F.2b}$$

$$N_{cell} = \frac{P_3 \cdot V_3}{R \cdot T_{cell,new}} \tag{F.2c}$$

APPENDIX G

FREUNDLICH ISOTHERM PARAMETERS FOR CARBON DIOXIDE ADSORPTION ISOTHERMS

CO_2 adsorption isotherms were fit to Freundlich isotherm in agreement with the weak adsorption of CO_2 on a heterogeneous surface. Figure G.1 show linearized form for Freundlich isotherm. All the lines are pretty much in the same range in accordance with weak adsorption of CO_2 on any surface within this study again.

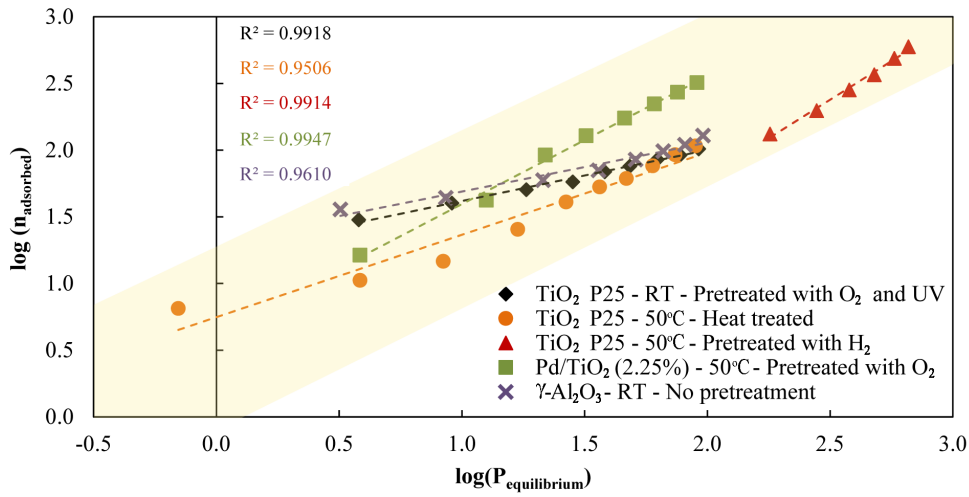

Figure G.1: Linearized form of Freundlich isotherm fitted to experimental data in this study

Table G.1 was formed according linearized form of Freundlich isotherm (Equation G.1a and Equation G.1b).

$$n_{ads} = K_F \cdot P_{eqb}^{1/n_F} \tag{G.1a}$$

$$log(n_{ads}) = log(K_F) + (1/n_F) \cdot log(P_{eqb}) \tag{G.1b}$$

Table G.1: Freundlich isotherm parameters for CO_2 adsorption on TiO_2 P25, Pd/TiO_2 and γ-Al_2O_3

Catalyst	n_F	K_F [$\mu mol \cdot g_{catalyst}^{-1} \cdot Torr^{-1/n_F}$]
TiO_2 P25 - RT - Pretreated with O_2 and UV	2.61	17.21
TiO_2 P25 - 50°C - Heat treated	1.62	5.59
TiO_2 P25 - 50°C - Pretreated with H_2	0.86	0.30
Pd/TiO_2(2.25%) - 50°C - Pretreated with O_2	1.04	4.31
γ-Al_2O_3 - RT - No pretreatment	2.72	20.99

APPENDIX H

TEMKIN ISOTHERM PARAMETERS FOR WATER ADSORPTION ISOTHERMS

Figure H.1 was plotted according linearized form of Temkin isotherm (Equation H.1a and Equation H.1b). Temkin isotherm is a two parameter isotherm where its parameters given in Table H.1.

$$n_{ads} = \frac{R \cdot T}{b_T} \cdot ln(K_T \cdot P_{eqb}) \tag{H.1a}$$

$$n_{ads} = \frac{R \cdot T}{b_T} \cdot ln(K_T) + \frac{R \cdot T}{b_T} \cdot ln(P_{eqb}) \tag{H.1b}$$

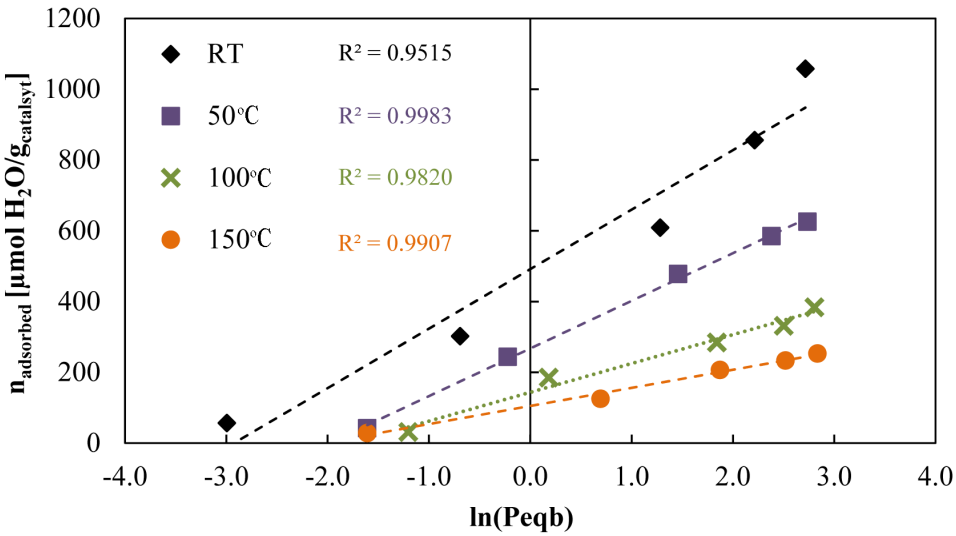

Figure H.1: Temkin isotherm parameters for H_2O adsorption isotherms on TiO_2 P25

Table H.1: Temkin isotherm parameters for H_2O adsorption on TiO_2 P25

Temperature	b_T [$J \cdot g_{catalyst} \cdot \mu mol^{-2}$]	K_T [$Torr^{-1}$]
RT	20.92	18.59
50°C	19.95	7.29
100°C	38.09	5.82
150°C	68.72	7.76

APPENDIX I

O_2 ADSORPTION ISOTHERMS IN DARK AND UNDER ILLUMINATION

O_2 adsorbed on fresh TiO_2 surface at room temperature in dark, under visible light illumination (room light) and under UV illumination. No difference was observed between the three isotherms (Figure I.1). However, before the O_2 adsorption on TiO_2 under illumination, the surface was exposed UV light during the evacuation period. Duration of illumination may resulted in surface modification via defect formation.

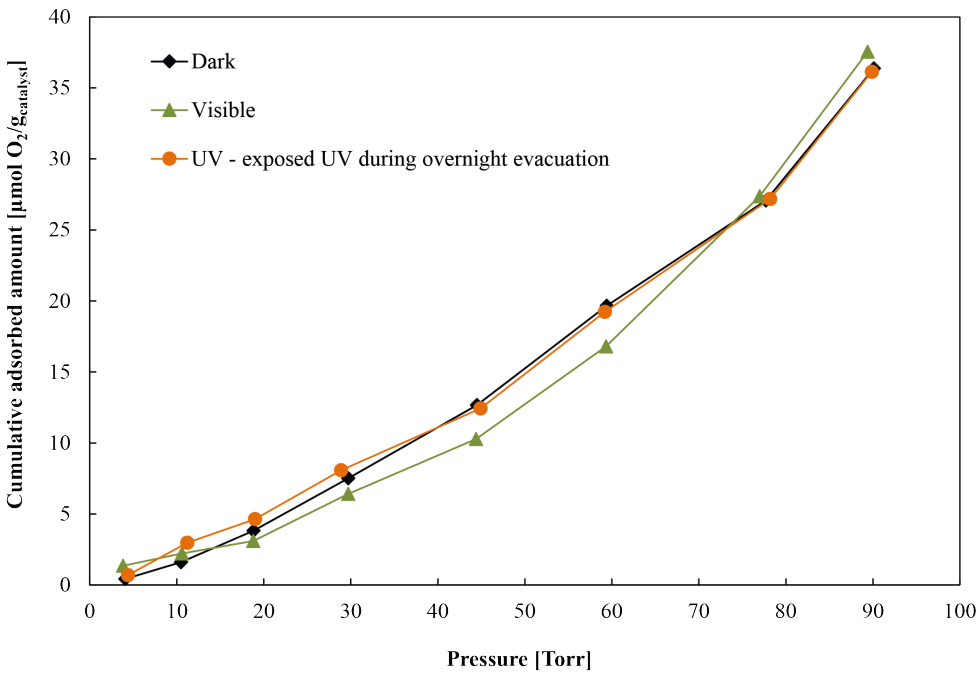

Figure I.1: O_2 adsorption isotherms on TiO_2 P25 obtained at room temperature in dark, under room light illumination and UV illumination

Then, O_2 adsorption isotherms were repeated under visible light at room temperature and in dark at 50°C (Figure I.2). Although, adsorption behavior seems similar, the results do not coincide exactly. Desorption observed in the beginning can be related with impurities on the surface.

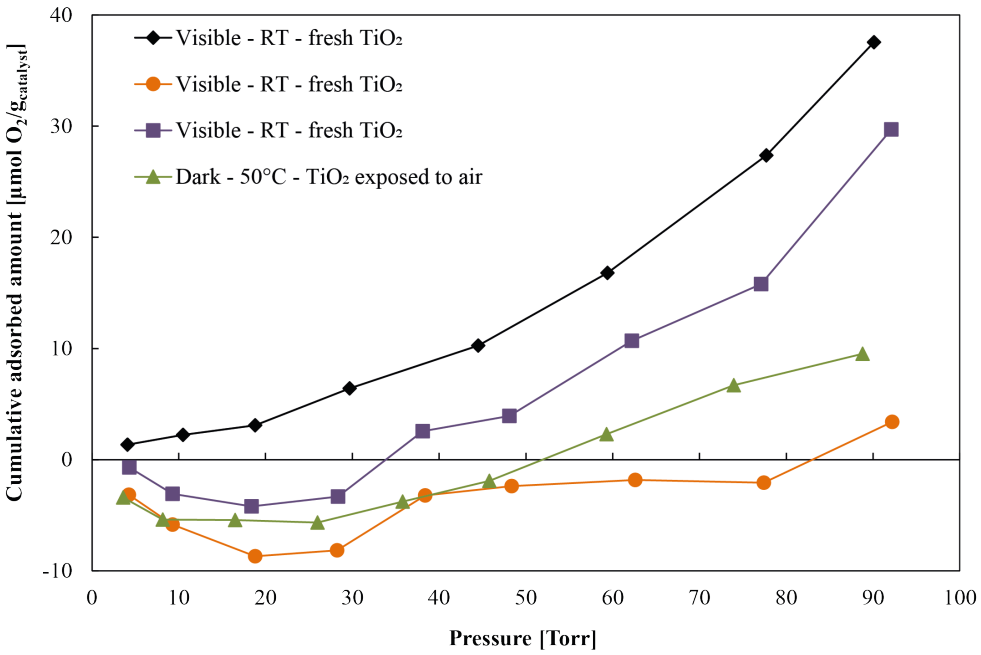

Figure I.2: O_2 adsorption isotherms on TiO_2 P25 obtained at room temperature and 50°C in dark and under room light illumination

APPENDIX J

MICROCALORIMETRY DATA

Table J.1: Incremental adsorbed amounts and corresponding absolute heat values for CO_2 adsorption on fresh TiO_2 P25 in Figure 4.2

Data number	Incremental $N_{adsorbed}/g_{sample}$ [mol/g_{sample}]	Absolute heat values [J/g_{sample}]
1	6.50E-06	0.7367
2	1.71E-07	0.3138
3	2.33E-07	0.1499
4	1.74E-06	0.1563
5	3.07E-06	0.1281
6	5.68E-06	0.037
7	5.71E-06	0.0609
8	4.55E-06	0.0683
9	2.06E-06	0.0603
10	8.52E-06	0.0543

Table J.2: Incremental adsorbed amounts and corresponding absolute heat values for CO_2 adsorption on TiO_2 P25 after first heat treatment in Figure 4.2

Data number	Incremental $N_{adsorbed}/g_{sample}$ [mol/g_{sample}]	Absolute heat values [J/g_{sample}]
1	6.50E-06	0.5511
2	4.04E-06	0.2492
3	4.11E-06	0.3362
4	1.08E-05	0.4054
5	1.54E-05	0.3571
6	1.21E-05	0.2925
7	8.28E-06	0.289
8	1.49E-05	0.2699
9	1.62E-05	0.4004
10	1.50E-05	0.3032

Table J.3: Incremental adsorbed amounts and corresponding absolute heat values for CO_2 adsorption on TiO_2 P25 after second heat treatment in Figure 4.2

Data number	Incremental $N_{adsorbed}/g_{sample}$ [mol/g_{sample}]	Absolute heat values [J/g_{sample}]
1	6.50E-06	0.4525
2	4.05E-06	0.3634
3	6.69E-06	0.3043
4	6.26E-06	0.4434
5	8.25E-06	0.405
6	1.09E-05	0.3539
7	1.22E-05	0.3300
8	1.36E-05	0.3463
9	1.88E-05	0.3342
10	9.82E-06	0.2875

Table J.4: Incremental adsorbed amounts and corresponding absolute heat values for CO_2 adsorption on H_2 pretreated TiO_2 P25 in Figure 4.4

Data number	Incremental $N_{adsorbed}/g_{sample}$ [mol/g_{sample}]	Absolute heat values [J/g_{sample}]
1	-8.42E-06	0.6502
2	-1.84E-07	0.1584
3	5.41E-07	0.1900
4	5.89E-06	0.2011
5	3.74E-06	0.1833
6	7.22E-06	0.1803
7	1.01E-05	0.1368
8	1.46E-05	0.163 0
9	1.46E-05	0.1598
10	8.37E-05	0.4625
11	6.58E-05	0.2516
12	8.47E-05	0.4509
13	8.47E-05	0.1836
14	1.20E-04	0.1294
15	1.09E-04	0.0676

Table J.5: Incremental adsorbed amounts and corresponding absolute heat values for H_2O adsorption on TiO_2 P25 at 50°C in Figure 4.12

Data number	Incremental $N_{adsorbed}/g_{sample}$ [mol/g_{sample}]	Absolute heat values [J/g_{sample}]
1	1.34E-04	11.4702
2	1.58E-04	9.4926
3	1.32E-04	6.0903
4	1.23E-04	4.6828
5	1.52E-04	3.2559
6	3.48E-06	4.6199
7	2.39E-04	1.0453

Table J.6: Incremental adsorbed amounts and corresponding absolute heat values for H_2O adsorption on TiO_2 P25 at 100°C in Figure 4.12

Data number	Incremental $N_{adsorbed}/g_{sample}$ [mol/g_{sample}]	Absolute heat values [J/g_{sample}]
1	3.12E-05	5.6770
2	1.54E-04	15.0875
3	9.91E-05	5.0031
4	4.72E-05	3.3260
5	5.24E-05	0.9236

Table J.7: Incremental adsorbed amounts and corresponding absolute heat values for H_2O adsorption on TiO_2 P25 at 150°C in Figure 4.12

Data number	Incremental $N_{adsorbed}/g_{sample}$ [mol/g_{sample}]	Absolute heat values [J/g_{sample}]
1	2.85E-05	4.5374
2	9.66E-05	10.4411
3	8.18E-05	5.8052
4	2.64E-05	1.8026
5	2.00E-05	0.5871

Table J.8: Incremental adsorbed amounts and corresponding absolute heat values for H_2 adsorption on 0.5% Pd/TiO_2 at 50°C for monitoring reduction in Figure 4.24

Data number	Incremental $N_{adsorbed}/g_{sample}$ [mol/g_{sample}]	Absolute heat values [J/g_{sample}]
1	1.358E-04	23.2260
2	1.011E-04	17.4877
3	1.042E-04	15.6819
4	1.290E-04	15.9500
5	1.225E-04	12.0604

Table J.9: Incremental adsorbed amounts and corresponding absolute heat values for H_2 adsorption on 2.0% Pd/TiO_2 at 50°C for monitoring reduction in Figure 4.24

Data number	Incremental $N_{adsorbed}/g_{sample}$ [mol/g_{sample}]	Absolute heat values [J/g_{sample}]
1	1.894E-04	44.9478
2	1.967E-04	39.6401
3	9.775E-06	2.6366
4	-2.247E-05	1.2302
5	9.661E-06	1.3169
6	1.422E-05	0.9133

Table J.10: Incremental adsorbed amounts and corresponding absolute heat values for H_2 adsorption on H_2 pretreated 0.5% Pd/TiO_2 at 50°C in Figure 4.26

Data number	Incremental $N_{adsorbed}/g_{sample}$ [mol/g_{sample}]	Absolute heat values [J/g_{sample}]
1	2.37E-05	2.7869
2	7.96E-06	1.0273
3	8.90E-06	1.0488
4	5.42E-06	1.7417
5	1.21E-05	1.4128
6	1.59E-05	1.6770
7	1.63E-05	1.3694
8	1.94E-05	1.3861
9	2.12E-05	0.9708

Table J.11: Incremental adsorbed amounts and corresponding absolute heat values for H_2 adsorption on H_2 pretreated 1.0% Pd/TiO_2 at 50°C in Figure 4.26

Data number	Incremental $N_{adsorbed}/g_{sample}$ [mol/g_{sample}]	Absolute heat values [J/g_{sample}]
1	5.89E-06	1.9991
2	2.86E-05	7.0193
3	3.99E-05	8.9608
4	7.54E-05	12.0396
5	8.18E-05	7.3646
6	1.08E-04	7.5132
7	8.40E-05	3.7465
8	8.84E-05	3.0418
9	1.31E-04	5.4504

Table J.12: Incremental adsorbed amounts and corresponding absolute heat values for H_2 adsorption on H_2 pretreated 2.0% Pd/TiO_2 at 50°C in Figure 4.26

Data number	Incremental $N_{adsorbed}/g_{sample}$ [mol/g_{sample}]	Absolute heat values [J/g_{sample}]
1	2.38E-05	5.6702
2	4.81E-05	13.8080
3	3.44E-05	7.3879
4	4.45E-05	8.8184
5	3.79E-05	5.8743
6	5.52E-05	-
7	2.82E-05	4.3612
8	3.04E-05	2.2269
9	3.15E-05	1.2210

Table J.13: Incremental adsorbed amounts and corresponding absolute heat values for CO_2 adsorption on O_2 pretreated 0.5% Pd/TiO_2 at 50°C in Figure 4.28

Data number	Incremental $N_{adsorbed}/g_{sample}$ [mol/g_{sample}]	Absolute heat values [J/g_{sample}]
1	1.630E-05	1.0568
2	2.581E-05	0.5267
3	4.957E-05	0.3988
4	3.634E-05	0.3898
5	4.537E-05	0.4643
6	4.837E-05	0.4177
7	4.955E-05	0.3319
8	4.871E-05	0.3195

Table J.14: Incremental adsorbed amounts and corresponding absolute heat values for CO_2 adsorption on H_2 pretreated 0.5% Pd/TiO_2 at 50°C in Figure 4.28

Data number	Incremental $N_{adsorbed}/g_{sample}$ [mol/g_{sample}]	Absolute heat values [J/g_{sample}]
1	3.546E-05	2.1160
2	3.552E-05	0.4623
3	3.844E-05	0.4005
4	3.998E-05	0.2813
5	6.461E-05	0.3115
6	5.353E-05	0.2688
7	6.340E-05	0.2240
8	7.025E-05	0.1670

Table J.15: Incremental adsorbed amounts and corresponding absolute heat values for CO_2 adsorption on 1.0% Pd/TiO_2 (exposed to air) at 50°C in Figure 4.28

Data number	Incremental $N_{adsorbed}/g_{sample}$ [mol/g_{sample}]	Absolute heat values [J/g_{sample}]
1	7.782E-06	2.2508
2	8.521E-07	0.8608
3	-2.528E-06	0.5682
4	-6.533E-07	0.3369
5	7.541E-06	0.3965
6	2.471E-06	0.1445
7	1.974E-06	0.1271
8	5.780E-06	0.0938

Table J.16: Incremental adsorbed amounts and corresponding absolute heat values for CO_2 adsorption on H_2 pretreated 1.0% Pd/TiO_2 at 50°C in Figure 4.28

Data number	Incremental $N_{adsorbed}/g_{sample}$ [mol/g_{sample}]	Absolute heat values [J/g_{sample}]
1	7.669E-06	2.0615
2	-2.485E-06	0.5283
3	-2.528E-06	0.2670
4	-6.533E-07	0.2088
5	4.800E-06	0.2518
6	8.776E-06	0.2094
7	5.396E-06	0.2023
8	6.036E-06	0.2050

Table J.17: Incremental adsorbed amounts and corresponding absolute heat values for CO_2 adsorption on O_2 pretreated 2.0% Pd/TiO_2 at 50°C in Figure 4.28

Data number	Incremental $N_{adsorbed}/g_{sample}$ [mol/g_{sample}]	Absolute heat values [J/g_{sample}]
1	7.983E-06	0.8180
2	8.246E-06	0.5695
3	8.636E-06	0.4200
4	7.566E-06	0.3190
5	1.341E-05	0.3316
6	1.146E-05	0.3197
7	1.453E-05	0.3310
8	1.008E-05	0.2453

Table J.18: Incremental adsorbed amounts and corresponding absolute heat values for CO_2 adsorption on H_2 pretreated 2.0% Pd/TiO_2 at 50°C in Figure 4.28

Data number	Incremental $N_{adsorbed}/g_{sample}$ [mol/g_{sample}]	Absolute heat values [J/g_{sample}]
1	4.226E-05	5.1549
2	1.613E-05	1.0514
3	8.636E-06	0.3301
4	1.002E-05	0.2147
5	1.192E-05	0.2233
6	7.829E-06	0.1858
7	7.829E-06	0.1597
8	1.188E-05	0.1376